AD-A141 958 MECHANISMS OF SMOKE REDUCTION IN THE HIGH-PRESSURE COMBUSTION OF EMULSIFI.. (U) SOUTHWEST RESEARCH INST SAN ANTONIO TX L G DODE ET AL. MAY 84 SWRI-6287/3 1/2

UNCLASSIFIED N00014-80-K-0460 F/G 21/2 NL

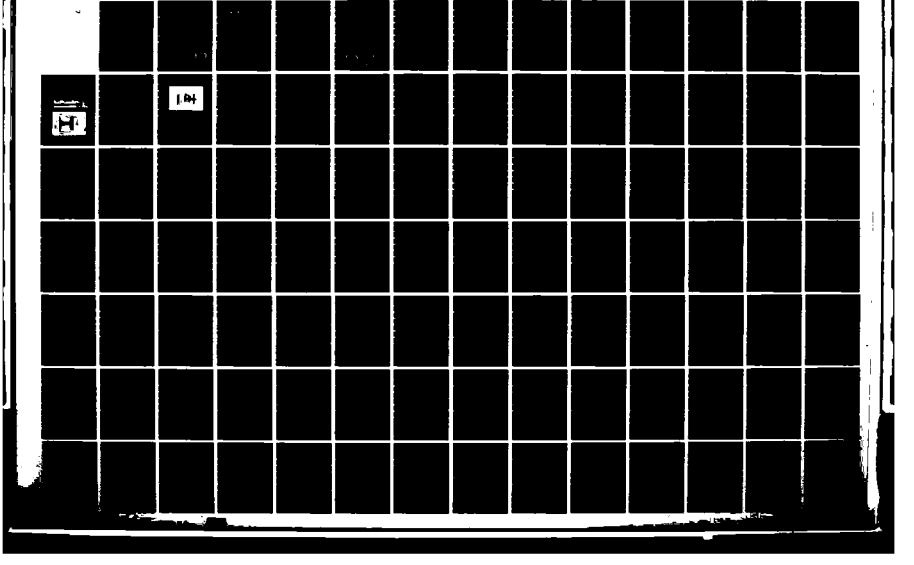

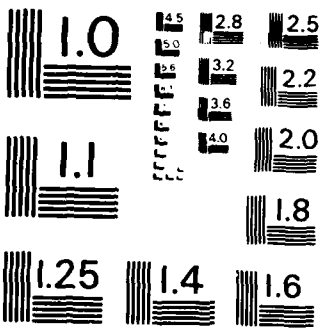

(12)

MECHANISMS OF SMOKE REDUCTION IN THE HIGH-PRESSURE COMBUSTION OF EMULSIFIED FUELS

Volume III — Experimental Measurements and Computer Modeling of Evaporating Emulsified and Neat Fuel Sprays

FINAL REPORT
NO. SwR-6287/3

Prepared by
Lee G. Dodge and Clifford A. Moses
Energy Systems Research Division
Southwest Research Institute

Prepared for
Office of Naval Research
Department of the Navy
800 N. Quincy Street
Arlington, Virginia 22217

Contract No. NOOO14-80-K-0460

Approved for public release;
distribution unlimited

May 1984

SOUTHWEST RESEARCH INSTITUTE
SAN ANTONIO HOUSTON

Unclassified
SECURITY CLASSIFICATION OF THIS PAGE (*When Data Entered*)

REPORT DOCUMENTATION PAGE	READ INSTRUCTIONS BEFORE COMPLETING FORM
1. REPORT NUMBER	2. GOVT ACCESSION NO. / 3. RECIPIENT'S CATALOG NUMBER
MECHANISMS OF SMOKE REDUCTION IN THE HIGH-PRESSURE COMBUSTION OF EMULSIFIED FUELS **Volume III — Experimental Measurements and Computer Modeling of Evaporating Emulsified and Neat Fuel Sprays**	5. TYPE OF REPORT & PERIOD COVERED Final Report 29 Sept '80 - 28 Feb '84
	6. PERFORMING ORG. REPORT NUMBER Final Rpt #SwR-6287/3
Lee G. Dodge and Clifford A. Moses	8. CONTRACT OR GRANT NUMBER(s) N00014-80-K-0460
9. PERFORMING ORGANIZATION NAME AND ADDRESSES Southwest Research Institute P.O. Drawer 28510 6220 Culebra Road San Antonio, Texas 78284	10. PROGRAM ELEMENT, PROJECT, TASK AREA & WORK UNIT NUMBERS
11. CONTROLLING OFFICE NAME AND ADDRESS Office of Naval Research Department of the Navy 800 North Quincy Street Arlington, Virginia 22217	12. REPORT DATE May 1984 13. NUMBER OF PAGES 107
14. MONITORING AGENCY NAME & ADDRESS (*if different from Controlling Office*)	15. SECURITY CLASS (*of this report*) Unclassified 15a. DECLASSIFICATION DOWNGRADING SCHEDULE

16 DISTRIBUTION STATEMENT (*of this Report*)

Approved for Public Release; distribution unlimited

17 DISTRIBUTION STATEMENT (*of the abstract entered in Block 20, if different from Report*)

18 SUPPLEMENTARY NOTES

19 KEY WORDS (*Continue on reverse side if necessary and identify by block number*)

Alternative Fuels	Drop-Size Measurements	Evaporation
Atomization	Drop Sizing	Fuel Drops
Combustion	Drops	Lasers
Combustors	Emulsified Fuels	Measuring Instruments

20. ABSTRACT (*Continue on reverse side if necessary and identify by block number*)

Measurements of drop-size distributions and vaporized fuel concentrations have been combined with a spray model in the comparative study of the evaporation of sprays of emulsified and non-emulsified (neat) fuels at elevated temperatures and pressures. The fuel spray was generated by a pressure jet atomizer and was polydisperse; the air stream was approximately one-dimensional turbulent flow in a constant area duct. Diagnostic techniques have been adapted or developed which

DD FORM 1 JAN 73 1473 EDITION OF 1 NOV 65 IS OBSOLETE

Unclassified
SECURITY CLASSIFICATION OF THIS PAGE (*When Data Entered*)

allow rapid measurements of overall drop-size distributions in the presence of evaporation in high-temperature high-pressure air, and also the fuel vapor concentration distribution within sprays. It was concluded that even in conditions of turbulence and high Reynolds number for drop motion relative to the air, some emulsified fuel drops apparently undergo microexplosions. Further, it was determined that the initial atomization quality depends on the air conditions, with better atomization at higher air densities. This implies that spray drop-size measurements performed at atmospheric conditions need to be corrected for air density and temperature effects to predict atomization quality for altitude relight or high-pressure combustion.

A spray model has been developed which represents the spray being studied and provides data in a form comparable to the experimental diagnostics. Comparisons are provided between the predicted and measured drop-size distribution and fuel-vapor concentrations during the evaporation process. Trends for changes in drop-size distribution (both average size and width of the distribution) with distance from the nozzle are predicted fairly well by the model except close (<10 mm) to the nozzle exit.

ABSTRACT

Measurements of drop-size distributions and vaporized fuel concentrations have been combined with a spray model in the comparative study of the evaporation of sprays of emulsified and non-emulsified (neat) fuels at elevated temperatures and pressures. The fuel spray was generated by a pressure jet atomizer and was polydisperse; the air stream was approximately one-dimensional turbulent flow in a constant area duct. Diagnostic techniques have been adapted or developed which allow rapid measurements of overall drop-size distributions in the presence of evaporation in high-temperature high-pressure air, and also the fuel vapor concentration distribution within sprays. It was concluded that even in conditions of turbulence and high Reynolds number for drop motion relative to the air, some emulsified fuel drops apparently undergo microexplosions. Further, it was determined that the initial atomization quality depends on the air conditions, with better atomization at higher air densities. This implies that spray drop-size measurements performed at atmospheric conditions need to be corrected for air density and temperature effects to predict atomization quality for altitude relight or high-pressure combustion.

A spray model has been developed which represents the spray being studied and provides data in a form comparable to the experimental diagnostics. Comparisons are provided between the predicted and measured drop-size distribution and fuel-vapor concentrations during the evaporation process. Trends for changes in drop-size distribution (both average size and width of the distribution) with distance from the nozzle are predicted fairly well by the model except close (< 10 mm) to the nozzle exit.

TABLE OF CONTENTS

LIST OF ILLUSTRATIONS

LIST OF ILLUSTLRATIONS (Cont'd)

Figure

LIST OF ILLUSTRATIONS (cont'd)

Figure

LIST OF ILLUSTRATIONS (cont'd)

I. INTRODUCTION

It has been shown by Moses,[1] Klarman et al.,[2] Spadaccini and Pelmas,[3] Kinney and Lombard,[4] and others that adding water to fuel in the form of emulsions can reduce soot in gas-turbine combustors. Callahan et al.[5] have also demonstrated soot reductions in diesel engines using emulsified fuels. Several reasons have been suggested for the soot reduction including: (a) a reduction in gas-phase pyrolysis reactions due to the lowered combustion temperature resulting from the increased heat used to vaporize water or an increase in endothermic reactions, (b) a reduction in liquid-phase pyrolysis due to lowered drop temperatures, (c) an increase in soot precursor oxidation due to an increased OH concentration, or (d) an improvement in fuel/air mixing resulting from "microexplosions" caused by superheating of the water in the fuel drop. Which mechanism dominates is still in question.

Recently published papers by Gollahalli et al.[6] and Rao and Bardon[7] show opposite effects on flame temperature resulting from emulsification for the two different flames studied, and attribute soot reduction to items (d) and (a) above, respectively. Although soot reductions for emulsions observed in full-scale tests have often been attributed to microexplosions, it has never been possible to observe them in these tests. Microexplosions can occur when water is contained in a fuel drop which has a higher boiling point than water. During the heatup of such a drop, the water may either be brought to the surface to evaporate, or, if that transport process is too slow and the drop exceeds the boiling point of water, the superheated water may violently boil and shatter the drop into many smaller drops. These smaller drops enhance mixing and reduce the probability of soot formation. Disruptive burning has been observed in single-drop laboratory experiments[8,9,10], but the fuels and/or air conditions have been chosen to maximize the probability of microexplosions and are not representative of the environment in a gas-turbine combustor. For example, the high relative drop/gas velocities in a gas-turbine combustor promote internal circulation in the fuel drops which reduce the probability of disruptive burning by transporting the more volatile water to the surface.[8] In one single-drop experiment, Lasheras et al.[10] limited internal circulation by keeping the Reynolds number of the drops to less than 0.5, while in a gas turbine the same size drop would have an initial Reynolds number about two or three orders of magnitude larger.

One of the goals of the work reported here was to examine the evaporation of emulsified fuels sprayed from a pressure jet atomizer into turbulent high-temperature high-pressure air, and look for evidence of microexplosions of emulsified drops. Comparative evaporation rates of emulsified and neat fuels were determined using a two-phase probe, and drop-size distributions were determined from the forward angle light diffraction pattern using a Malvern Model 2200 modified for use in evaporating sprays. Measurements were made at air temperatures to 700 K and pressures to 586 kPa using both Jet-A and a single-component fuel, both in em ified and neat form. Modifications required for drop-size measurements in flames a also described.

In addition to the interest in microexplosions, another t of this program has been to develop a better understanding of fuel spray evaporat. by coupling the drop-size and fuel vapor concentration measurements with a computer model of spray evaporation. As indicated in Faeth's[11] review article, there are a number of spray models which have been written, but the verification data is very sparse. Data generated in this program directly address this void.

This report describes the high-temperature, high-pressure spray test facility, the operation and modifications to the Malvern drop-sizing instrument, the two-phase probe, and the computer spray model that were employed in this research program. The results obtained using these diagnostics to study fuel-spray evaporation for emulsified and non-emulsified fuels are presented. Five publications/presentations resulted from this work and are referenced in Appendix B. These papers include descriptions of: (1) a calibration procedure for the Malvern instrument which significantly improves accuracy and is now becoming widely accepted, (2) several modifications to the Malvern which allow it to be used in evaporating sprays, and (3) several papers which show results from these measurements and model predictions.

II. EXPERIMENTAL APPARATUS

Four principal pieces of experimental apparatus have been assembled or purchased for this program. They are: (1) the high-temperature high-pressure test section and disc-in-duct combustor, along with the air factory, nozzles, and other associated hardware, (2) the Malvern laser-diffraction, drop-sizing instrument as modified for these experiments, (3) the two-phase, or phase-discriminating probe used for fuel vapor measurements, and (4) the computer model for spray evaporation.

2.1 High-Temperature High-Pressure Test Section

Almost all of the experiments described in this report were spray evaporation studies without combustion, conducted in uniform-temperature fully-developed turbulent flow in a constant area duct. A few experiments were attempted in burning fuel sprays, but the data were of poor quality and difficult to interpret. The same test section was used for the non-combusting and combusting experiments except that a disc coaxial with the circular duct was inserted for the combustion experiments to provide a recirculation zone for flame stabilization.

Unvitiated compressed air is supplied to the test cell by three compressors and a gas-fired preheater which provide up to 1.1 kg/sec at pressures ranging from 138 kPa (1.36 atm) to 1620 kPa (16.0 atm) and temperatures up to 1090 K.

The test section shown in Figure 1, consists of a type 316 stainless steel pipe, 16.83 cm OD, 12.50 ID, 2.17 cm wall thickness, with quartz windows on each side having a clear aperture of 9.2 cm by 6.7 cm. A smooth transition section 5.5 cm long is provided on each end of the windows, as shown in Figure 2, to reduce recirculation zones. Each window is purged by air on both top and bottom. Air is supplied to each window by a total of 10 tubes of nominal 0.635 cm OD and then diffused and exhausted by a convergent section parallel to the window surface.

For the evaporation tests, a fuel nozzle is mounted about even with the upstream edge of the windows. The nozzle is supported with a 12.7 mm OD stainless steel tube which follows the test section centerline for a distance of about 25 cm upstream from the nozzle and then makes a right angle bend and exits from the test section. The

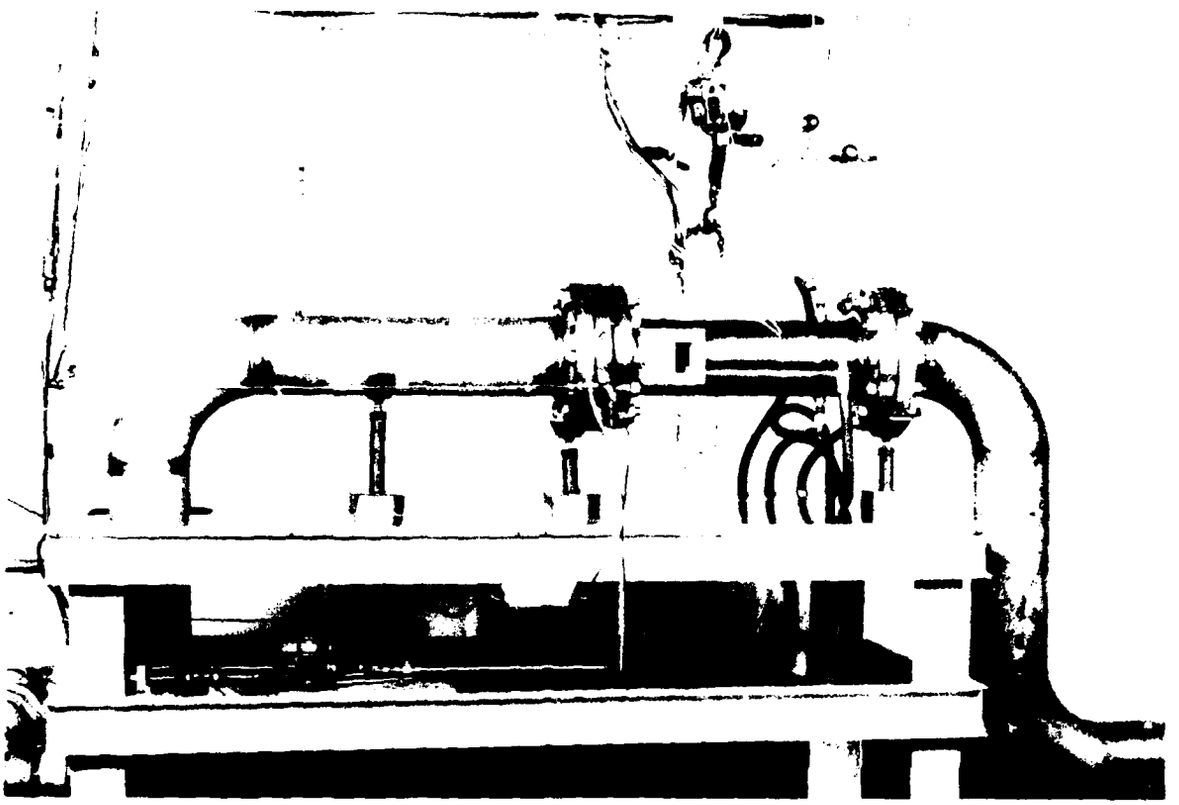

FIGURE 1. OVERALL VIEW OF TEST SECTION

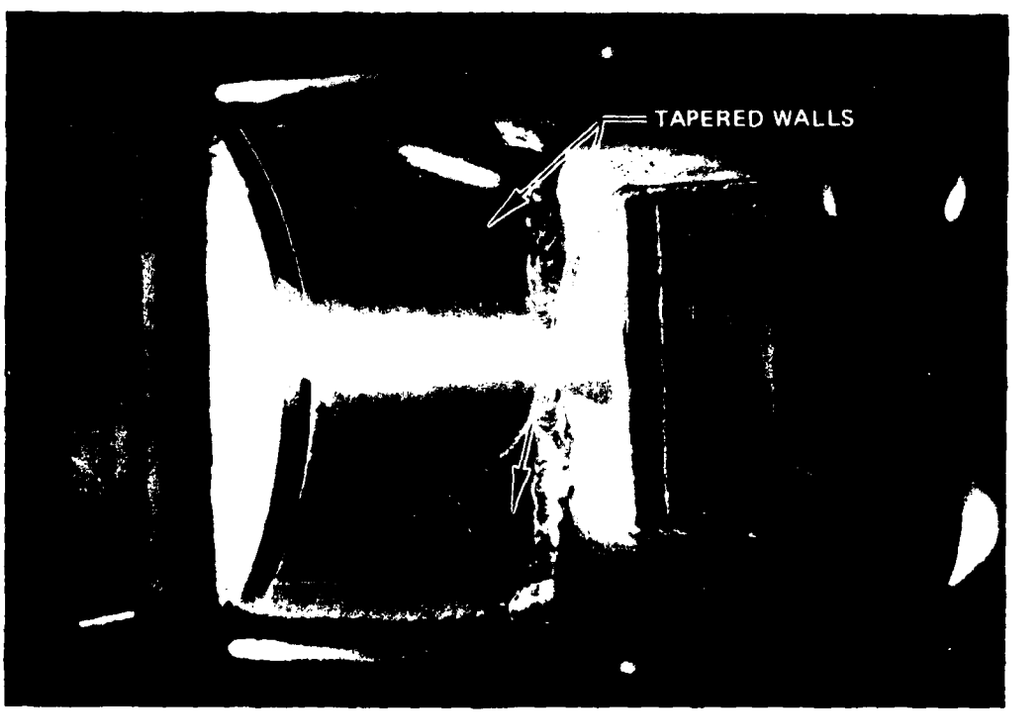

FIGURE 2. INSIDE OF TEST SECTION SHOWING
WINDOW TRANSITION REGION

12.7 mm OD tube carries cooling water and a separate parallel 6.35 mm OD stainless steel tube is the water return line. Another 6.35 mm OD stainless steel tube is mounted inside the 12.7 mm water cooling tube and carries fuel to the nozzle. Fuel temperature is regulated by controlling the water temperature.

For the spray tests with combustion, a 7.22 cm diameter disk holding the fuel nozzle in the center and an igniter is mounted in the center of the duct as shown in Figure 3. The disk stabilizer follows the design by Mellor and coworkers at Purdue, and occupies 1/3 of the area of the duct. Control of the fuel temperature is the same as that described above for the evaporation tests. For some experiments, the flame was also stabilized without the disc by using two rectangular flame holders, 6.4 mm thick, 25.4 mm high, and 50mm long, placed 25 mm apart at the upper and lower edges of the spray, 42 mm downstream of the nozzle.

The two nozzles used are simplex pressure atomizers producing a hollow cone spray. The model type was Delavan Corp. WDA 45° hollow cone with nominal flow rates of 3.79 liters/hour (1 gallon/hour) and 11.3 liters/hour (3 gallons/hour) at 862 kPa (125 psi) differential pressure using water.

The operation of the test cell is monitored with a Hewlett-Packard 9820 programmable calculator which is coupled to a 50 channel scanner. A test report including the average and statistical variation of all the important parameters is available immediately after a test. The sensing systems consist of strain-gage pressure transducers, thermocouples, and turbine flowmeters.

2.2 Malvern Drop-Sizing Instrument

Drop size data were obtained with a Malvern Model 2200 Particle Sizer based on principles of forward-light scattering or Fraunhofer diffraction. When illuminated by a beam of monochromatic, coherent, collimated light from a HeNe laser, the smaller drops diffract light at larger angles to the optical axis than the larger drops and a unique diffraction pattern is formed. Detection is accomplished with a 30 annular ring set of solid state detectors. Detector outputs are multiplexed and the data signal-averaged with a Commodore PET computer. A computer routine proprietary to Malvern is used to interpret the light scattering pattern of the polydisperse drop

FIGURE 3. TEST SECTION AS DISC-IN-DUCT COMBUSTOR

systems. The drop-size data are available as either a set of two parameters defining a Rosin-Rammler, log-normal, or normal distribution, or as a histogram of 15 size classes of drops without any assumption about the shape of the distribution. Although all of the distributions have been tried, the Rosin-Rammler has generally provided the best fit and was used throughout this program. A 300 mm focal length f/7.3 lens was used to collect the scattered light. The laser beam diameter was 9 mm with a Gaussian intensity distribution truncated at the edge by the 9 mm aperture.

The standard Malvern system is not suitable for use with evaporating sprays due to beam-steering problems; further complications are introduced if the spray is burning because the laser signal must be separated from the flame radiation. Modifications were made to the Malvern system to address both of these problems.

The laser beam-steering problems at elevated air temperatures were caused by refractive index gradients due to both temperature gradients and fuel vapor concentration gradients. The problem is identical to "heat waves" observed over buildings in the summer. The result is that the unscattered portion of the laser beam of the drop sizer, which normally is focused onto the central detector, is caused to wander onto some of the other nearby detectors which are used to measure light scattered by the drops in the spray. Since large drops scatter light at the smallest angle and their scattered light is focused onto the inner detectors, the extra signal intensity due to the beam steering is interpreted by the instrument as more large drops than actually exist. Fortunately, the additional signals due to beam steering are typically limited to the inner six or eight of the thirty detectors in non-burning evaporating sprays early in the evaporation process. The detector radii increase rapidly in going away from the center spot, so that the beam steering perturbations, which affect the first couple of detectors at any elevated temperature must become much larger in magnitude to progress outward through the larger radii detectors.

The signals from the 30 detectors are paired together for adjacent detectors to form 15 data which are used to determine the two parameters specifying the Rosin-Rammler distributions. Mathematically, this represents an overdetermined set of 15 data to determine 2 coefficients, and some of these data are unnecessary except to improve the statistics in determining the fit. Thus, in some cases the data from the inner detectors (up to 8) may be ignored and a reasonable fit to the Rosin-Rammler

distribution obtained. This approach has been used successfully and is described in more detail by Dodge and Cerwin.[12] This modification allows the use of this type of automated sizing instrumentation in elevated temperature and pressure sprays for the first time.

Additional changes were required for burning sprays. Three modifications were made to discriminate against flame radiation. First the laser beam was chopped at 667 Hz and the differential signal at each detector ring was sampled for 20 cycles. This necessitated slowing the multiplexing rate in the electronics from about 1.3 ms/channel to 30 ms/channel. It was also necessary to sample on the "clean" part of the signal when the beam was completely blocked or completely transmitting as the chopper blade edge produces a large spurious signal when passing through the laser beam due to its own diffraction pattern. The second modification was the use of a 3 nm band pass interference filter centered at the HeNe laser wavelength of 632.8 nm in front of the lens on the drop sizer. All measurements were made with the 300 mm focal length lens which has a maximum effective acceptance angle of about 2.7° from the normal axis for light reaching the detector. The transmission of the filter changes less than one percent for rays at this angle or less relative to the normal axis through the filter. However, if the 100 mm or 63 mm focal length lenses (the other standard sizes) were used, the acceptance angle increases to about 8.1° or 12.8°, respectively, and wider band pass filters would be necessary. The third modification involves the use of an aperture of diameter 32 mm located about 130 mm from the lens to block radiation from the flame which is not within the scattering volume of the laser beam. These modifications are discussed in more detail by Dodge and Cerwin.[12]

The modifications to the instrument to discriminate against flame radiation were successful in allowing the light scattered by the drops to be detected while discriminating against flame radiation which was orders of magnitude higher in intensity. However, for the conditions examined, the extreme temperature gradients caused such large beam steering excursions that reasonable drop-size data were not obtained for burning sprays.

In addition to the various modifications already discussed, a calibration procedure has been developed and described in Reference 3 of Appendix B which substantially improves the accuracy of the Malvern instrument. This procedure involves

determining the responsivity of each of the 30 detectors using a uniform light source. After using this procedure, the instrument response agrees with calibration standards within the accuracy of those standards.

2.3 Two-Phase Probe

The temperature-controlled two-phase probe is shown in Figure 4. The operation of various two-phase probe designs has been described by Collins,[13] McVey et al.,[14] and Wadleigh and Oman.[15] The concept is to transport gases past a sample probe (the vapor-only probe) at a high velocity and to pull a small amount of vapor and air out of the high speed stream for analysis. The streamlines into the vapor-only tube bend so sharply that drops larger than a few micrometers cannot make the sharp turn, and centrifugal force causes them to be separated from the vapor and air sample. This sample can then be analyzed for fuel vapor concentration. A second tube concentric with the vapor-only tube, but larger, is shown in Figure 4. It is called the boundary-layer suction tube, and it prevents drops from impinging on the vapor-only tube and then being sucked in. Guidelines for operation of the boundary-layer suction tube are given by Wadleigh and Oman.[15] Flow was established in both the boundary layer suction tube and the main probe without pumps, but rather using the pressure differential between the test section (448 kPa) and atmospheric pressure. A valve was used in the boundary layer tube to restrict flow and was adjusted to give a minimum reading (actually zero) for the vapor-only tube gases while sampling a hexadecane spray at room temperature. Flow through the main probe was not restricted to achieve a maximum velocity at the vapor/drop separation point. The main tube is 4.93 mm id and 610 mm long. Computations indicated that the flow should be friction-choked, or close to it, in the main probe, with an entrance mach number of about 0.40. Differential measurements of the static and stagnation pressure indicated an entrance mach number of about 0.35.

The boundary layer suction tube is 2.57 mm id. The vapor-only tube is located 25 mm from the entrance to the main probe and is 1.08 mm id. The probe is maintained at about 478 K with recirculating silicon oil which is temperature-controlled by electric heaters and water cooling. The two-meter long sample line was teflon and heated to about 505 K. The analysis of the vapor-only sample was made with a heated (422 K) flame ionization detector.

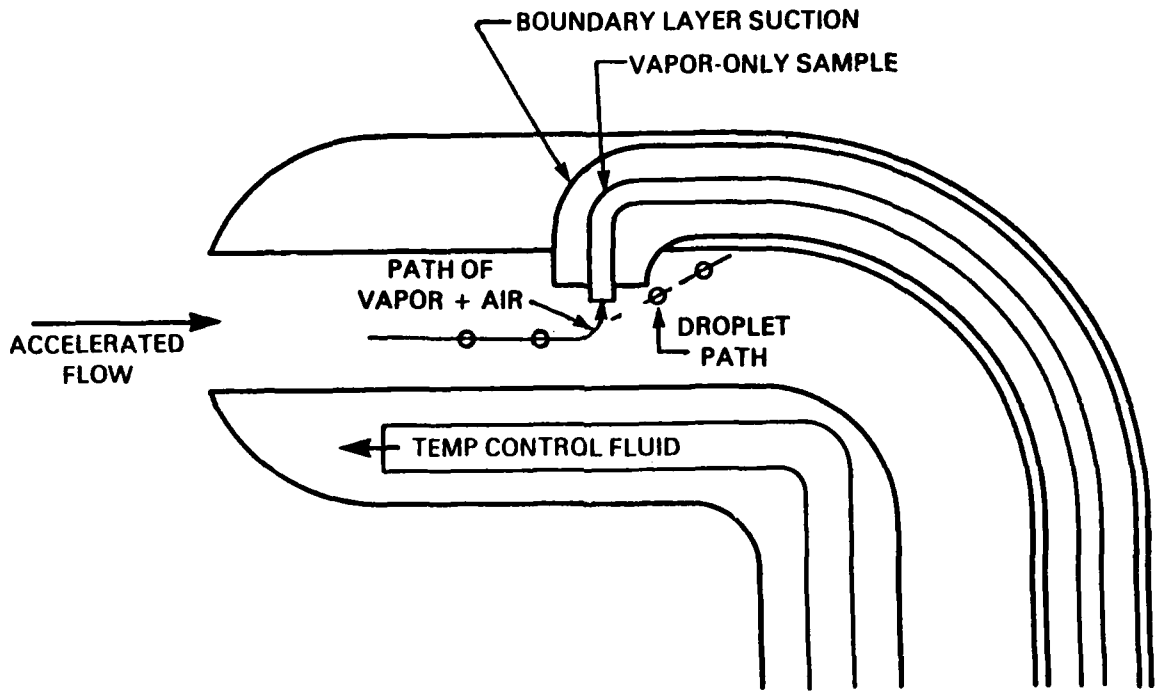

FIGURE 4. TEMPERATURE-CONTROLLED TWO-PHASE PROBE

2.4 Spray Trajectory and Evaporation Model

A computer model based on an array of different-sized, noninteracting drops has been developed to study the heat-up, final "wet-bulb" drop temperature, evaporation rates, trajectories and resulting size-distribution parameters at locations downstream from the nozzle. The trajectory part of the model should be considered as a straightforward and simple one based on an average drop path (neglecting turbulent statistical fluctuations) in a one-dimensional flow field. This corresponds to the experimental situation being studied. The thermodynamic part of the model, however, is very detailed and computes the transient heat-up and final drop temperature in greater detail than many spray models. The environment surrounding the drop is calculated based on the properties of both the fuel vapor and air rather than air alone as in some spray models. The convective effects on evaporation are included and constantly updated as the different size drops are decelerated to the air-stream velocity. The effects of temperature and pressure on air and fuel properties is included, and the steady-state "wet-bulb" temperature is iteratively calculated using the equations for the vapor pressure and temperature-dependent fuel and air properties. This model assumes uniform drop temperatures (infinite heat transfer rates within the drop) and single-component fuels.

Some spray models have predicted the change in drop-size distribution for a quiescent spray as a function of time, but results from this model show the considerable distinction between drop-size distributions as measured at a given location along the nozzle axis, at which drops arrive after different transit times (depending on diameter), as contrasted with the variation with time. For example, in this experiment, the spray initially has a higher axial velocity than the air and the small drops decelerate more rapidly than the large ones, resulting in a higher concentration in the measurement volume for the small drops and a longer time-of-arrival. These effects must be included in any model which is intended to be used for comparison with experimentally measured changes in size distribution.

In developing a model which can be used to compare with experimental results, it is necessary to consider the interaction of the measuring device with the spray. The added weighting of the small drops due to their more rapid deceleration has been discussed. In addition, the small drops are caught up in the air stream and tend to

populate the center of the spray while the large drops maintain their initial velocity longer and tend to fill the outer edges of the spray. This disparity is magnified by the fact that at the exit of a hollow-cone swirl nozzle (the type used in these tests) the majority of the fluid consists of larger drops in the outer cone of the spray, while smaller drops fill in the less dense spray in the center of the cone. Thus, it is necessary to model these inhomogeneities in size distribution through the spray and also the location, diameter, and intensity distribution of the laser beam relative to the spray. At this time, the model does account for the different trajectories of the large and small drops, but assumes that all the spray is initially at a fixed cone angle. The drop-size distribution is calculated for a complete cross section of the spray at a given axial location, without regard for the laser beam sampling volume. The model also assumes that spray breakup is complete and no secondary atomization or drop agglomeration occurs beyond some point from the nozzle exit. An initial size distribution at that point is an input to the model. Thus, the model is not applicable very close to the nozzle ($\lesssim$10mm).

Results from the model are presented in the following sections, while the detailed mathematics of the model are presented in Appendix A. A general flow chart of the model is presented in Figure A1. Most of the model has been constructed from pieces of existing models. The thermodynamic part of the model follows closely the work of Chin and Lefebvre at Purdue University, while the aerodynamic equations for drag, drop velocity, etc. are based on a model developed at the University of Sheffield by Swithenbank, Boyson, Ayers and others. (See Appendix A for detailed references).

The capabilities of the model can probably be best understood by examining some typical output data and also comparing the model results with experimental results. Some information available from the model is shown in Table 2 which represents a spray of n-hexadecane into air at 450 K and 4.42 atm. The motion of the fuel spray and air are illustrated in Figure 5. The air velocity was assumed to be a uniform one-dimensional axial flow of 8.54 m/s, while the initial fuel velocity was 20.76 m/s at an angle of 22.5° to the axis (45° cone angle) and a fuel temperature of 311 K. The computed drop size data assuming a Rosin-Rammler distribution are shown on the top line and include the two Rosin-Rammler parameters, $\bar{x}$ and N which specify a size and a width for the distribution, and the Sauter mean diameter (SMD) which is an "average" drop size. By definition, if all drops in the spray were equal in size to the

Table 2. Output of Spray Model

R-R XBAR (UM)	R-R N	CORR. COEF.	SMD
46.8	2.11	0.988	27.76

Fraction of Fuel Evaporated = 0.0279 at Dist. = 0.016
Fraction of Fuel Still in Liquid Phase in Gas Stream = 0.9721
Air Temperature = 435.3 K 323.6 F
Air Velocity = 7.262 M/s, 23.821 FT/S
Fuel Vapor Mass Fraction in Air = 0.5584E-02
Fuel Vapor Mole Fraction in Air = 11426. PPMC
Fuel Vapor Mole Frac Integrated Over SPRRAD = 0.1577E+07 (PPMC)(MM)**2 Where SPR Rad Equals 6.6 MM

Initial Diam	Diam	Time	X Drop	Y Drop	Z Drop	U-Vel	V-Vel	W-Vel	FTEMP	FRAC
5.6	2.6	0.001	0.016	0.002	0.000	8.540	0.000	0.000	433.5	0.010
7.0	5.1	0.001	0.016	0.002	0.000	8.540	0.000	0.000	433.5	0.014
8.8	7.5	0.001	0.016	0.002	0.000	8.541	0.002	0.000	433.5	0.021
11.1	10.3	0.001	0.016	0.003	0.000	8.549	0.007	0.000	433.5	0.032
14.0	13.6	0.001	0.016	0.003	0.000	8.615	0.056	0.000	433.5	0.046
17.6	17.5	0.001	0.016	0.004	0.000	8.923	0.286	0.000	415.6	0.065
22.2	22.2	0.001	0.016	0.005	0.000	9.875	0.996	0.000	396.8	0.089
28.0	28.0	0.001	0.016	0.006	0.000	11.519	2.224	0.000	377.3	0.117
35.2	35.2	0.001	0.016	0.006	0.000	13.305	3.558	0.000	359.9	0.141
44.4	44.4	0.001	0.016	0.006	0.000	14.517	4.463	0.000	346.5	0.152
55.9	55.9	0.001	0.016	0.006	0.000	15.074	4.879	0.000	336.6	0.138
70.5	70.5	0.002	0.016	0.006	0.000	15.545	5.230	0.000	329.0	0.096
88.8	88.8	0.002	0.016	0.006	0.000	15.967	5.546	0.000	323.7	0.046
111.9	111.9	0.002	0.016	0.006	0.000	16.366	5.844	0.000	319.9	0.013
141.0	141.0	0.002	0.016	0.006	0.000	16.737	6.121	0.000	317.2	0.002
177.6	177.6	0.002	0.017	0.007	0.000	17.050	6.354	0.000	315.3	0.000
223.8	223.8	0.001	0.016	0.007	0.000	17.357	6.583	0.000	314.0	0.000
282.0	282.0	0.001	0.016	0.007	0.000	17.629	6.787	0.000	313.1	0.000
355.2	355.2	0.001	0.016	0.007	0.000	17.850	6.952	0.000	312.5	0.000
447.6	447.6	0.001	0.017	0.007	0.000	18.044	7.097	0.000	312.0	0.000
563.9	563.9	0.001	0.016	0.007	0.000	18.227	7.233	0.000	311.7	0.000

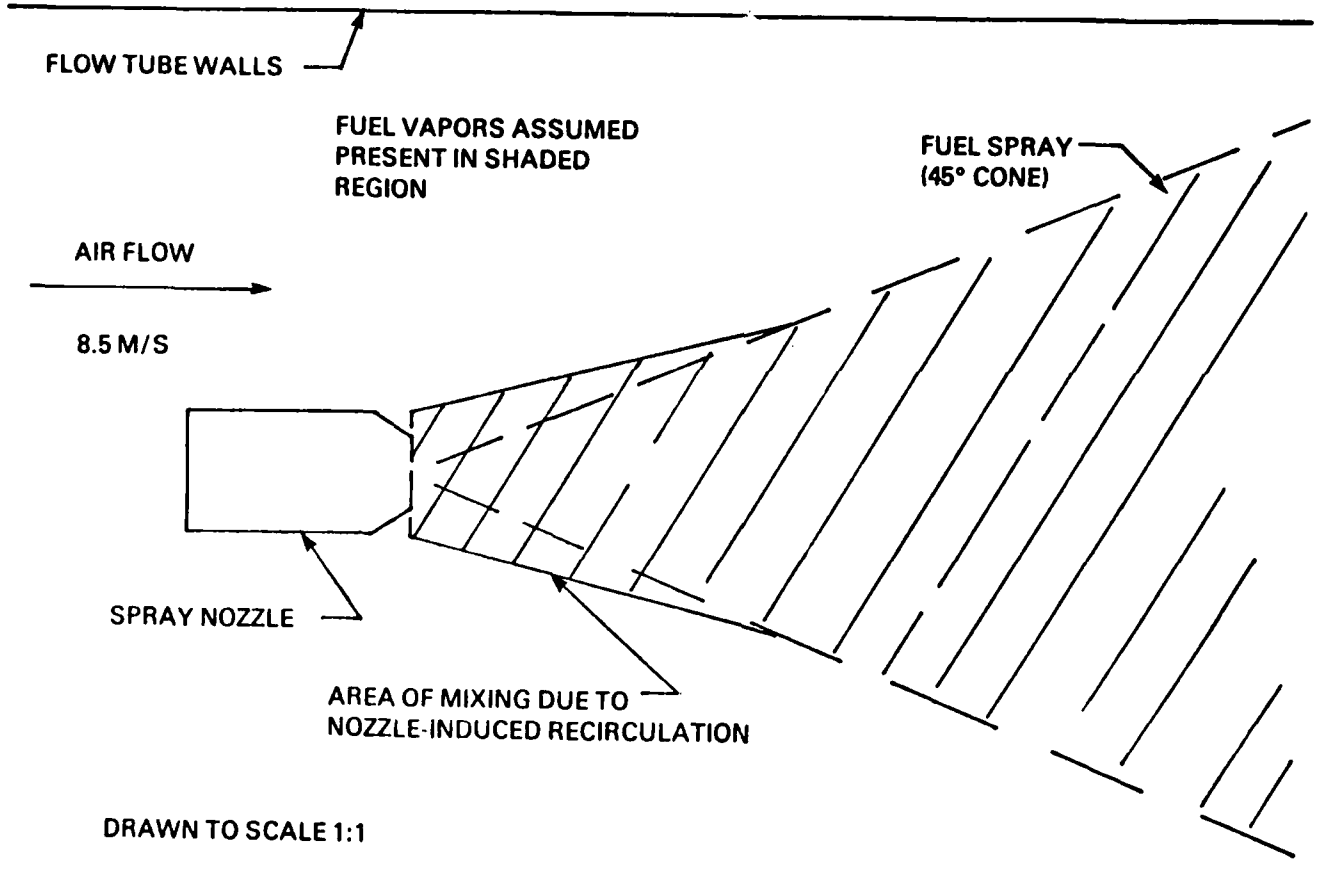

FIGURE 5. ASSUMED AREAS OF FUEL VAPOR CONCENTRATION FOR COMPUTER CALCULATIONS

SMD, than the volume-to-surface-area ratio of the imaginary monodisperse spray would be equal to the actual spray. This ratio is chosen because surface area regulates evaporation rates while the volume indicates the quantity of fuel. The initial drop sizes are shown in column 1, and the initial relative population of drops in each class were computed to correspond exactly to a Rosin-Rammler distribution specified as an input to the program. (Those values were $\bar{x}$ = 52 and N = 1.75 for the example shown). Because of the evaporation and the more rapid deceleration of the small drops (resulting in an increased weighting for the small drops), the size distribution changes at positions downstream from the nozzle. The drop-size distribution no longer corresponds exactly to the Rosin-Rammler distribution, and the degree to which it does fit that distribution is given by the correlation coefficient. For the cases examined, the correlation coefficient has been in excess of 0.97, but under some conditions it could be worse. These distribution parameters are calculated from information shown for individual drop size classes in the lower part of Table 2.

The initial drop sizes (in μm) are shown in Column 1, while the instantaneous drop sizes are shown in column 2 at a distance from the nozzle of 16 mm as shown in column 4 and a time (in seconds) as specified in column 3. When the drops evaporate completely, the time and location are frozen at the point where the drop disappeared and those drops are not used in calculating the Rosin-Rammler parameters. Note that in this example, the model calculates spray data at a given axial distance from the nozzle (X DROP) and not at a given time from injection. The model can also use time as a target. The smaller drops take longer to reach the specified location due to their lower velocity as specified in column 7 by U-VEL in m/s. The smaller drops decelerate to the air stream velocity of 8.54 m/s more rapidly than the large drops. The coordinate system is cylindrical with the axial coordinate being x with velocity u, the corresponding radial components y and v, and the corresponding angular components (assumed zero presently) z and w. Distances are in meters and velocities in meters/seconds.

Note the difference in trajectories and velocities for the different size classes. All non-evaporated drops are at the same axial (X DROP) location, but the radial location (Y DROP) of the small drops is less than the large ones due to their being caught up in the air stream sooner as shown by the axial (U-VEL) and radial (V-VEL)

velocities. The importance of convective effects in heat and mass transfer is obvious from these values, and hence, the shortcomings inherent in quiescent spray models.

The instantaneous drop temperature (FTEMP) is shown in the next to the last column. The initial fuel temperature was 311 K and the "wet-bulb" final steady-state drop temperature is about 433 K at these conditions. The normal boiling point of n-hexadecane is 560 K. Note that the small drops heat up and evaporate almost instantaneously while the "uniformly mixed" temperature of the largest drops is predicted to be close to the initial fuel temperature. Due to finite-rate heat transfer, the surface temperature of the large drops would be higher, but experimental evidence is lacking to predict temperature profiles within the drop. Complex models have been developed to predict these profiles, but they are too cumbersome for this effort and generally lack verification.

Note the importance of modeling the transient nature of the drop before it reaches the steady-state temperature. Of the 21 drop size classes shown in Table 2, only five size classes have reached the steady-state temperature. As the pressure and convective effects are increased, the length for the transient period relative to the steady-state period increases[16]. Thus, models that assume no mass transfer until the drop reaches its steady-state temperature are not representative of many realistic conditions in gas turbines and are insufficient to compare with experimental results generated in this program.

The top part of Table 2 is computed from the data for the individual size classes shown in the bottom of Table 2. The first line of the middle section indicates the fraction of the fuel which has evaporated at a given axial location measured from the nozzle exit (in meters), and the second line indicates the fuel remaining in liquid form. The fuel vaporization absorbs heat from the surrounding air in the spray cone and the resulting air temperature is shown on the third line. Momentum transfer from the spray to the air is not included in this model, but the effect of lowered temperature on increasing air density and reducing air velocity in the spray cone is included, as shown on the fourth line. The quantity of vaporized fuel is calculated and assumed to be uniformly distributed at a given axial location over the region shown in Figure 5. The fuel vapor concentration expressed as a mass fraction is shown on the fifth line and as mole fraction on the sixth line. In order to compare these values with those measured

by the probe, the mole fraction integrated over a cross-section of the spray cone at a given axial location is given in line seven.

In addition to the drop array data just discussed, the model has been used to examine the steady-state "wet-bulb" temperature and the quiescent, evaporation rate of the fuel, which are both independent of drop size, as a function of air pressure and temperature. At atmospheric pressure, the steady-state drop temperature is lower than the normal boiling point due to the cooling effect of energy used in vaporizing the fuel. As the pressure increases, the boiling point increases and the steady-state temperature increases. Obviously the fuel and air properties are important in determining this temperature. Steady-state temperatures for three normal paraffins - octane (C_8H_{18}), dodecane ($C_{12}H_{26}$), and hexadecane ($C_{16}H_{34}$) - were calculated over a range of conditions with the results as shown in Figures 6 to 8. At low air temperatures, the drop temperatures converge to the air temperature. As the air temperature increases, the increased vaporization cools the drop below the air temperature, but increased pressure markedly increases the allowable drop temperature. The spontaneous nucleation temperature for water indicated in the figures is discussed in a later section. The critical pressure for hexadecane is 1421 kPa (14.02 atm) and for dodecane 1820 kPa (17.96 atm), and data are not shown for pressures higher than the critical pressure.

Droplet evaporation follows a D-squared law which relates the drop diameter D to the initial size D_o and the time t by[17].

$$D^2 = D_o^2 - \lambda t \qquad (1)$$

where the proportionality constant λ is the evaporation constant. The mass transfer rate of fuel from the drop, $\dot{m}_F$, at quiescent conditions is related to the evaporation constant by,

$$\dot{m}_F = (\pi/4)\,\lambda\,\rho_F\,D \qquad (2)$$

where ρ_F is the fuel density. The evaporation constant is increased by convection, with a correction factor given by Frossling[18] for cases where heat transfer rates are controlling of,

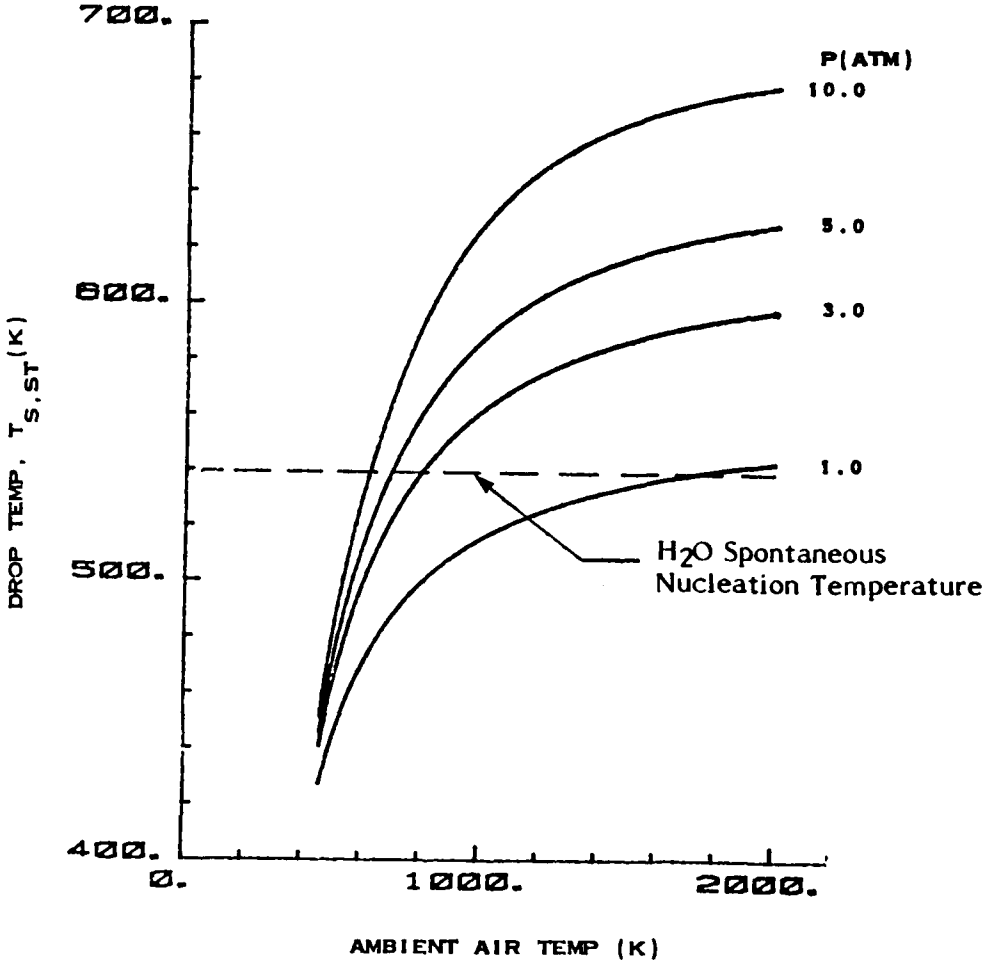

FIGURE 6. COMPUTED STEADY STATE DROP SURFACE TEMPERATURE FOR N-NEXADECANE

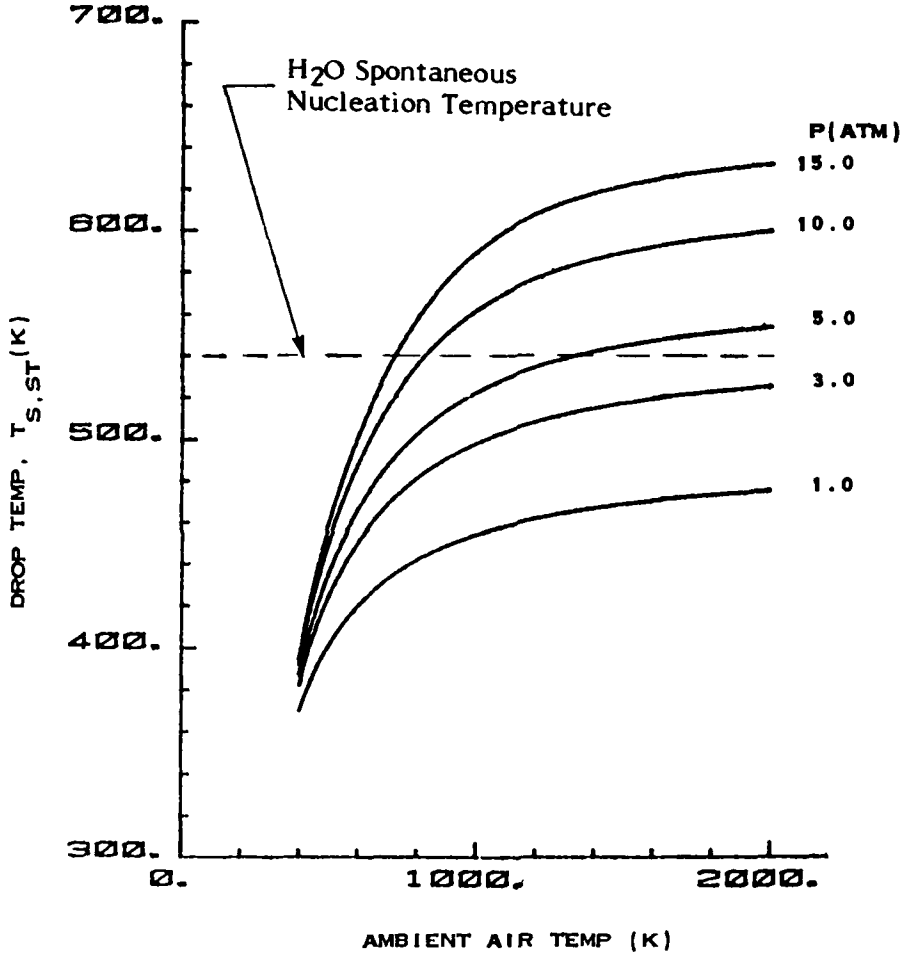

FIGURE 7. COMPUTED STEADY STATE DROP SURFACE TEMPERATURE FOR N-DODECANE

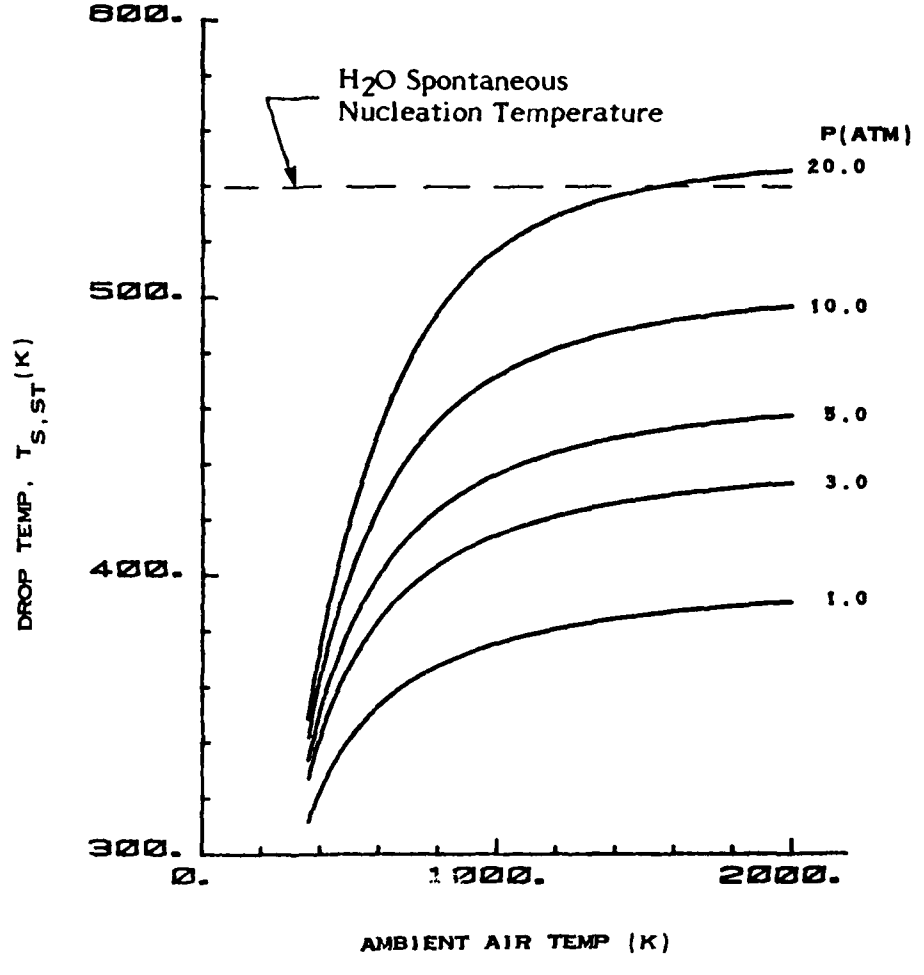

FIGURE 8. COMPUTED STEADY STATE DROP SURFACE TEMPERATURE FOR N-OCTANE

$$\lambda_{Conv.} = \lambda_{Quies.} (1 + 0.276\, Re_D^{0.5}\, Pr_g^{0.33})$$

where Re_D is the Reynolds number of the gas relative to the drop and Pr_g is the Prandtl number of the gas.

In summary, the computer model, while not completely comparable with experimental results in its present form, does provide insight into much of the thermodynamics affecting drop evaporation. It also shows quantitatively how the smaller drops are caught up in the air stream much more quickly than the larger ones. It also indicates the importance of modeling evaporation during the transient heat-up phase, particularly for realistic sprays at high pressures and Reynolds numbers. It shows the effect of air pressure on the steady-state drop temperature, and how increasing air pressure leads to increased drop temperatures which enhance the probability of initiating microexplosions.

III. EXPERIMENTAL PROCEDURES AND RESULTS

Experimental results include the effects of fuel properties, nozzle pressure drop, air temperature, and air pressure on the initial atomization of fuels and the change in drop-size distribution during evaporation. The properties of the fuels used in these tests are given in Table 1. Most of these tests were comparative studies for the fuels emulsified with 20 percent water and the same fuels in non-emulsified or "neat" form. The 20 percent emulsion was chosen to accentuate the differences between the emulsified and neat fuel. The changes in the experimentally determined drop-size distributions with distance from the nozzle are compared with values computed from the spray model. The spray model was also used to compute drop temperatures to help interpret the experimental results. Experimental results are also reported for the two-phase probe measurements of the comparative vaporization rates of emulsified and neat fuels.

3.1 Spray Drop-Size Measurements

3.1.1 General Characteristics of Sprays

A comparison of the spray data on centerline and at the edge of the spray is instructive in understanding the features of fuel sprays from swirl nozzles. Typically, the attenuation of the laser beam of the drop sizer by the edge of the spray is about comparable to that for the beam passing through the center of the spray, although the path length through the edge is much shorter than the center. This can be understood by considering that in swirl atomizers, the majority of the fuel goes into larger drops along the outer edge of the cone, with an inner core composed of smaller drops at a much lower density. Figure 9 shows a comparison of the characteristic drop sizes, represented by the Sauter mean diameter (SMD), measured along the edge of the spray and the centerline. These data are for a nozzle similar in design but larger in capacity than for other data in this report, but the nozzle spray pattern is representative. These results are consistent with the above description of the spray in that near the nozzle the measurements are close to the same place (considering the 9 mm diameter of the measuring beam), and SMD's are similar, while further downstream the edge measurements are weighted towards the large drops and the centerline measurements are more representative of the overall distribution. Further evidence for this view of

Table 1. Some Properties of Fuels Used

Jet A (AL-10112F)

Viscosity at 40°C 1.72 cS
Specific Gravity at 60°F 0.8049
Heat of Combustion 46.904 MJ/kg
Hydrogen Content 14.15%
Flash Point: 355K
Boiling Point Distribution (GC)

Wt% Off	Deg K
0.1	436
10	468
20	484
30	490
40	494
50	502
60	506
70	510
80	518
90	527
99	548
100	796

20% H_2O/2% Surfactant/78% Jet A (AL-10112F)

Viscosity at 40°C 4.47 cS
Specific Gravity at 60°F 0.8618

Hexadecane (95% purity)

Viscosity at 40°C 2.98 cS
Specific Gravity at 60°F 0.7774
Boiling Point (nominal) 560K

20% H_2O/2% Surfactant/78% Hexadecane

Viscosity at 40°C 5.55 cS
Specific Gravity at 60°F 0.8249

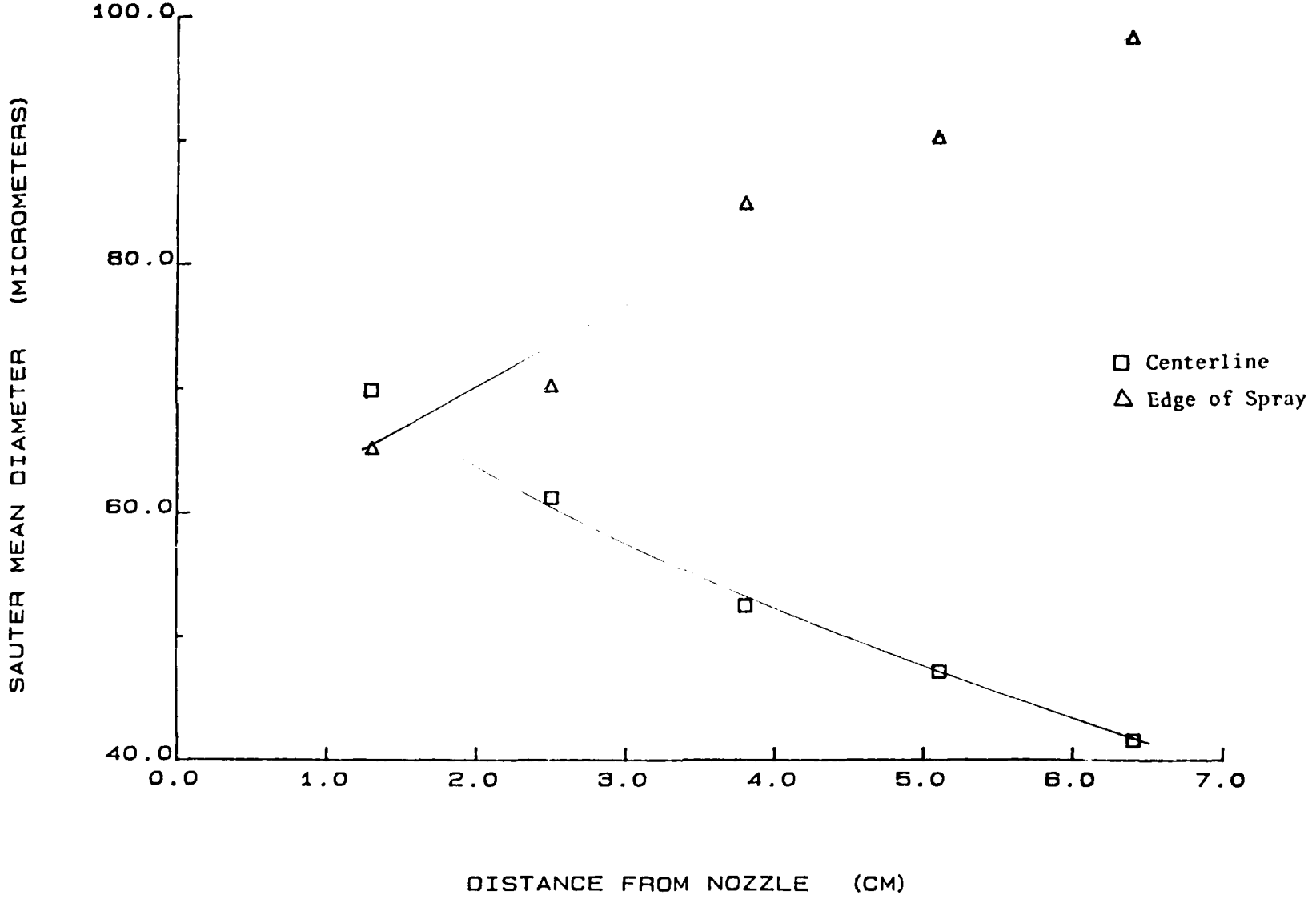

FIGURE 9. COMPARISON OF SMD ON CENTERLINE AND EDGE OF SPRAY

the spray structure is shown in Figure 10 which compares the Rosin-Rammler N parameter for the edge and centerline measurements. The N parameter is defined by,[19,20]

$$R = \exp(-((d/\bar{X})^N)) \quad (1)$$

where R is the cumulative volume fraction of drops larger than size d, $\bar{X}$ is a size parameter, and N measures the width of the distribution. Large values of N imply narrow distributions and vice versa. Thus, Figure 10 shows that close to the nozzle, the measurements agree, as they should, while further from the nozzle the edge measurements show a much narrower distribution consisting of just the larger drops (from Figure 9), while the distribution through the centerline remains relatively broad since both larger drops on the edges and smaller drops in the center of the cone are being sampled. For completeness, it should also be noted that the SMD can be computed from the two Rosin-Rammler parameters by[20]

$$SMD = X/\Gamma(1-1/N) \quad (2)$$

where Γ is the gamma function.

Further evidence of the non-homogeneity of the spray size distribution is shown in Figure 11 for a 5.68 liter/hr (1.5 gph) 80° hollow cone nozzle. This figure shows the SMD and N values at a fixed axial distance of 25 mm at different distances from the centerline. Again the measured size distribution through the spray is the smallest in average size and broadest in distribution through the center of the spray, while the edges are more monodisperse and much larger in average size.

Several other comments can be made concerning the trends in SMD and N values as a function of distance from the nozzle. Returning to Figure 9, the SMD's on the centerline decrease in going downstream from the nozzle. This is probably due mostly to the fact that close to the nozzle, the laser beam samples more of the larger drops along the top and bottom edges of the spray, while further downstream it is weighted more heavily towards the smaller drops in the center of the spray cone. Two other effects contribute to this trend. First, when sampling very close to the nozzle, ($\leq$ 12 mm) the SMD is larger due to the fact that atomization is not complete.

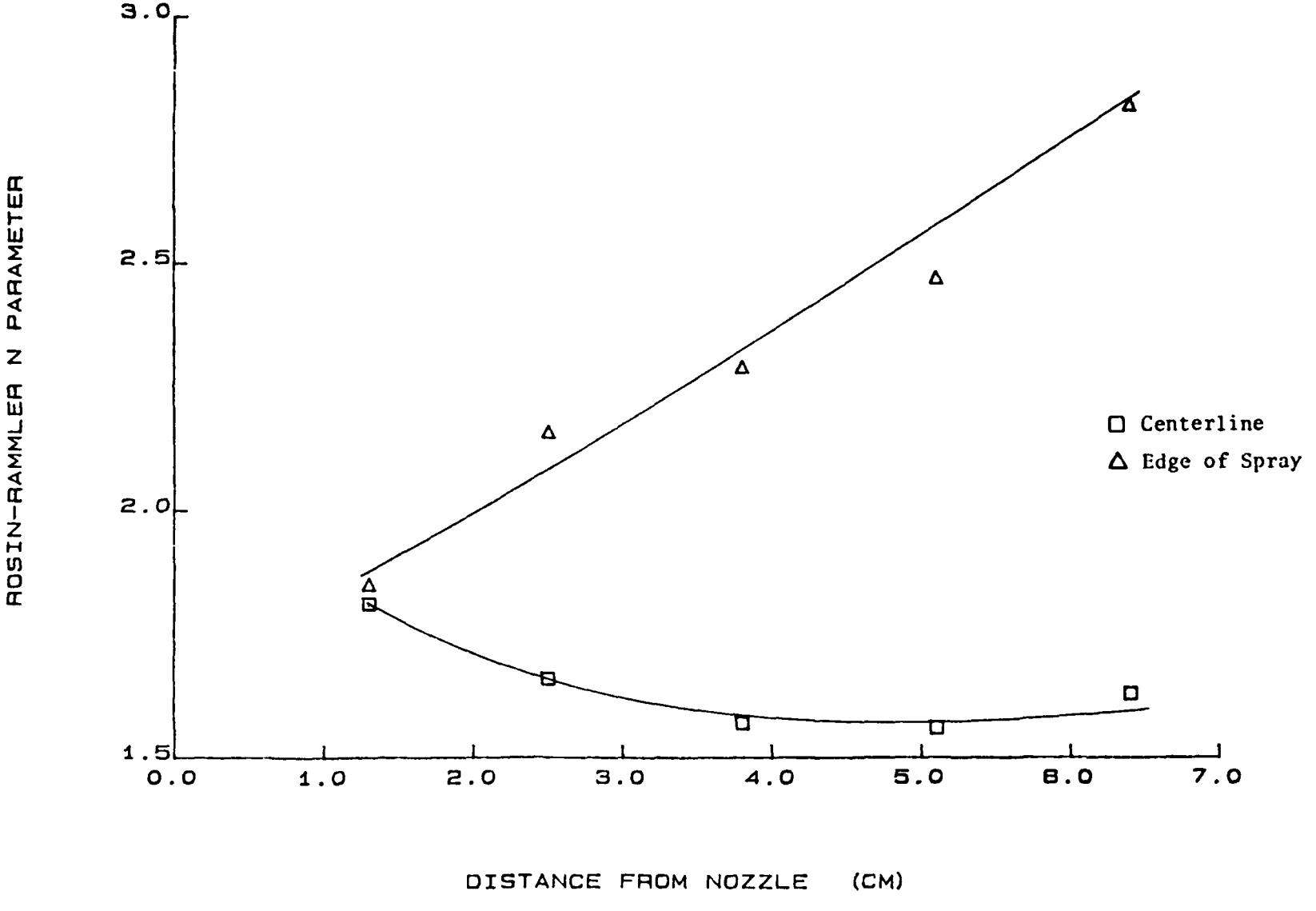

FIGURE 10. COMPARISON OF ROSIN-RAMMLER N PARAMETER ON CENTERLINE AND EDGE OF SPRAY

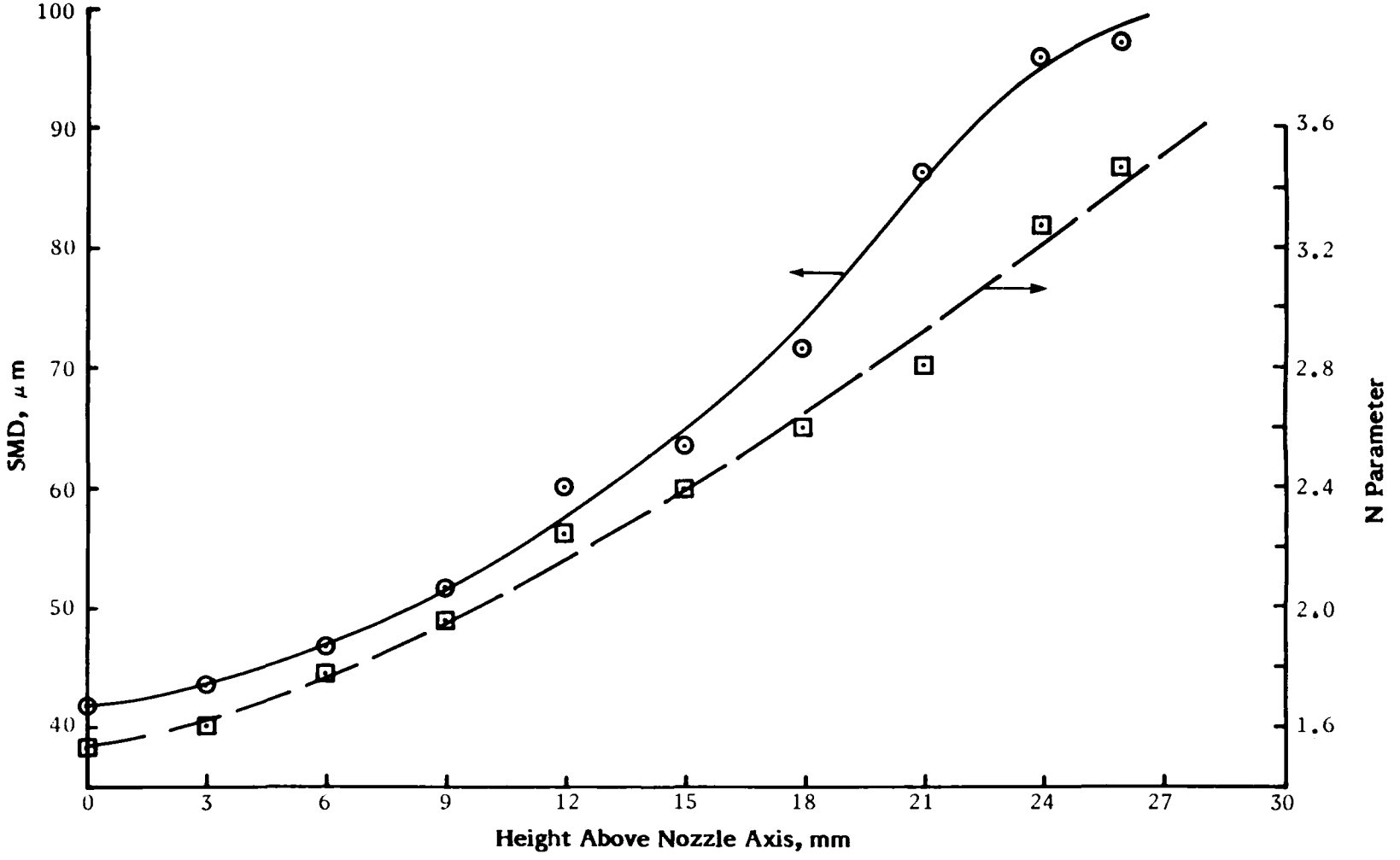

FIGURE 11. CHANGE IN DROP-SIZE DISTRIBUTION WITH DISTANCE FROM CENTERLINE
3.78 liter/hr, 80° hollow cone, ΔP=689 kPa

Second, in the first few centimeters downstream of the nozzle the small drops slow down to the air stream velocity more rapidly than the large drops (see Table 2), increasing their relative population in the laser beam sampling region. Thus, in a non-evaporating spray, the SMD decreases over the first 5 to 10 cm and then levels out.

Evaporation of the fuel drops has some interesting effects on SMD and the N parameter. If the spray were monodisperse (single-sized drops) then the SMD would decrease with evaporation. Sprays from pressure atomizers are very polydisperse (broadly distributed in size) with N parameters on the order of 2. The effect of evaporation is to preferentially evaporate the smaller drops, in accordance with the d^2-law, reducing the width of the distribution and increasing the average size for those drops remaining. Thus, at elevated temperatures, it is expected that in going downstream from the nozzle, the SMD and N values should both increase through the early stages of evaporation. This is predicted by the computer model and has been observed experimentally, as will be shown in the following results.

Another way of examining the fuel distribution from a spray nozzle is to measure the quantity of fuel sprayed at different angles relative to the nozzle axis. The results of such a test for the 3.79 liter/hr, 45° hollow-cone nozzle are shown in Figure 12 for the cumulative fraction of fuel within different cone angles measured from the centerline. The fuel fraction at a given angle is proportional to the derivative of the curve, so the inner 10° on each side of the nozzle axis (20° total included angle) contains little fuel, while the majority falls between 12° and 22° from the axis. The nozzle is specified at 45° total cone angle, corresponding to 22½° from the axis, and about 86 percent of the fuel falls within the 45° cone.

Pressure drop across the nozzle has a significant effect on the average size and width of the spray distribution as shown in Figure 13. Increasing pressure drop causes a reduction in SMD and a broadening of the size distribution. Also the SMD increases slightly with viscosity, the viscosities of the solvent, Jet-A, and the emulsion at 40°C being 1.00 cS, 1.72 cS, and 4.47 cS, respectively.

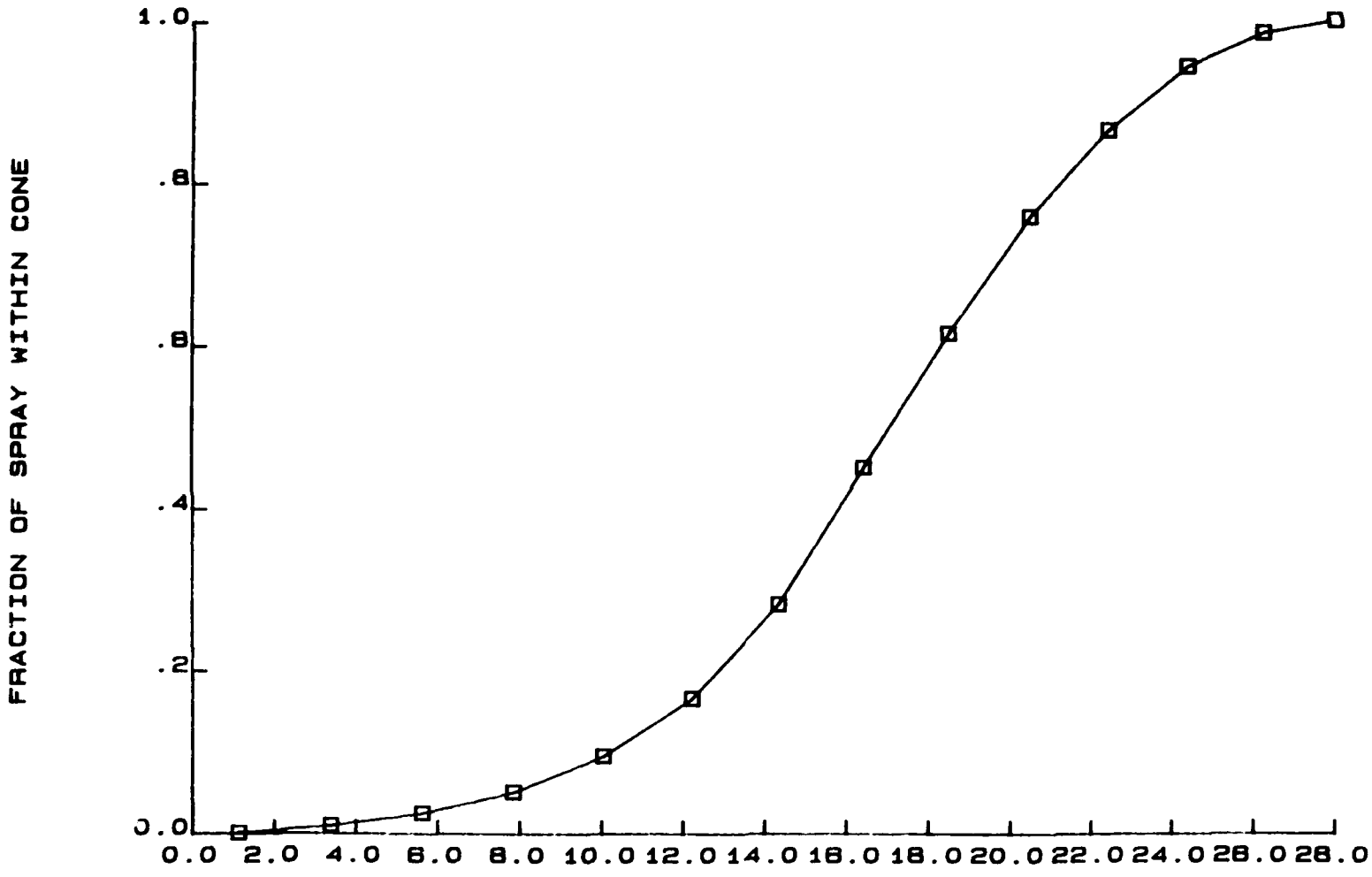

FIGURE 12. ANGULAR DISTRIBUTION OF CUMULATIVE FUEL FRACTION,
50 mm from 3.79 liter/hr 45° Hollow Cone Nozzle

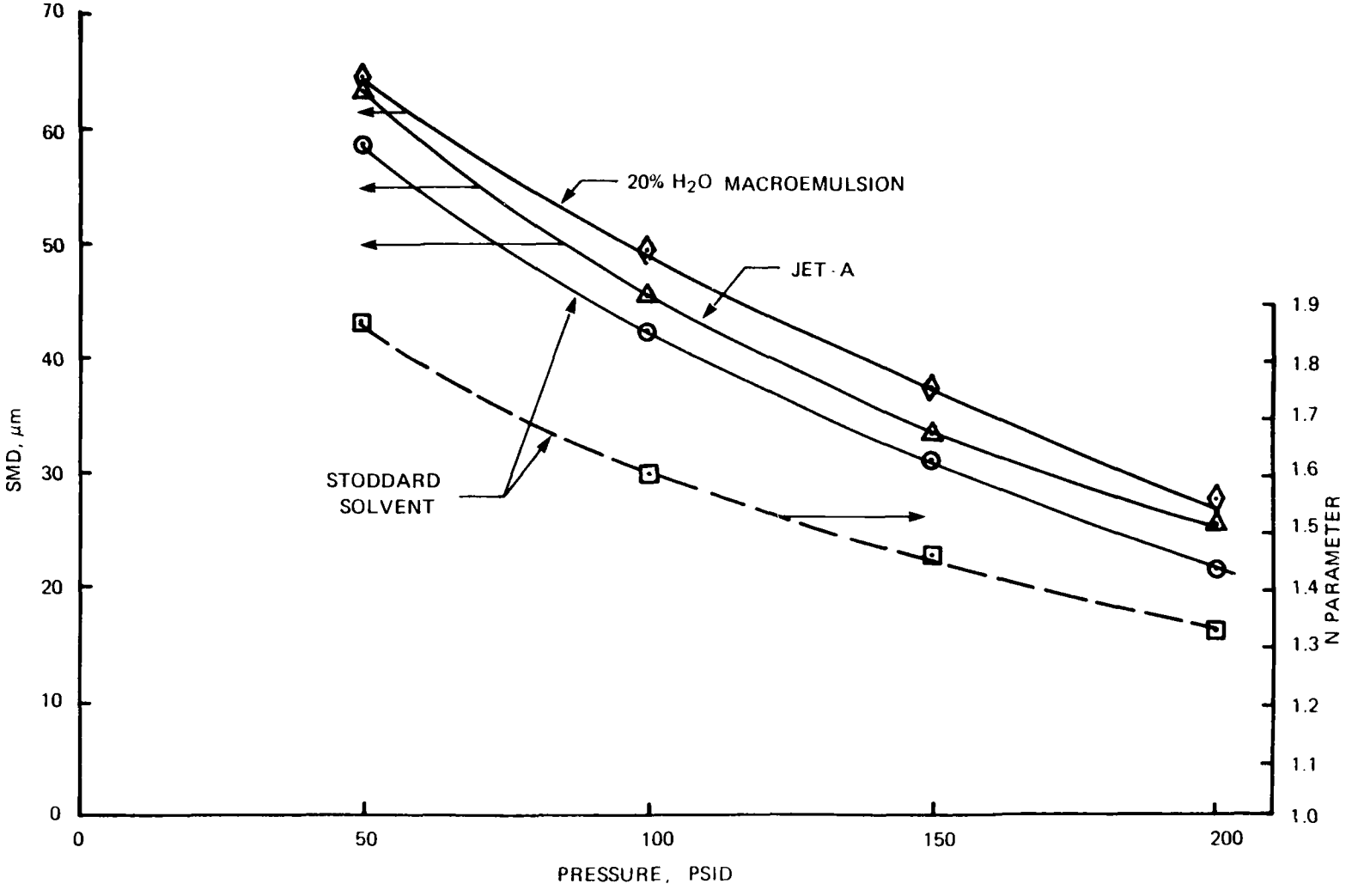

FIGURE 13. EFFECT OF INJECTION PRESSURE ON SMD; JET-A, WATER/JET-A MACROEMULSION, CALIBRATION FLUID

3.1.2 Effect of Elevated Temperature and Pressure on Size-Distributions for Emulsified and Neat Jet-A

One of the goals of this program was to study the effects of emulsification on the evaporation of jet fuel. The effects of air temperature at constant air pressure on the fuel spray drop-size distribution shown in Figures 14-18. Compared with non-evaporating (relatively) sprays at room temperature, it can be seen that the SMD increases during the evaporation process and the higher the temperature the more rapid the increase. The N values also increase going downstream from the nozzle. Both of these trends are in agreement with the idea previously discussed that the preferential evaporation of the smaller drops leads to a narrower distribution and increased average size for the remaining drops. Both the SMD and N values are affected by errors caused by beam steering, and these errors limit how far downstream measurements were reported at temperatures of 547 K and above. The N values are affected more strongly than the SMD's. These errors tend to increase SMD and decrease N from their actual values. The initial atomization of emulsified and neat jet-A is similar for each of these conditions. Differences in initial drop sizes are probably due mainly to differences in pressure drop across the nozzle and differences in temperatures of the fuels. At 450 K, the emulsified and neat fuels show similar trends. At 589 K and 644 K, the SMD's for the emulsified and neat fuel diverge with the emulsified fuel producing smaller drops downstream of the nozzle. All of the SMD data shown in Figures 14-18 are compared in Figure 19a, normalized to make comparisons easier. The 450 K and 506 K data are normalized to the average of the first two data closest to the nozzle. At the higher temperatures of 589 K and 644 K, the evaporation is so rapid that only the first points closest to the nozzle are used to normalize the data. The normalized SMD's at a fixed distance of 16 mm from the nozzle are shown as a function of temperature in Figure 19b, with the emulsified fuel compared with the neat fuel. Figures 19a and 19b show clearly the similarity of the trends for drop-size distributions during evaporation at the lower temperatures and the divergence at the elevated temperatures with the emulsified fuels producing smaller drops during the evaporation process. Similar trends were observed previously with a larger capacity (11.4 liters/hr) nozzle.[21]

There are at least two possible explanations for the smaller drop sizes for the emulsified fuel relative to the neat fuel at the higher temperature conditions. One

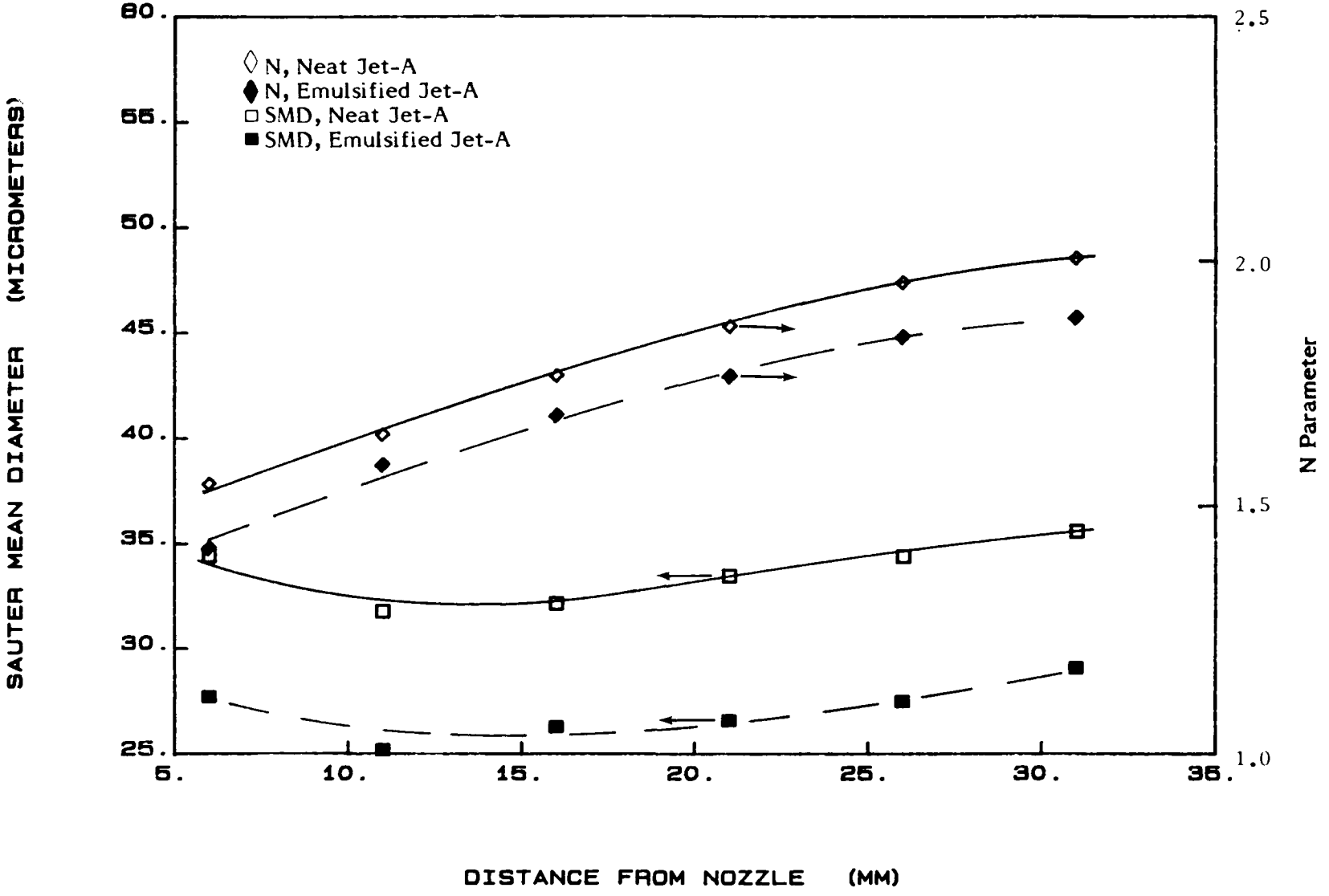

FIGURE 14. CHANGE OF SMD AND N WITH DISTANCE FROM THE NOZZLE, JET-A 450 K, 448 kPa

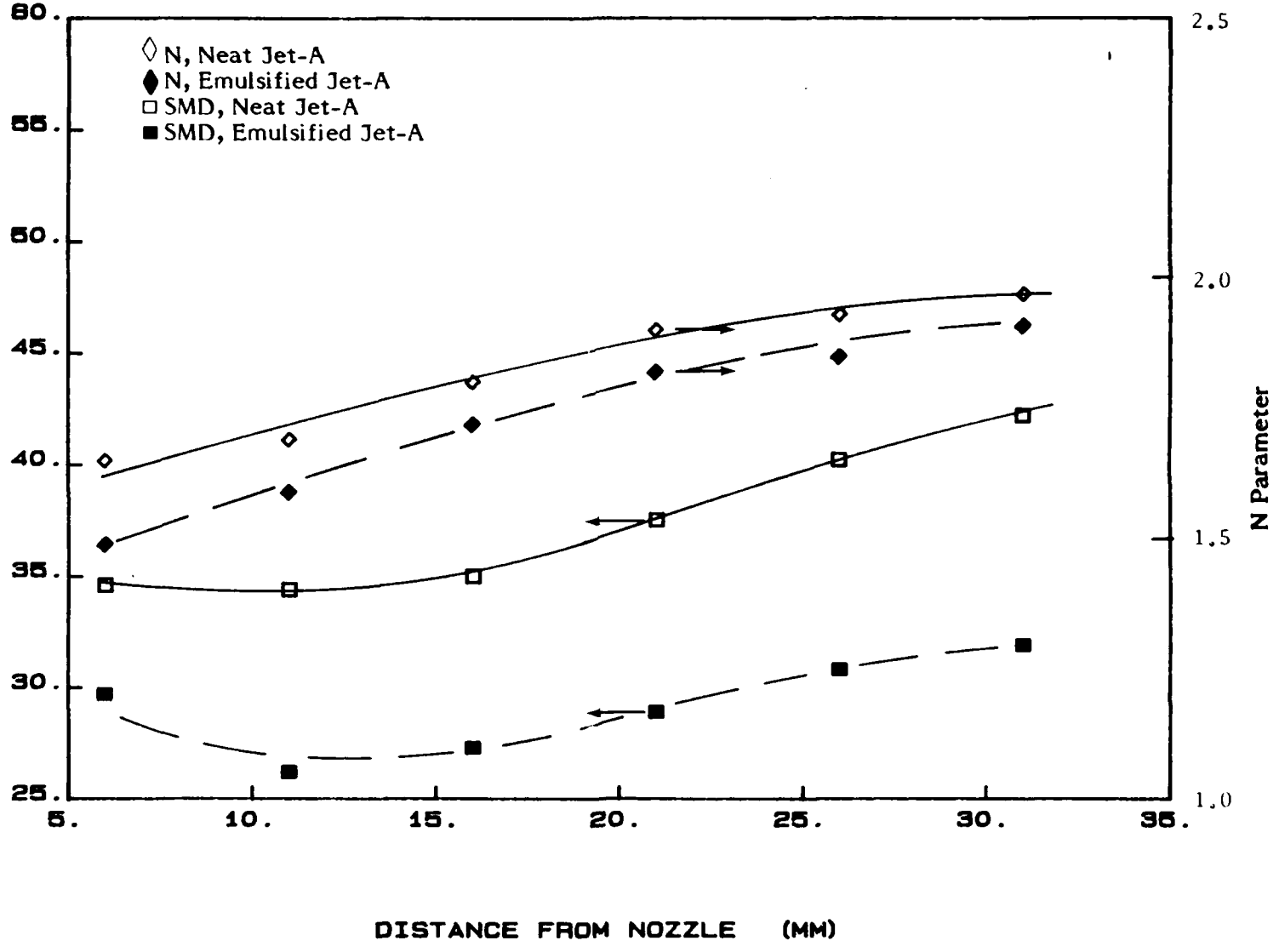

FIGURE 15. CHANGE OF SMD AND N WITH DISTANCE FROM THE NOZZLE, JET-A 506 K, 448 kPa

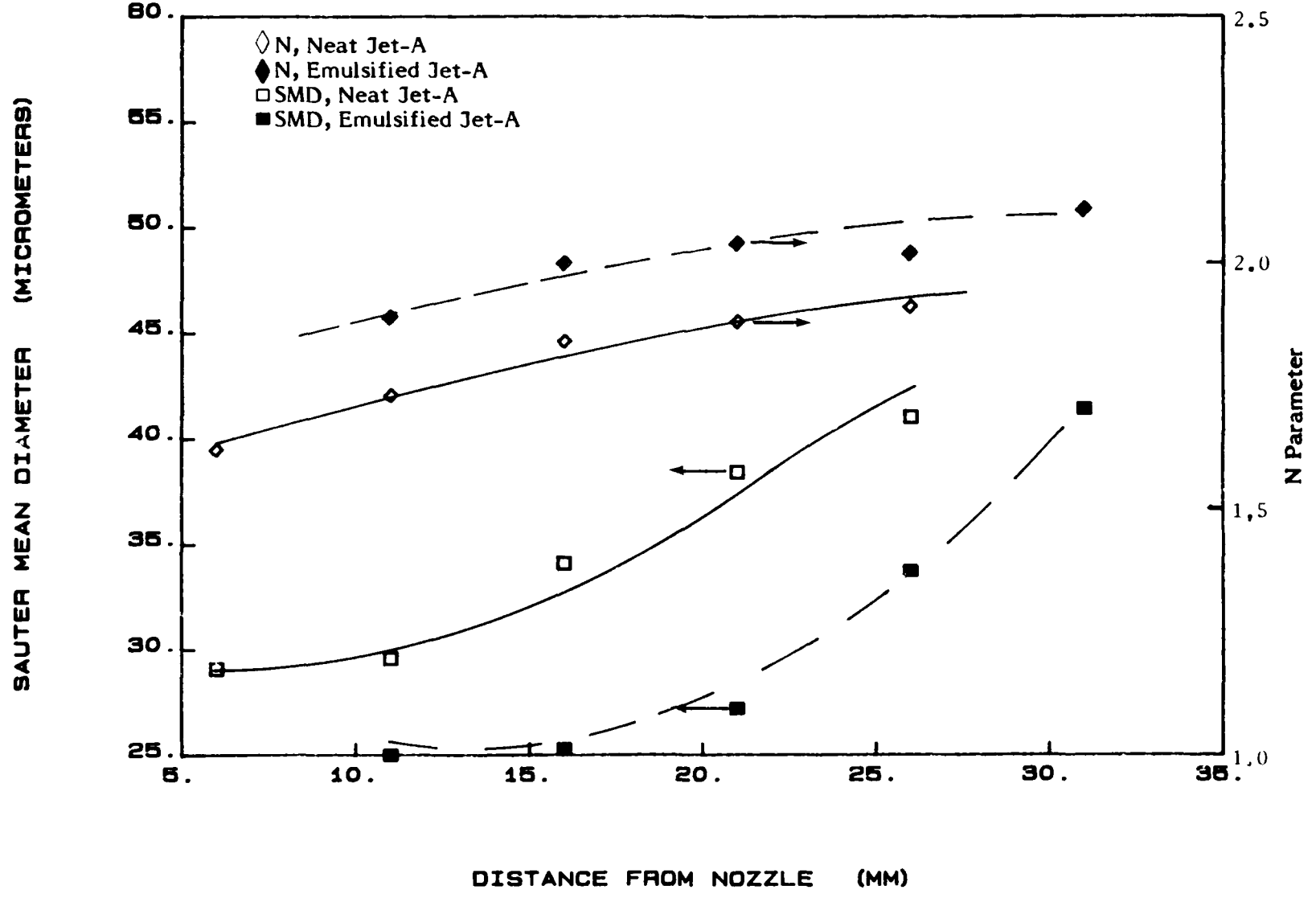

FIGURE 16. CHANGE OF SMD AND N WITH DISTANCE FROM THE NOZZLE, JET-A 547 K, 448 kPa

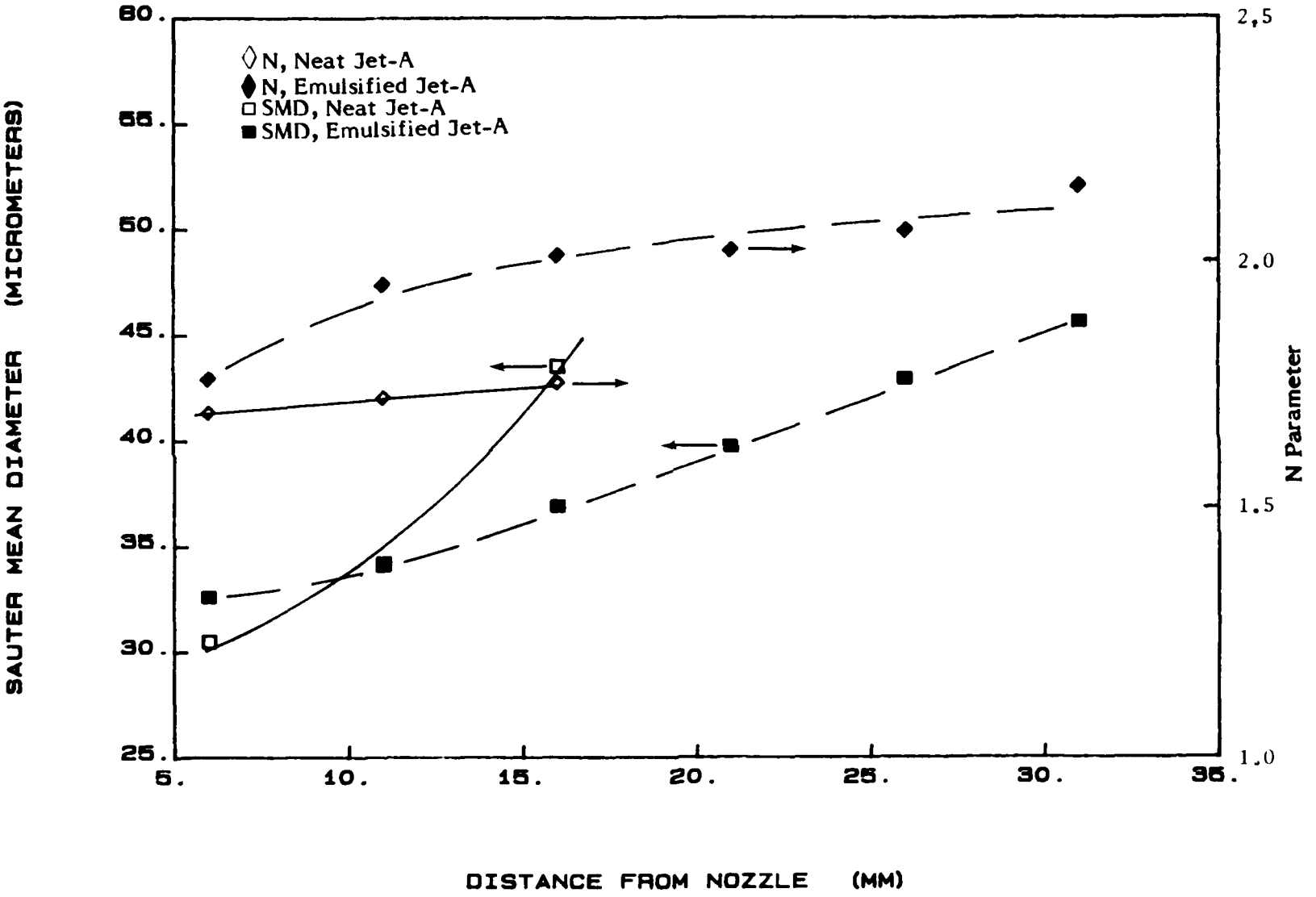

FIGURE 17. CHANGE OF SMD AND N WITH DISTANCE FROM THE NOZZLE, JET-A 589 K, 448 kPa

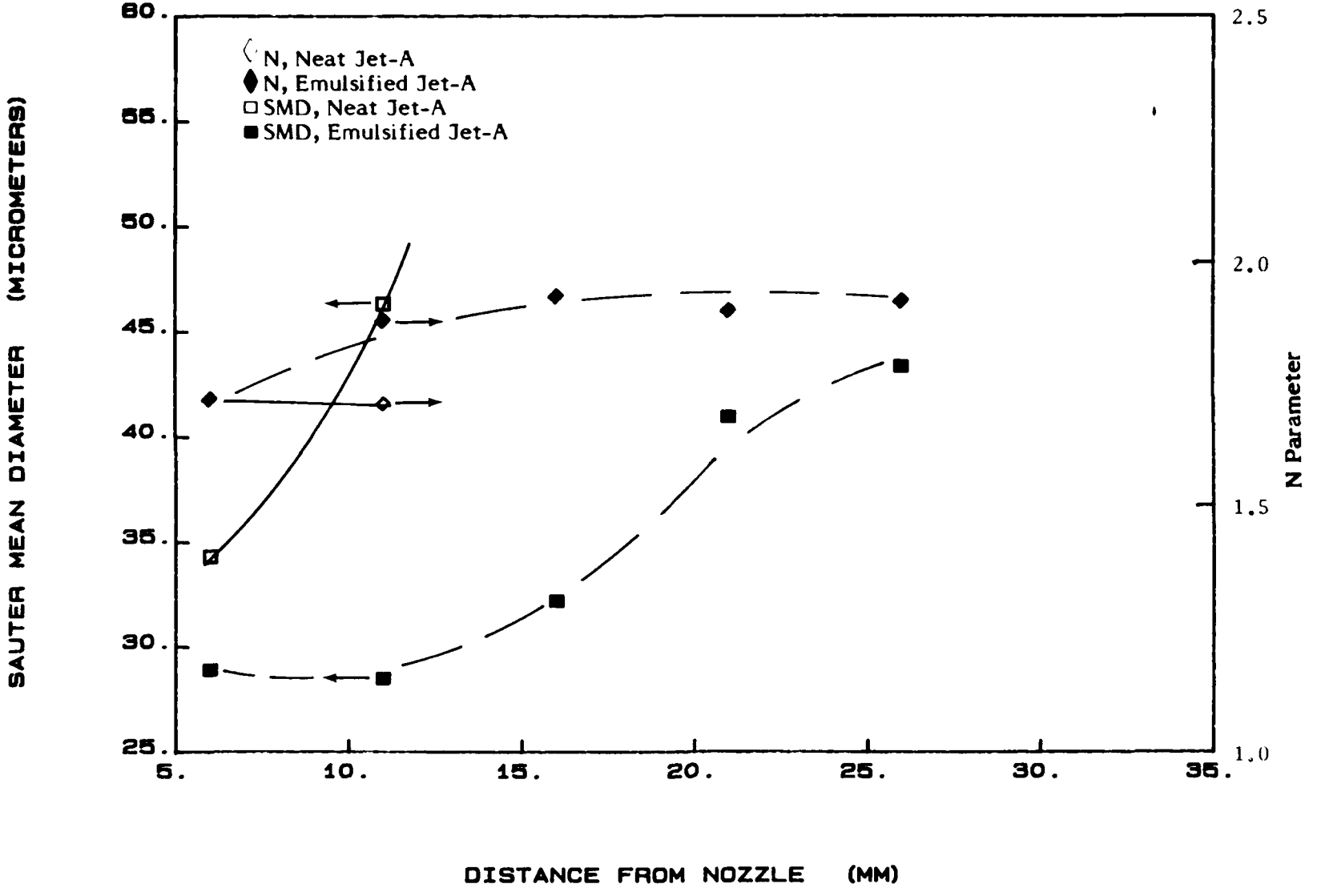

FIGURE 18. CHANGE OF SMD AND N WITH DISTANCE FROM THE NOZZLE, JET-A 644 K, 448 kPa

Open Symbols: Neat Jet-A

Closed Symbols: Emulsified Jet-A

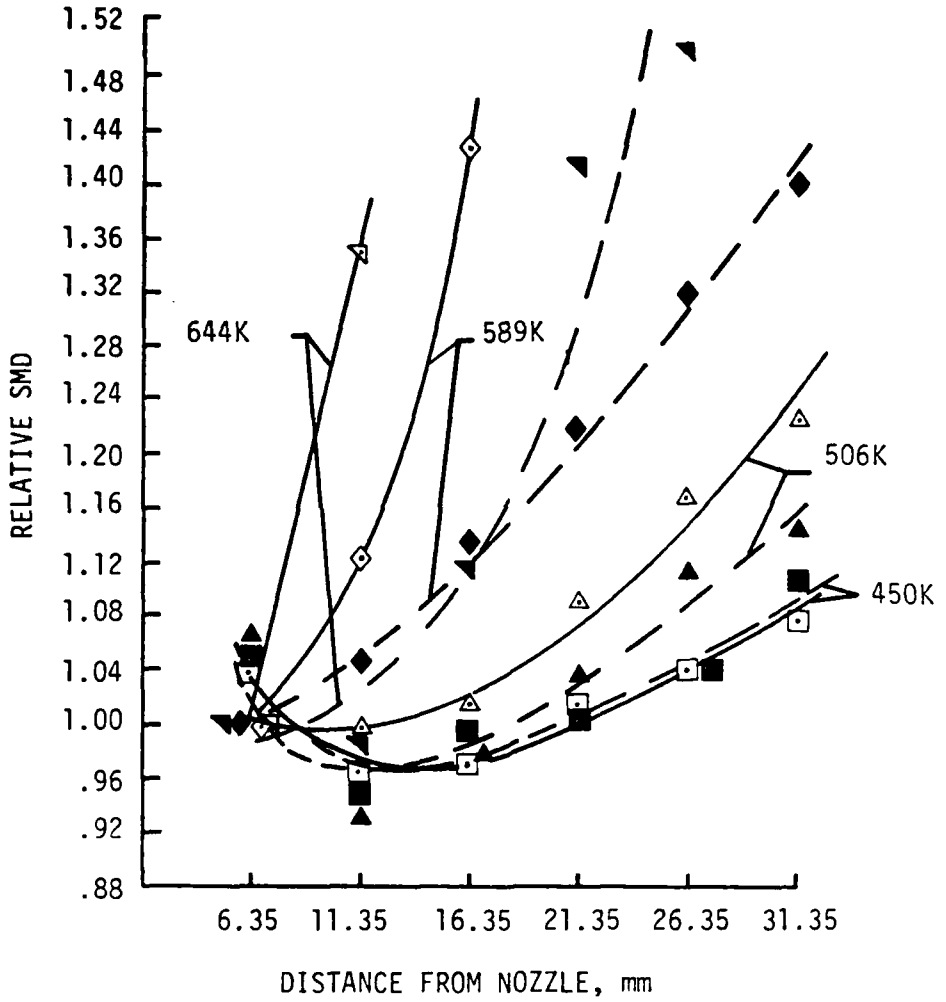

FIGURE 19a. EFFECT OF AIR TEMPERATURE ON ATOMIZATION AND EVAPORATION-RELATIVE SMD VERSUS DISTANCE FROM NOZZLE
3.8 liters/hr, 45°HC DELAVAN NOZZLE, 8.5 m/s, 448 kPa

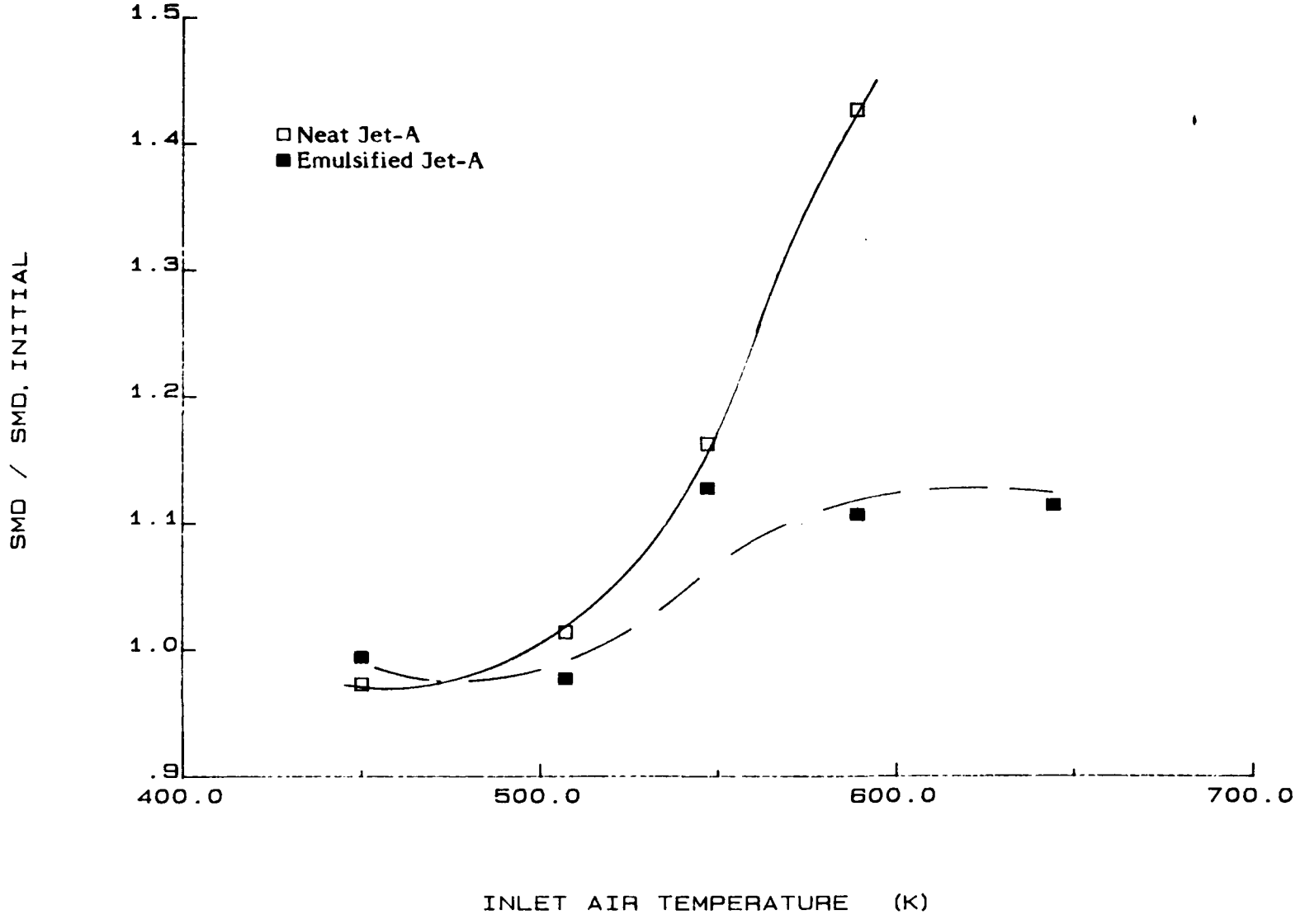

FIGURE 19b. EFFECT OF AIR TEMPERATURE ON SMD OF EMULSIFIED AND NEAT JET A AT 16 mm, AIR PRESSURE 448 kPa

possible explanation for reduced drop sizes for emulsified fuels relative to neat fuels is microexplosions, as previously discussed. The boiling points of many fuels are sufficiently high that water could reach its spontaneous nucleation point and cause the emulsified drop to explode if the water is not transported to the surface fast enough and allowed to evaporate. The spontaneous nucleation temperature of water in hexadecane has been estimated by Avedisian to be about 539 K,[22,23] and varies only slightly with pressure. This is an upper limit for clean, degassed water in hexadecane to begin boiling; the actual boiling point for these emulsions could occur within the range of 373 K to 539 K depending on the presence of bubbles or particles within the water, and particularly at the interface between the water and the fuel.

A second possible explanation for the reduced average drop sizes of the emulsified fuel relative to the neat fuel is that the heat of vaporization of water is about eight times that of jet-A, although the boiling point of water (373 K) is significantly less than that of the "average" (50 percent) boiling point of jet-A (502 K). The higher heat of vaporization of water reduces evaporation rates for emulsified fuels, but the lower boiling point increases it. If the net evaporation rate of the emulsified fuels is reduced relative to the neat fuels, then trends such as those shown in Figures 14–19 could result.

Another similar set of experiments was performed with emulsified and neat jet-A in which the air temperature was held constant and the air pressure was varied. Law[24] has suggested that an increase in air pressure at constant temperature should favor the occurrence of microexplosions because the steady state drop temperature increases with air pressure, as was shown in Figures 6-8. Thus, for a fixed air temperature of 547 K, the spray drop sizes were determined as a function of distance from the nozzle at pressures of 165 kPa shown in Figure 20, 207 kPa in Figure 21, 345 kPa in Figure 22, and 448 kPa in Figure 23. At the lowest air pressure, the emulsified fuel shows larger drops throughout the evaporation process, but at higher pressures, which raise the steady state drop temperature, the SMD's further downstream of the nozzle are smaller for the emulsified fuels. These trends are also evident in Figure 24a in which the SMD's for Figures 20-23 are all shown together. Another way of examining the pressure dependence is to compare the SMD's at a fixed distance from the nozzle as a function of pressure. Such a comparison for a distance of 26 mm is shown in Figure 24b, which indicates the SMD's after normalization to the

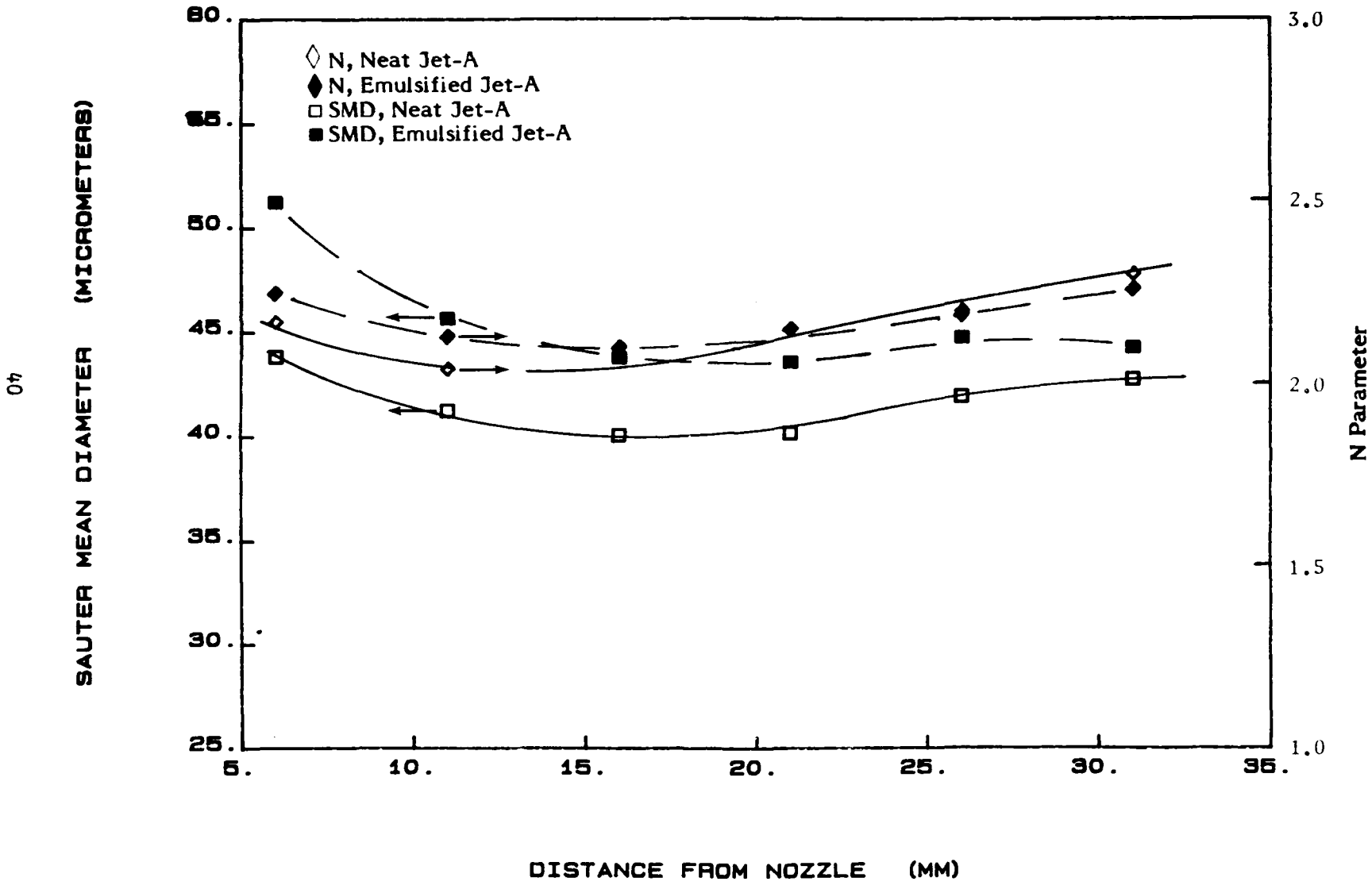

FIGURE 20. CHANGE OF SMD AND N WITH DISTANCE FROM THE NOZZLE, JET-A, 547 K, 165 kPa

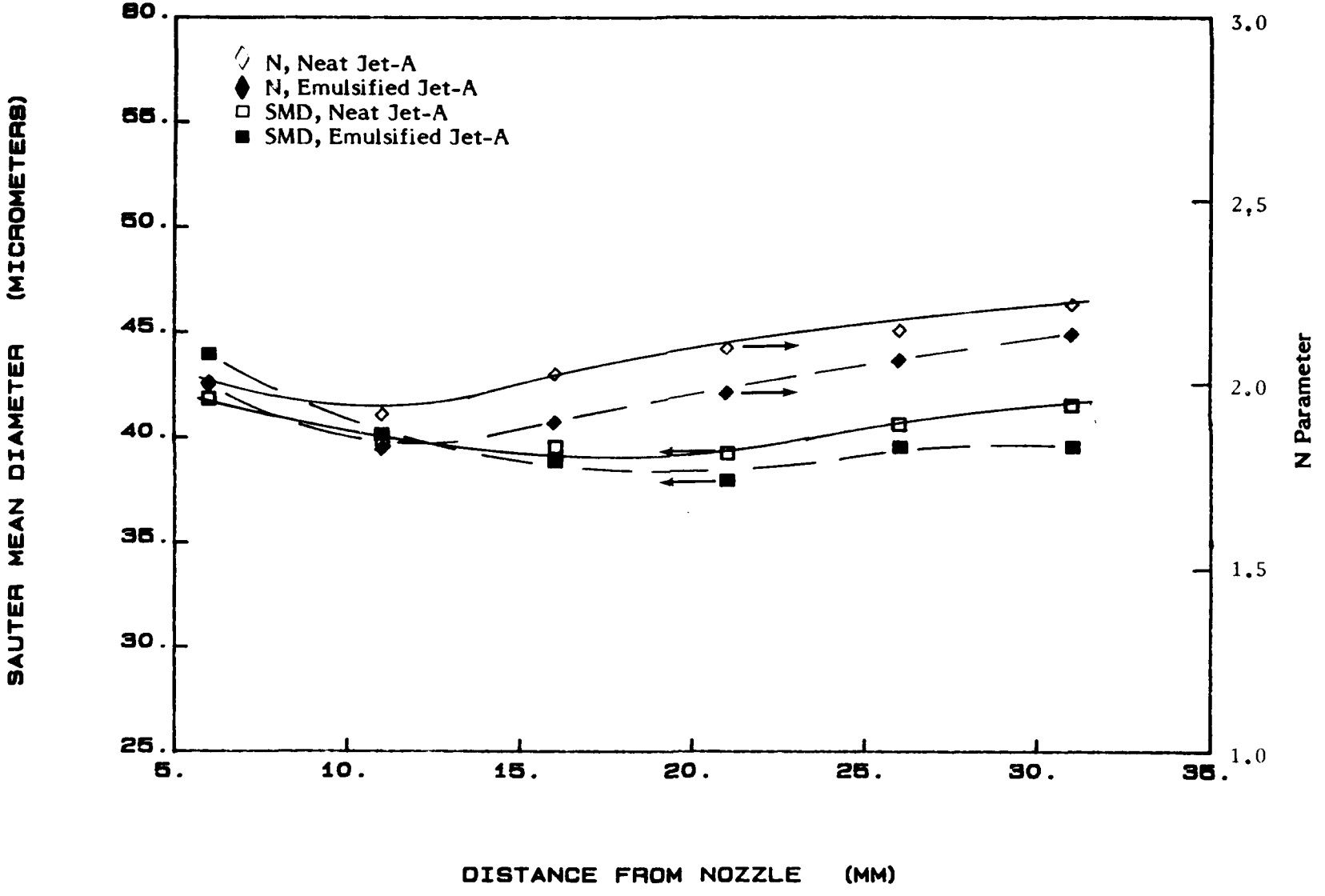

FIGURE 21. CHANGE OF SMD AND N WITH DISTANCE FROM THE NOZZLE, JET-A, 547 K, 206 kPa

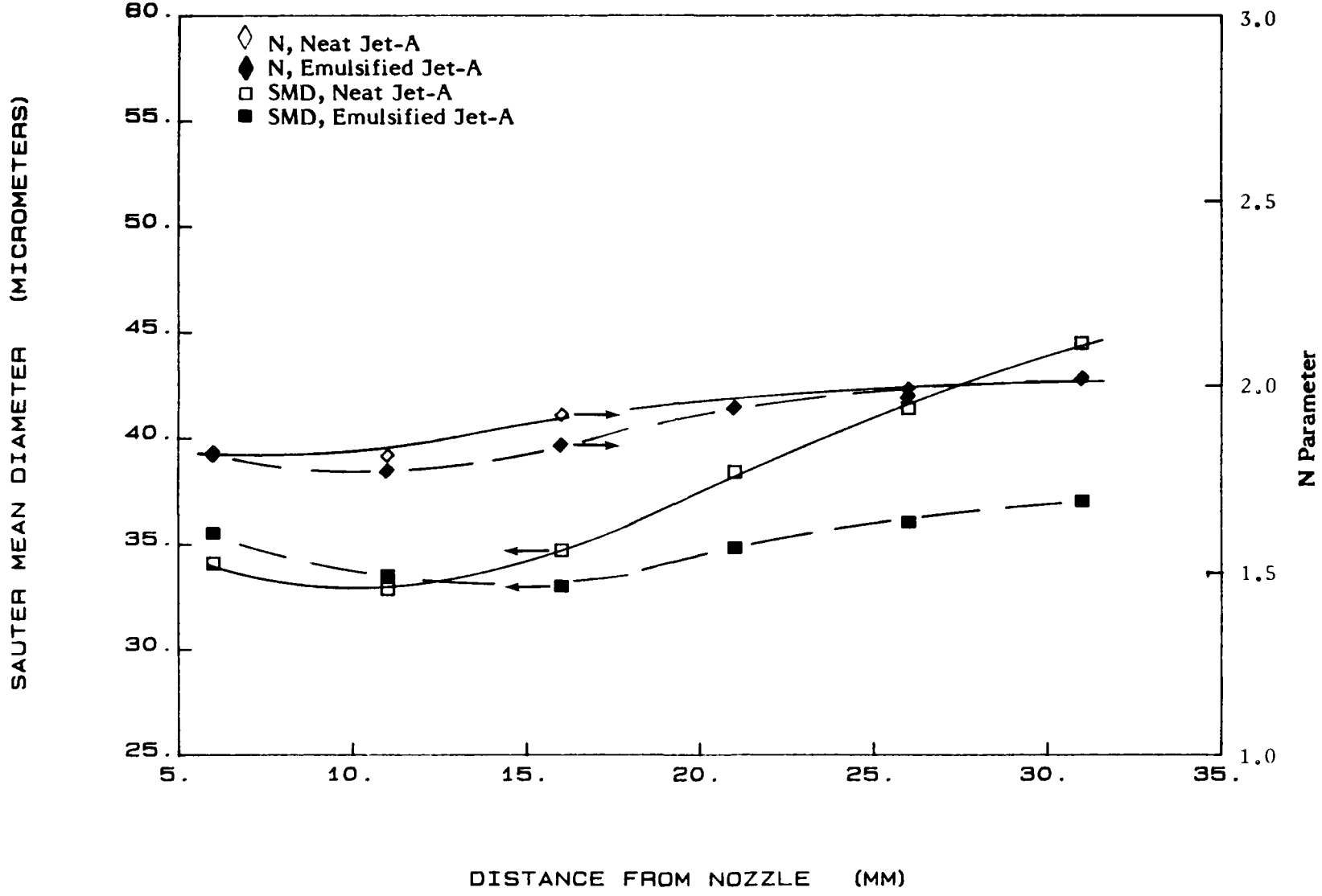

FIGURE 22. CHANGE OF SMD AND N WITH DISTANCE FROM THE NOZZLE, JET-A, 547 K, 345 kPa

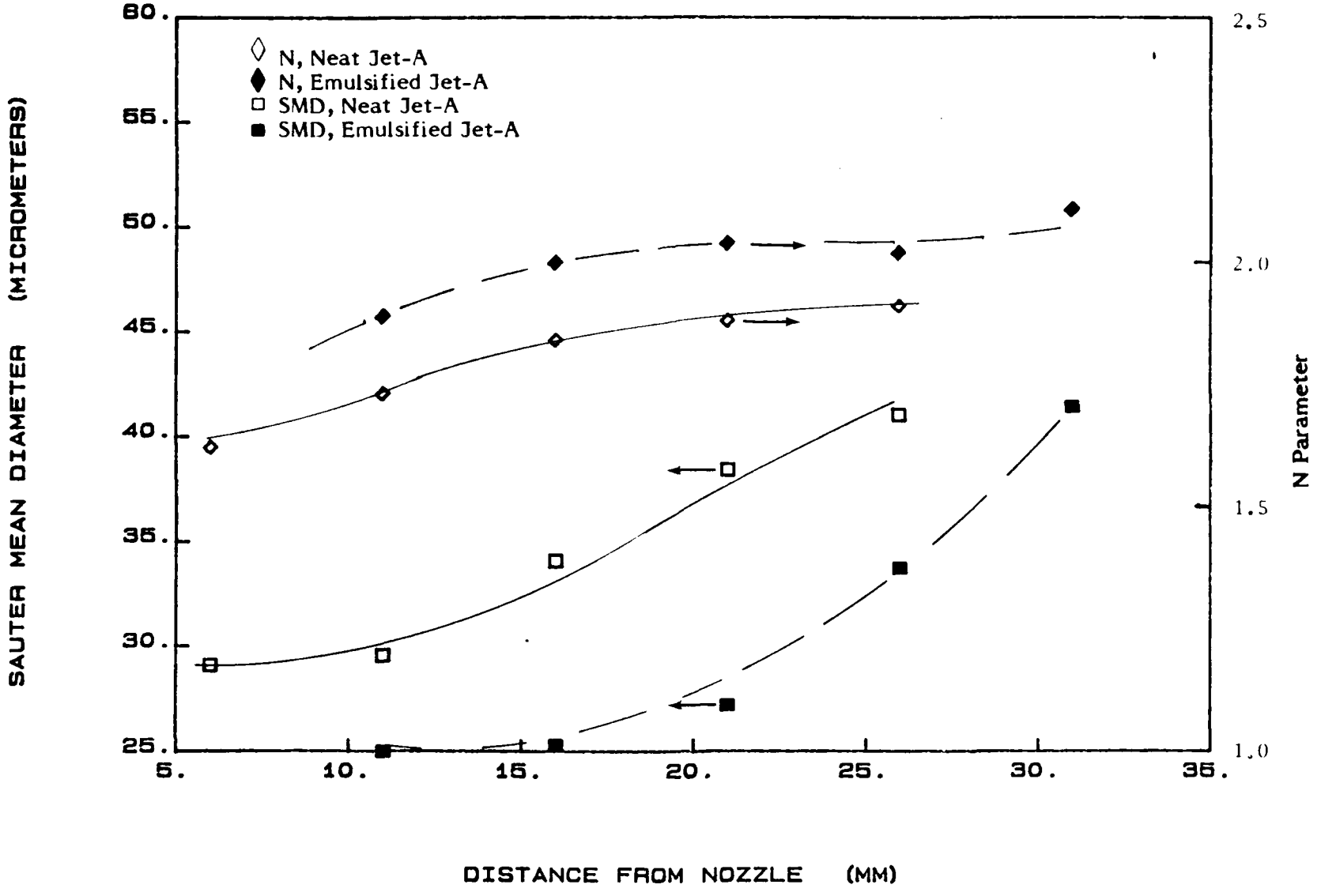

FIGURE 23. CHANGE OF SMD AND N WITH DISTANCE FROM THE NOZZLE, JET-A, 547 K, 448 kPa

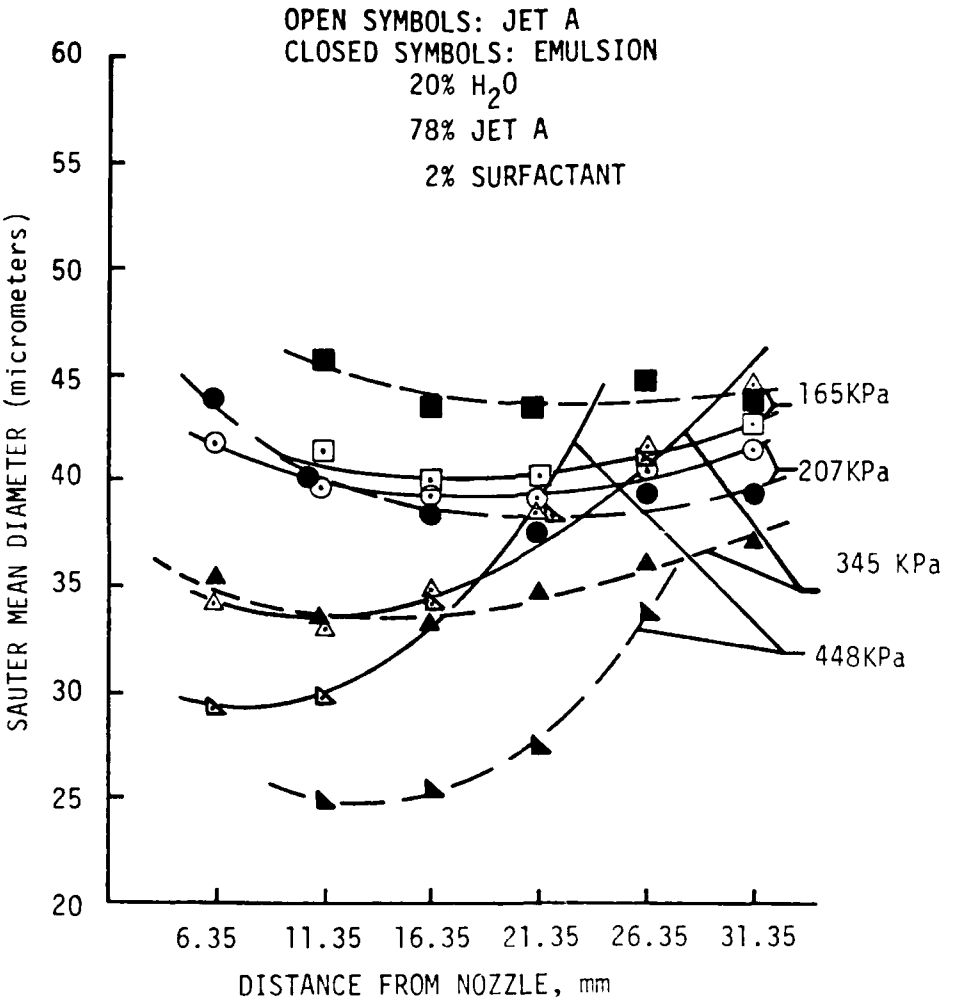

FIGURE 24a . EFFECT OF AIR PRESSURE ON ATOMIZATION AND VAPORIZATION-SMD VERSUS DISTANCE FROM NOZZLE
3.8 liters/hr 45°HC DELAVAN NOZZLE, 8.5 m/s, 547 K

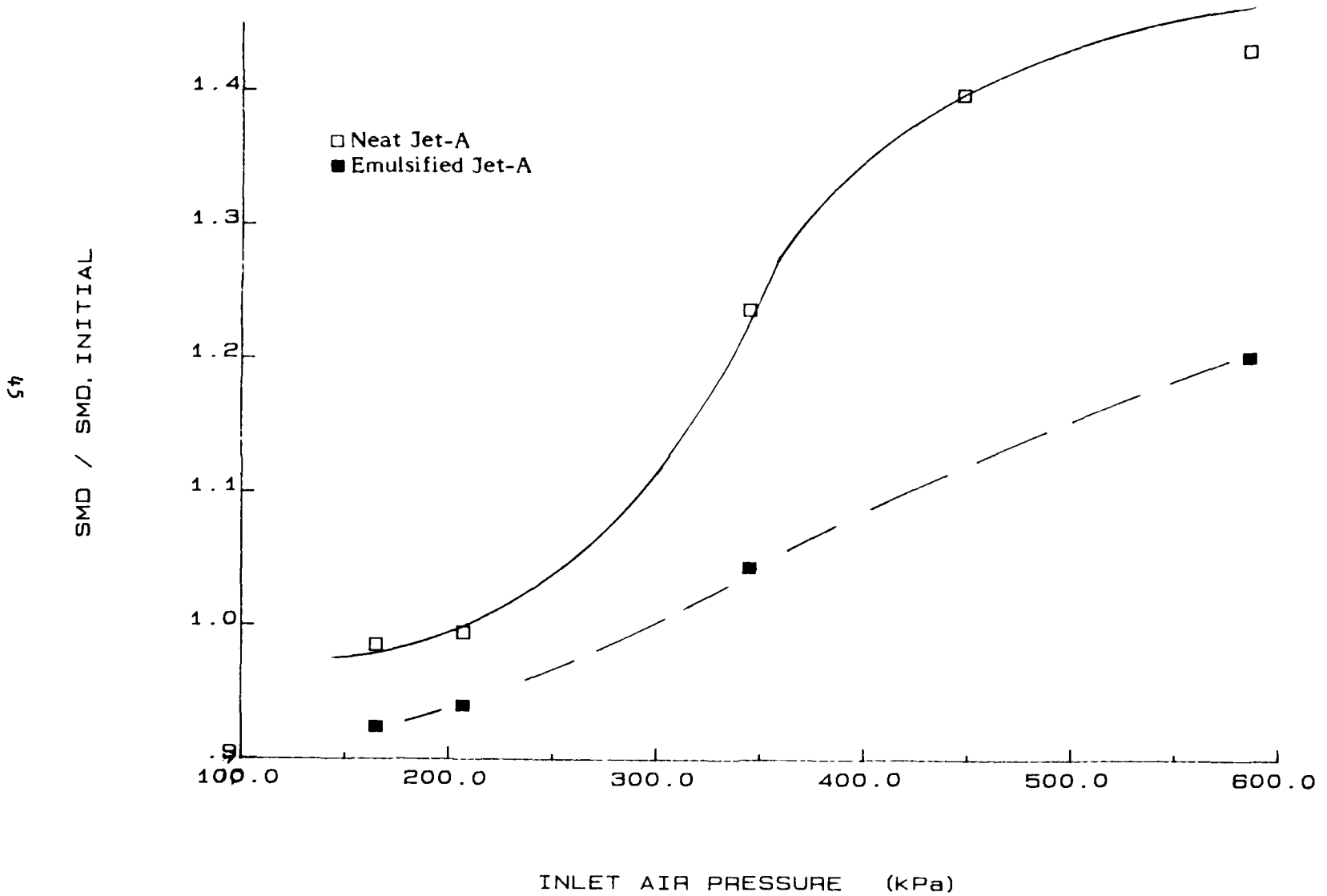

FIGURE 24b. EFFECT OF AIR PRESSURE ON SMD OF EMULSIFIED AND NEAT JET A AT 26 mm, AIR TEMPERATURE 547 K

initial SMD close to the nozzle. (The normalization is necessary because initial atomization depends on air density.) The divergence of drop sizes at higher pressures is consistent with the microexplosion phenomena.

In addition to the effects of pressure on the comparative evaporation of neat and emulsified fuels, note that the increased air density has a significant effect on improving the initial atomization close to the nozzle. This fact is very significant in that it implies that nozzle drop-size calibrations performed at atmospheric conditions cannot be used to predict spray evaporation at elevated pressure or subatmospheric conditions without correcting for this air density effect. Since evaporation times are proportional to the square of the initial drop sizes, the differences shown in Figure 24a for initial sizes represent even larger differences when considered in terms of spray evaporation times.

3.1.3 Effect of Elevated Temperature and Pressure on Size-Distribution For Emulsified and Neat Hexadecane

The evaporation of a multiple component petroleum fuel such as jet-A is difficult to model even without the addition of water. In order to allow for a more quantitative analysis of the evaporation process, experiments similar to those already discussed for jet-A were conducted with emulsified and neat hexadecane. The evaporation of these sprays was studied by taking drop-size measurements at a fixed pressure and varying temperature and visa versa. At a fixed pressure of 448 kPa (4.42 atm), the results are shown for a series of temperatures: 450 K in Figure 25, 506 K in Figure 26, 547 K in Figure 27, 589 K in Figure 28, 644 K in Figure 29, and 700 K in Figure 30. The SMD data for Figures 26-30 and data for 728 K are also shown in Figure 31a after normalization for an overall comparison of behavior. (The SMD data for emulsified hexadecane at 506 K were identical to 547 K and are not shown.) The normalized SMD's in Figure 31a for a distance of 26 mm from the nozzle are replotted in Figure 31b as a function of air temperature to illustrate the temperature dependence more clearly. At 450 K and 506 K, the emulsified and neat fuels evaporate in such a way that the drop sizes are very similar. At 589 K, 644 K, 700 K, and 728 K the initial atomization is similar, but the emulsified fuels produce smaller drops than the neat fuels downstream of the nozzle. These trends are similar to those observed for jet-A and are consistent with the behavior expected if microexplosions

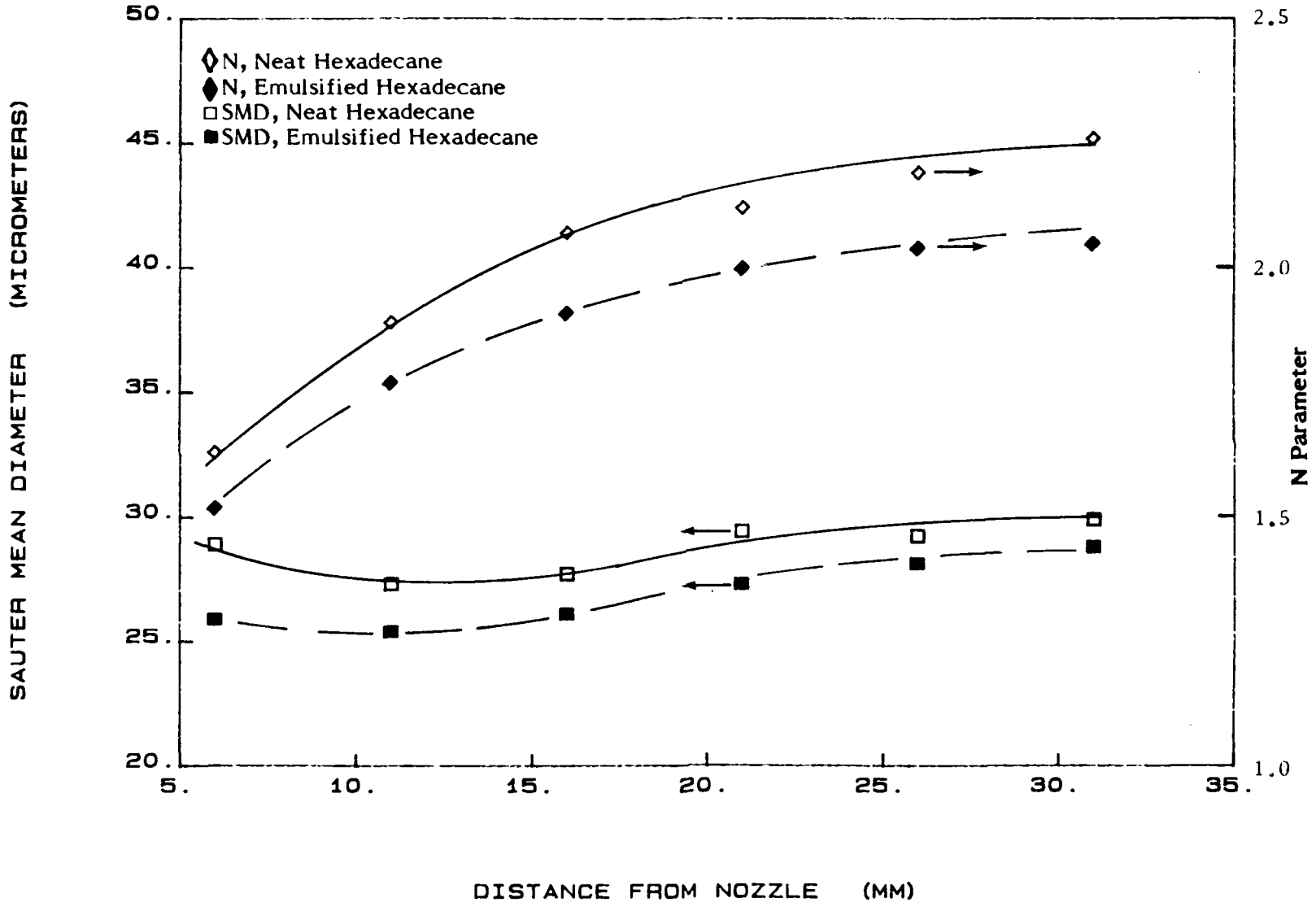

FIGURE 25. CHANGE OF SMD AND N WITH DISTANCE FROM THE NOZZLE, HEXADECANE 450 K, 448 kPa

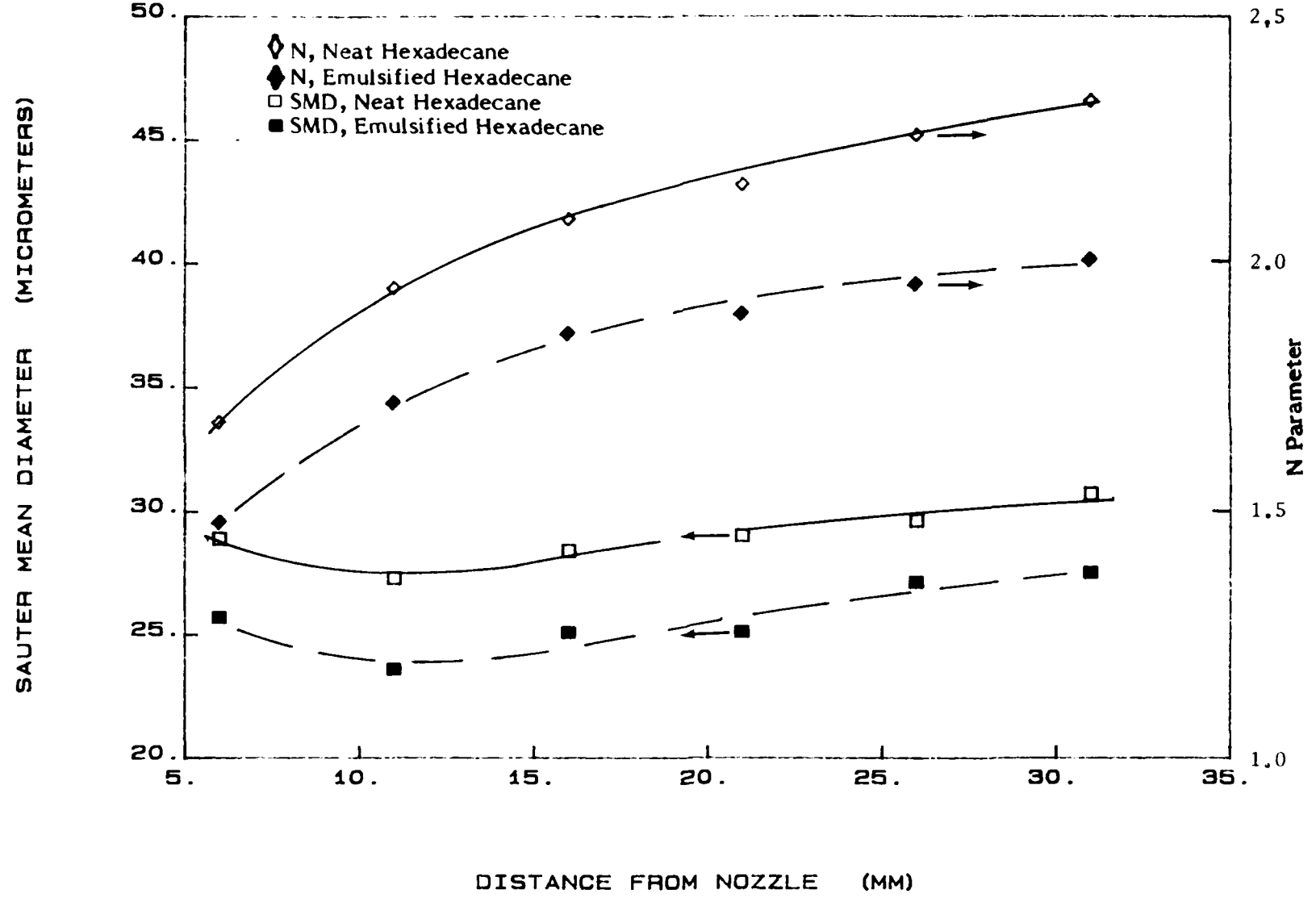

FIGURE 26. CHANGE OF SMD AND N WITH DISTANCE FROM THE NOZZLE, HEXADECANE 506 K, 448 kPa

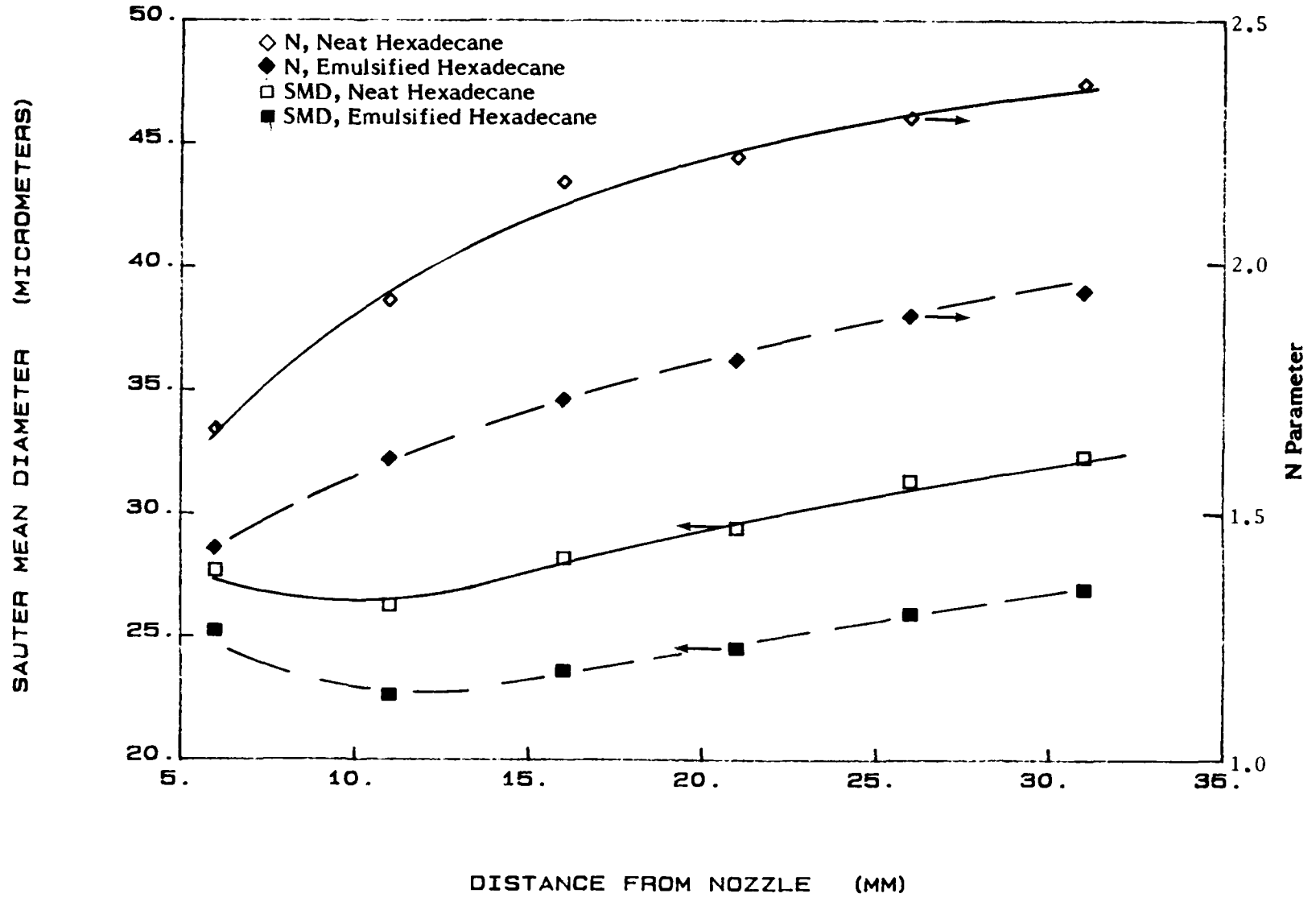

FIGURE 27. CHANGE OF SMD AND N WITH DISTANCE FROM THE NOZZLE, HEXADECANE 547 K, 448 kPa

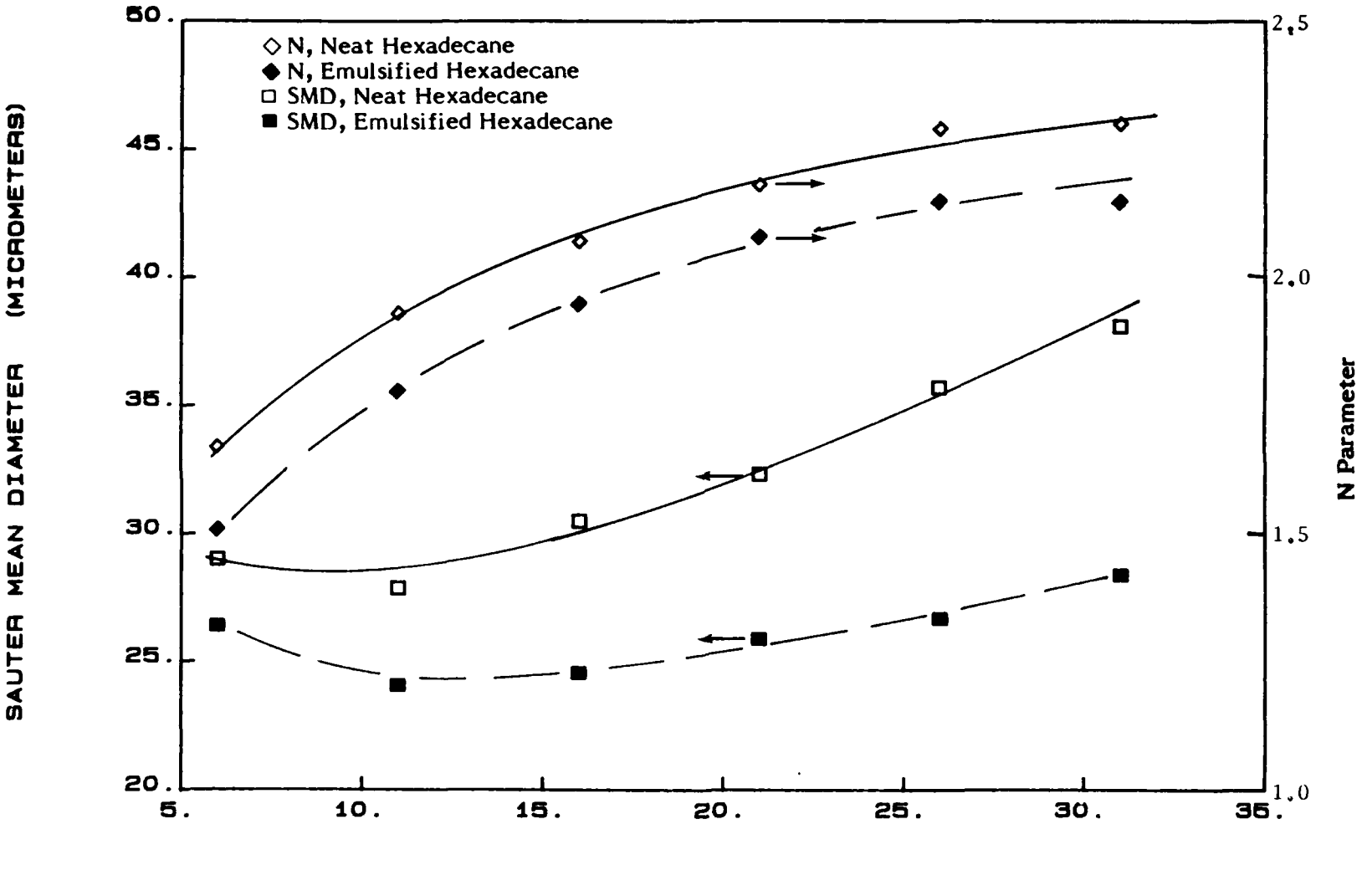

FIGURE 28. CHANGE OF SMD AND N WITH DISTANCE FROM THE NOZZLE, HEXADECANE 589 K, 448 kPa

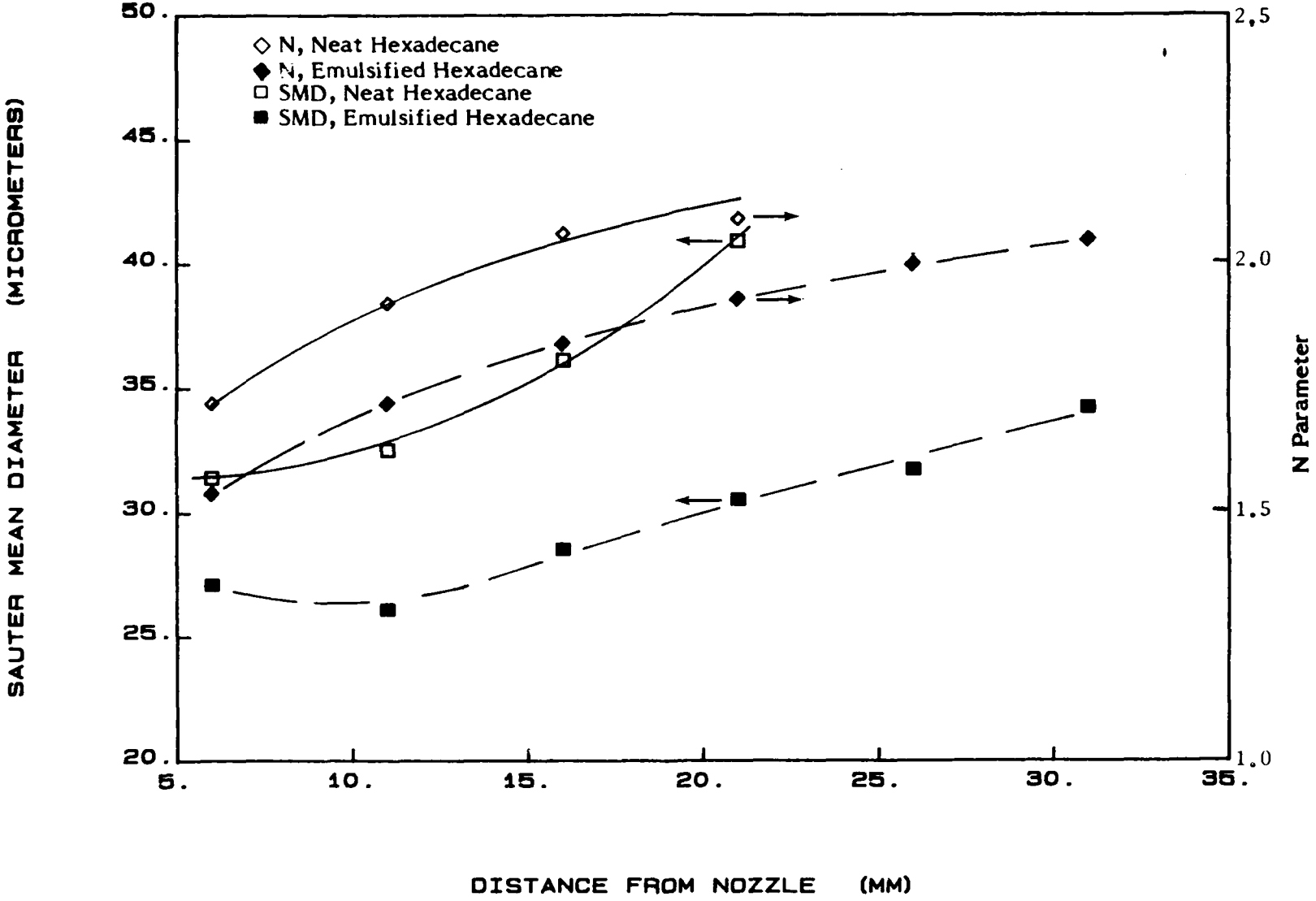

FIGURE 29. CHANGE OF SMD AND N WITH DISTANCE FROM THE NOZZLE, HEXADECANE 644 K, 448 kPa

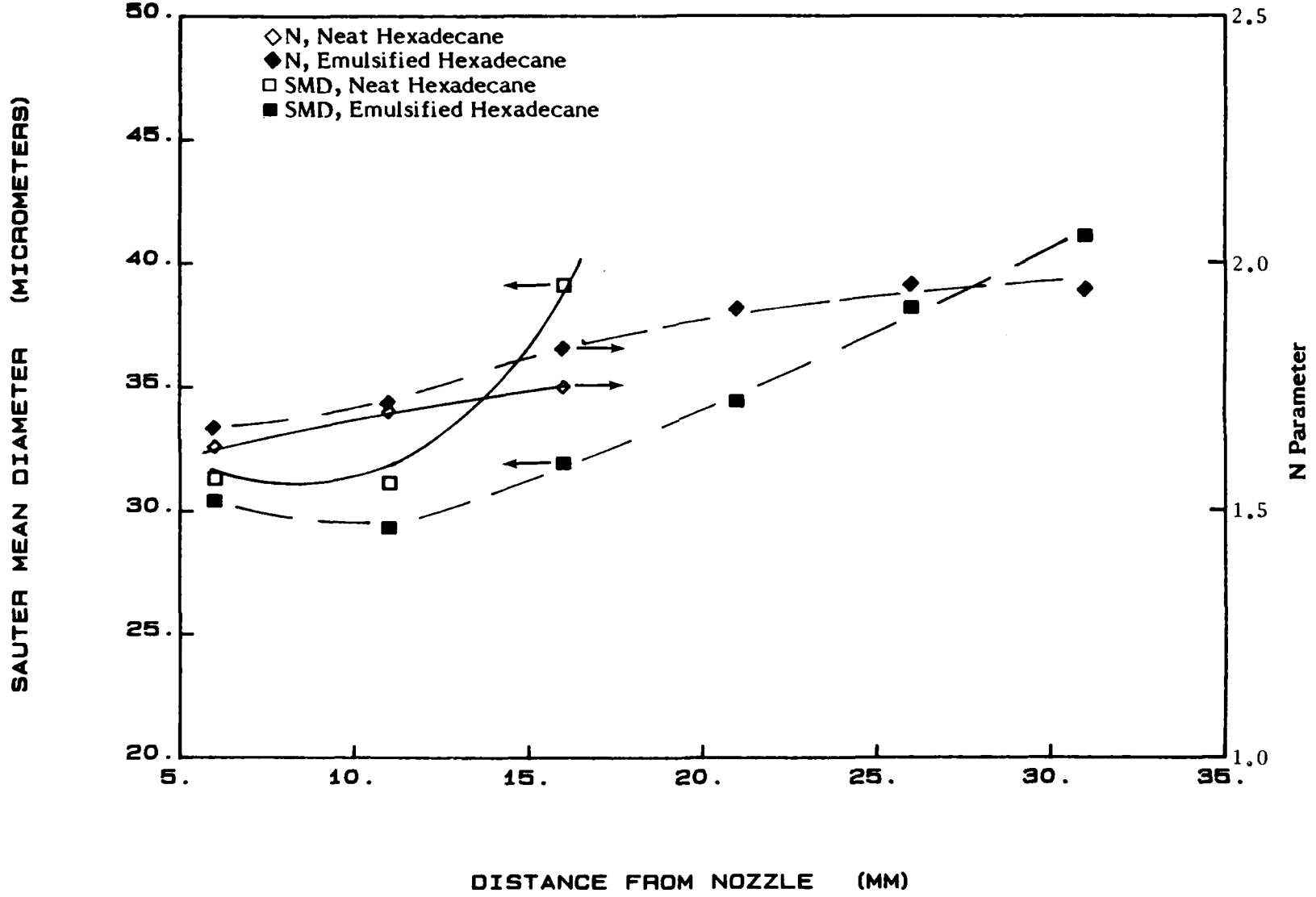

FIGURE 30. CHANGE OF SMD AND N WITH DISTANCE FROM THE NOZZLE, HEXADECANE 700 K, 448 kPa

Table 3. Computer Predicted Steady-State Drop Surface Temperature for Hexadecane at Conditions Corresponding to Figure 31 (P_{air} = 448 kPa (4.42 atm))

Air Temperature (K)	Drop Temperature (K)
506	469
547	488
589	503
644	520
700	535
728	541

Table 4. Computer Predicted Steady-State Drop Surface Temperature for Hexadecane at Conditions Corresponding to Figures 32-35 (T_{air} = 644 K)

Air Pressure (kPa)	(atm)	Drop Temperature (K)
165	1.63	491
241	2.38	502
345	3.40	512
448	4.42	520

were occurring. However, the advantage to using a single-component fuel is that it is possible to predict the steady state drop temperature, and if the assumption is made that the less volatile (hexadecane) component controls the evaporation rate for the emulsified fuel after some initial period, then these predicted single-component values should be reasonable estimates for the emulsified drops. The steady-state drop temperatures for hexadecane predicted by the computer model described previously are shown in Table 3 for conditions corresponding to Figure 31a. The emulsified and neat fuels diverge in drop-size behavior for an air temperature of about 589 K to 644 K, corresponding to a drop temperature of 503 K to 520 K. The temperature for microexplosions to occur depends on the purity and amount of bubbles at the water/hexadecane interface, but the upper limit for spontaneous nucleation for a pure bubble-free system is about 539 K at atmospheric pressure, with only a slight pressure effect.[22,23] It is reasonable to expect that the presence of bubbles and impurities may have reduced the effective spontaneous nucleation temperature from a predicted drop temperature of 539 K to the range of 503 K to 520 K, in agreement with the observed point of divergence of emulsified and neat fuels. The water/hexadecane/surfactant system used in these experiments was recirculated through an ultrasonicator before usage to maintain a well-mixed blend, but this may have added a considerable number of bubbles into the fuel, lowering the effective spontaneous nucleation temperature from the theoretical limit.

As drop temperatures increase, the likelihood of microexplosions increases. Drop temperatures may be increased by an increase in air temperature (at constant air pressure), as discussed above and shown in Table 3, or by an increase in air pressure (at constant temperature) as shown in Table 4. A set of experiments was performed to examine the effects of air pressure, and the corresponding steady-state drop temperatures, on the comparative drop-size distributions of emulsified and neat hexadecane at a constant air temperature of 644 K. Data for four different air pressures were recorded. The results for 165 kPa (1.63 atm) are shown in Figure 32, for 241 kPa (2.38 atm) in Figure 33, for 345 kPa (3.40 atm) in Figure 34, and for 448 kPa (4.42 atm) in Figure 35. The SMD's at a fixed distance of 26 mm from the nozzle in Figures 32-35 are shown as a function of air pressure in Figure 36. The SMD's in Figure 36 have been normalized relative to the initial SMD close to the nozzle at the same condition, so that the change in SMD with distance is clearer. Comparing the emulsified versus neat fuels in Figures 32-36, the trends for SMD's are similar for pressures of 345 kPa

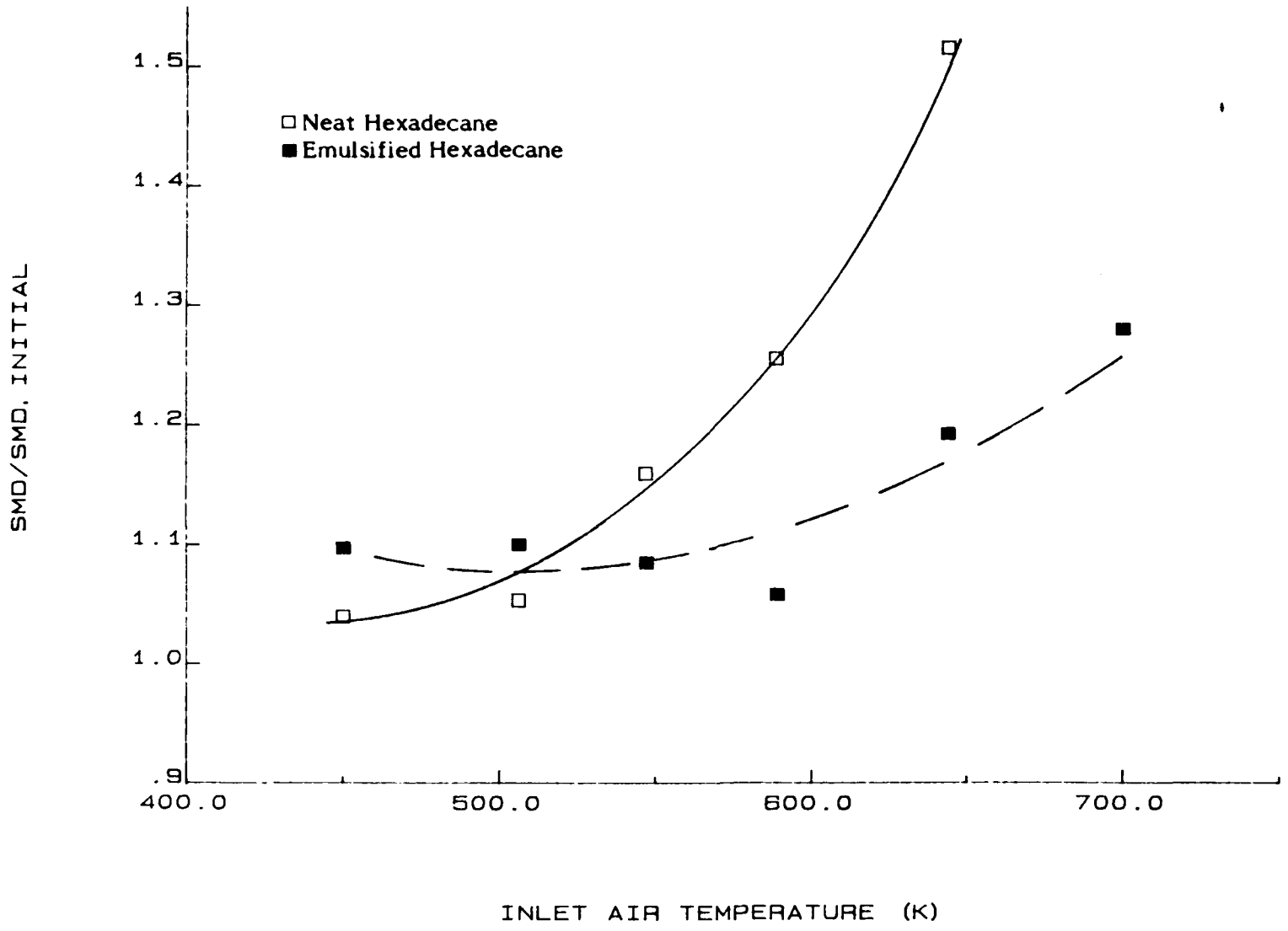

FIGURE 31b. EFFECT OF AIR TEMPERATURE ON SMD OF EMULSIFIED AND NEAT HEXADECANE AT 26 mm FROM NOZZLE, AIR PRESSURE OF 448 kPa (4.42 ATM)

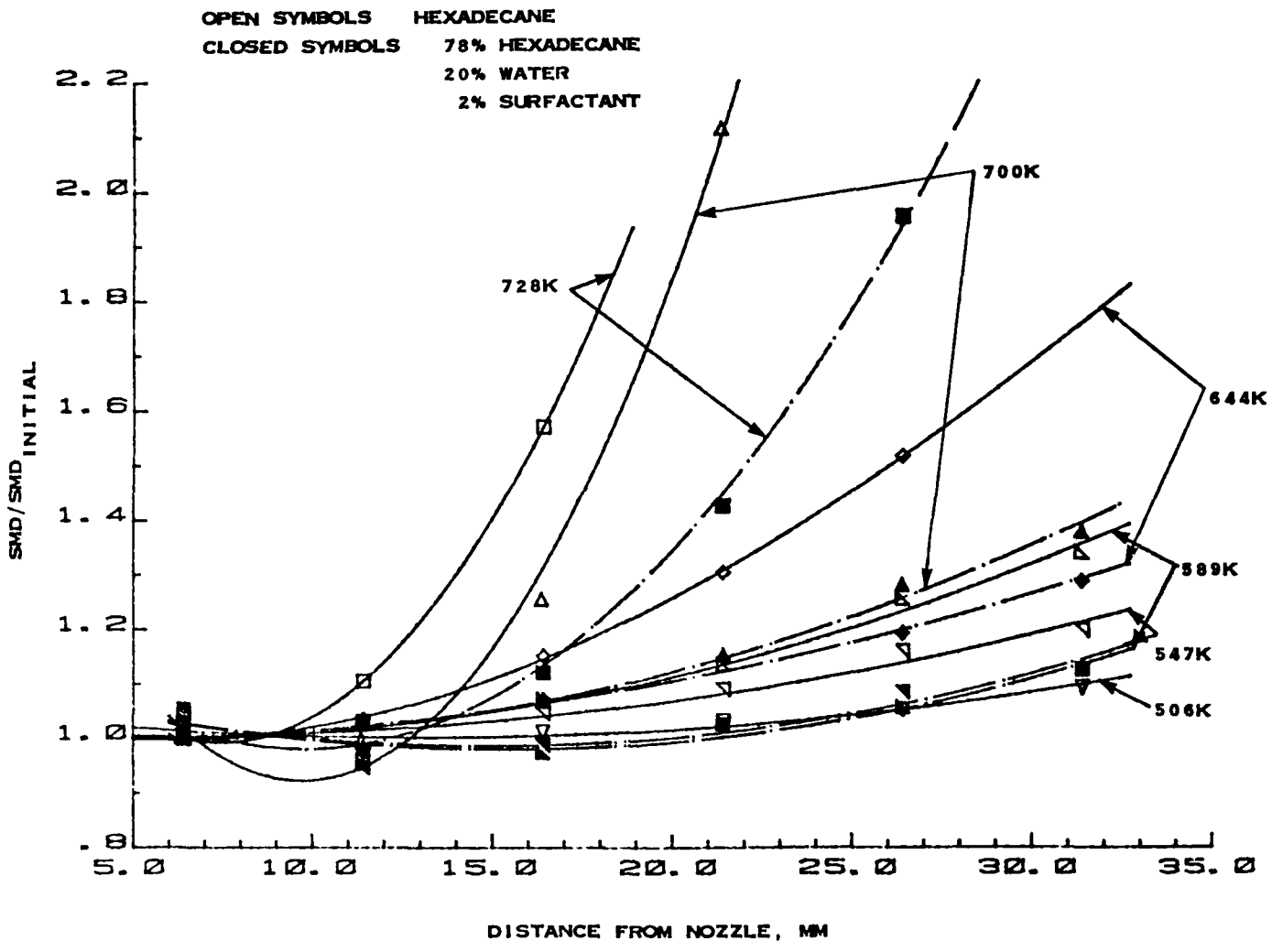

FIGURE 31a. COMPARISON OF RELATIVE SMD FOR EMULSIFIED AND NEAT HEXADECANE AT CONSTANT PRESSURE (4.42 atm, 448 kPa) AND VARIOUS TEMPERATURES (DELAVAN WDA 3.8 LITERS/HR 45° HOLLOW CONE, ΔP=483kPa). $SMD_{initial} \cong 28\ \mu m$

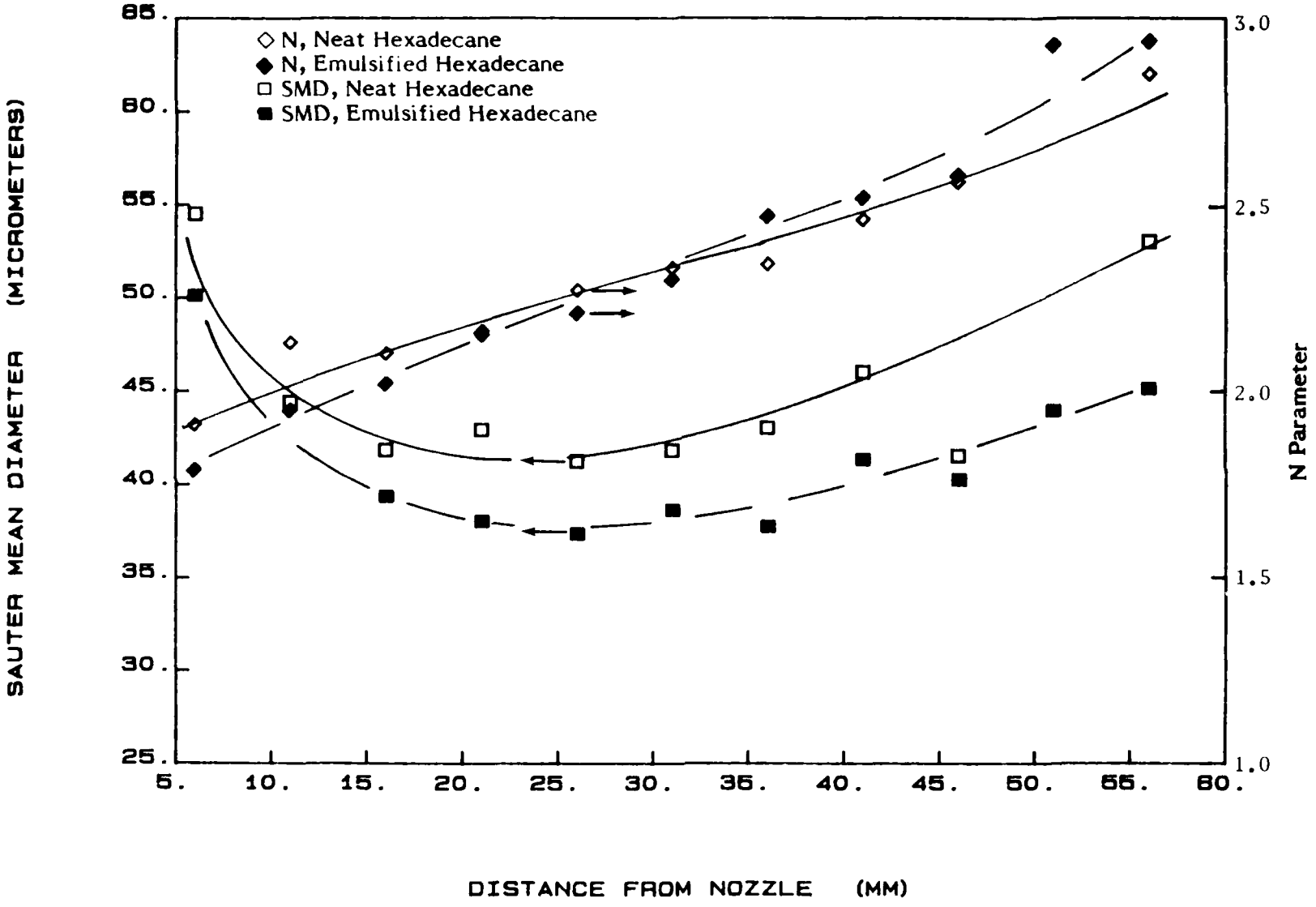

FIGURE 32. CHANGE OF SMD AND N WITH DISTANCE FROM THE NOZZLE, HEXADECANE 644 K, 165 kPa

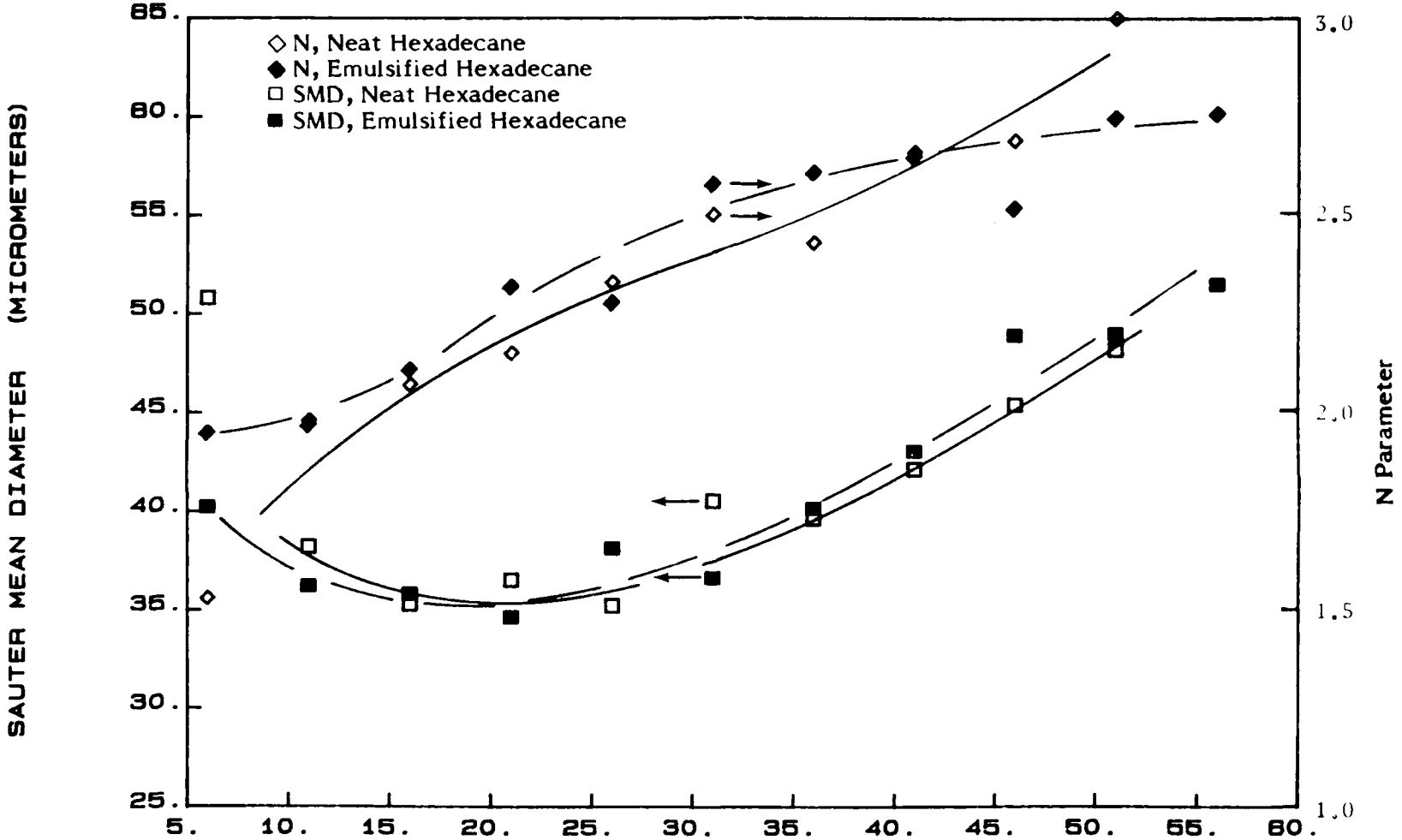

FIGURE 33. CHANGE OF SMD AND N WITH DISTANCE FROM THE NOZZLE, HEXADECANE 644 K, 241 kPa

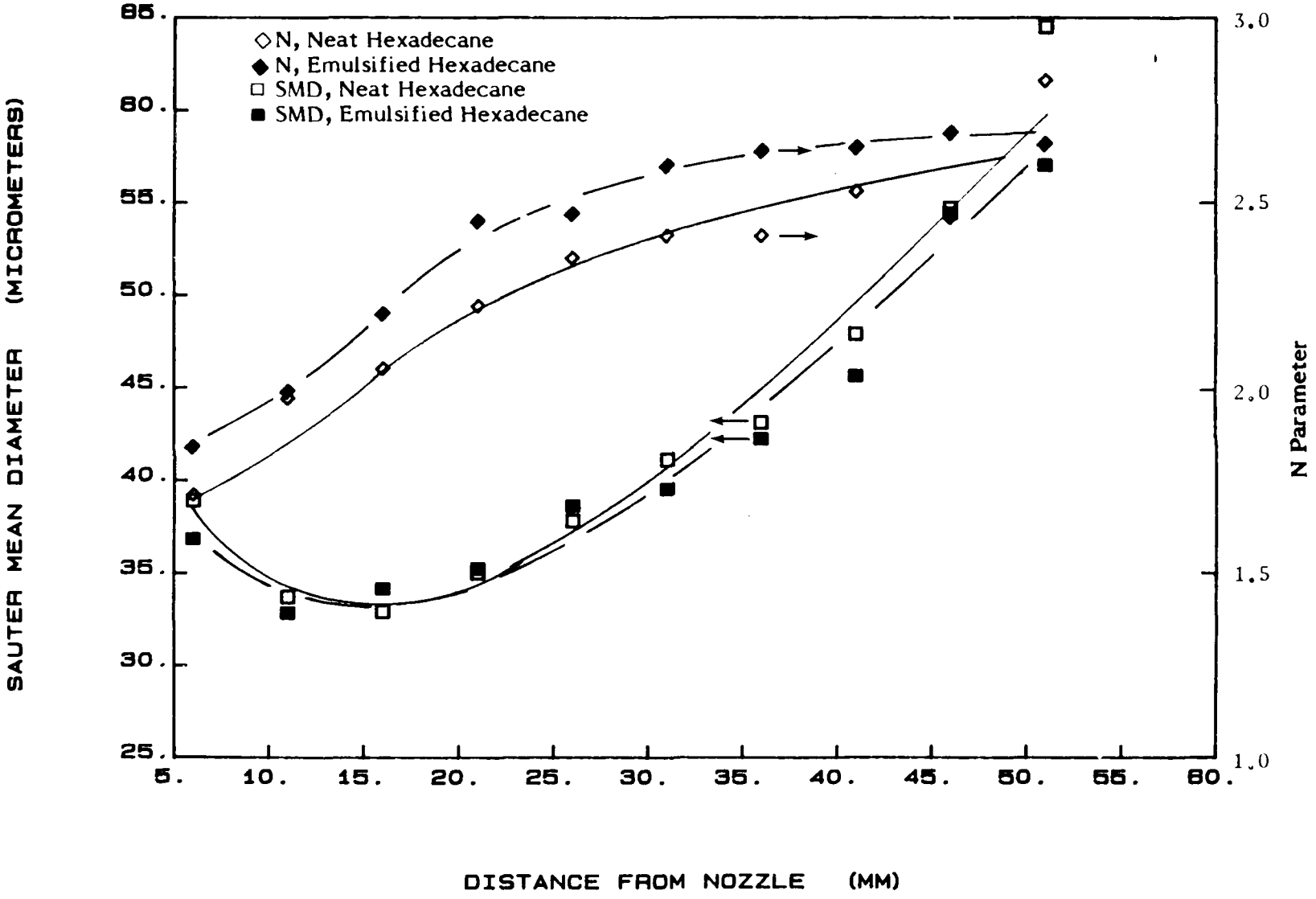

FIGURE 34. CHANGE OF SMD AND N WITH DISTANCE FROM THE NOZZLE, HEXADECANE 644 K, 345 kPa

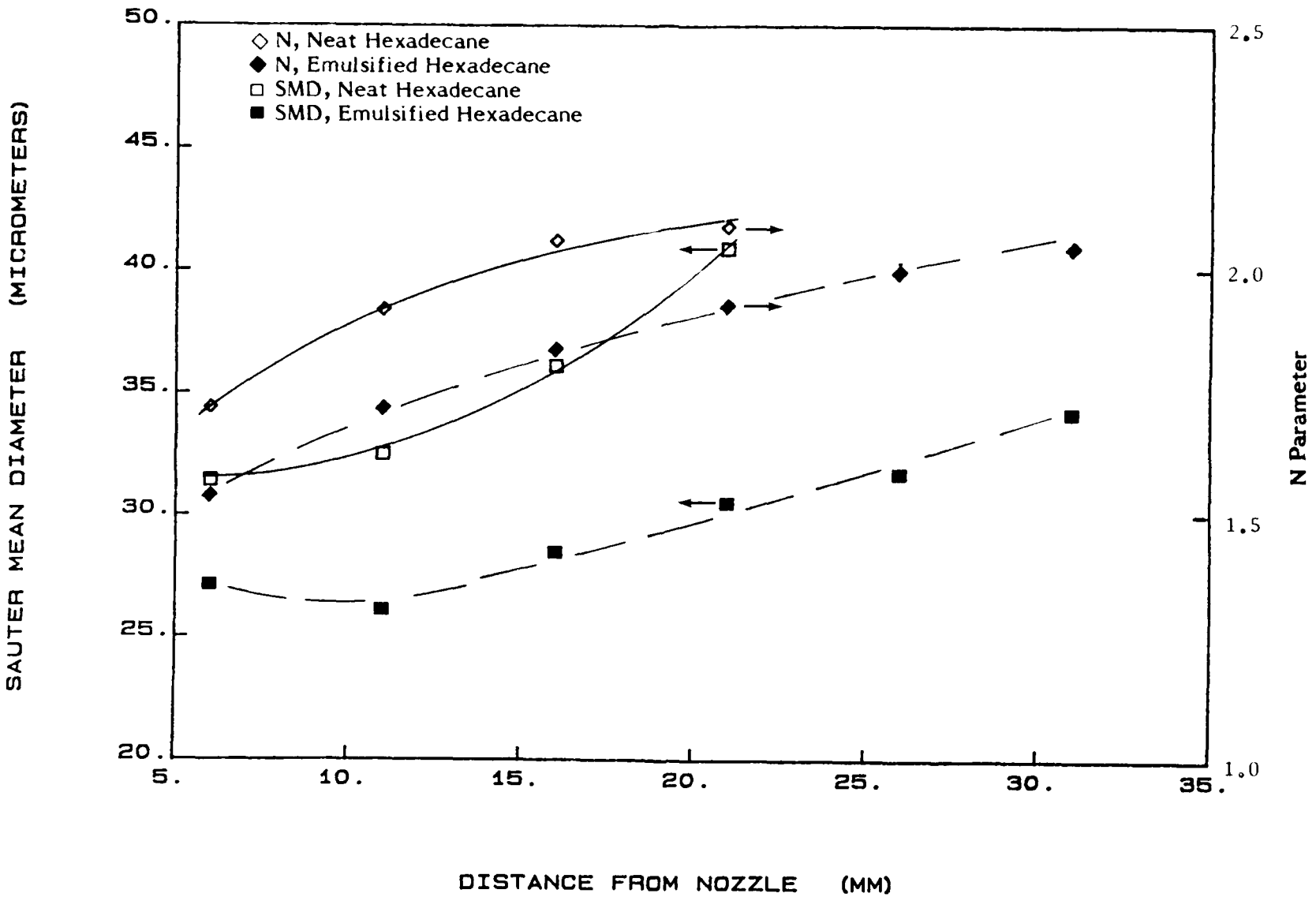

FIGURE 35. CHANGE OF SMD AND N WITH DISTANCE FROM THE NOZZLE, HEXADECANE 644 K, 448 kPa

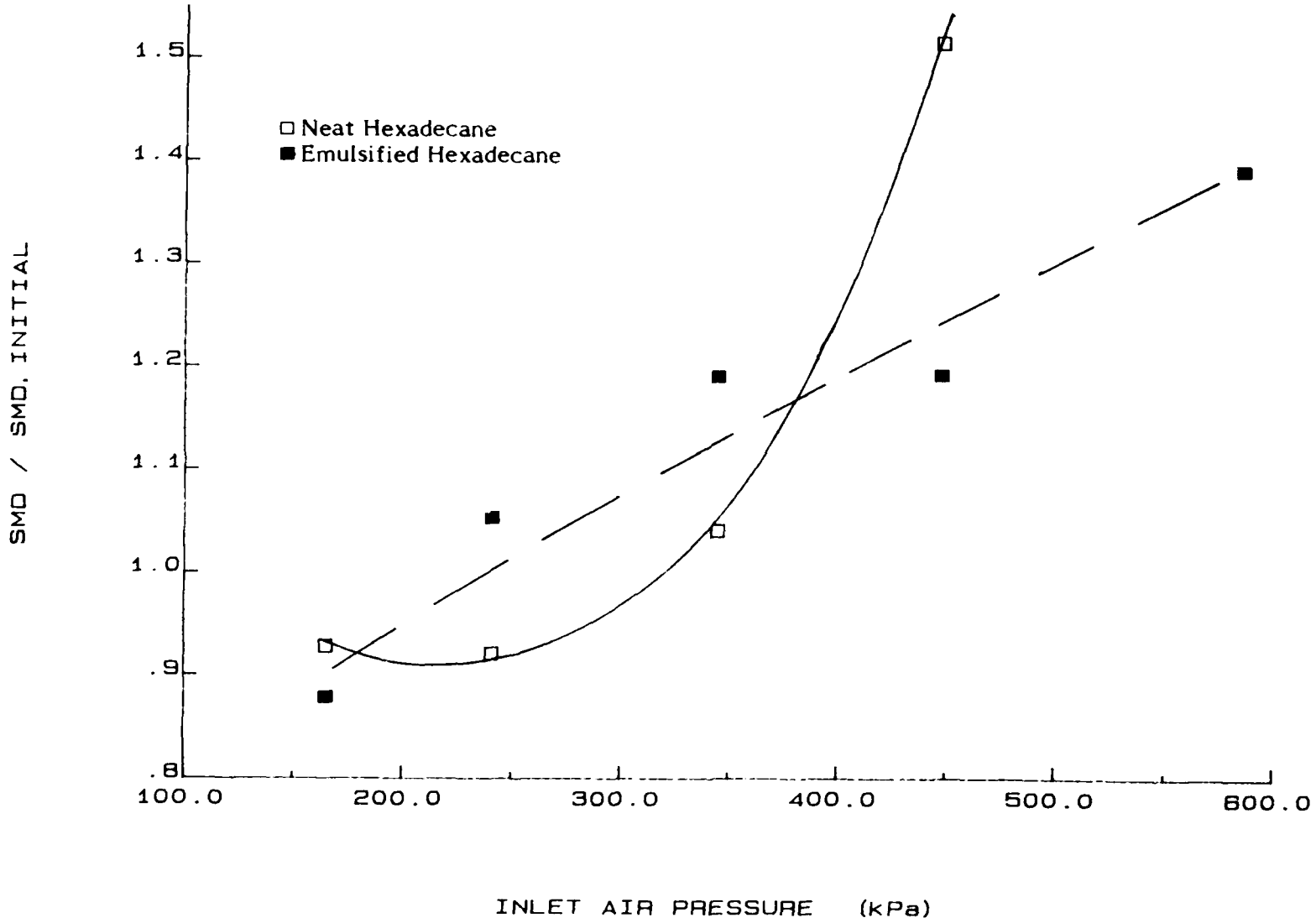

FIGURE 36. EFFECT OF AIR PRESSURE ON SMD OF EMULSIFIED AND NEAT HEXADECANE AT 26 mm FROM NOZZLE, AIR TEMPERATURE OF 644 K

and below, but diverge at 448 kPa with the emulsified fuels showing smaller drop sizes. These air conditions allow certain steady-state drop temperatures to be reached, as shown in Table 4. The divergence in drop-size distributions between 345 kPa and 448 kPa (at a fixed air temperature of 644 K) corresponds to drop temperatures in the range of 512 K to 520 K. Thus, for variations in air pressure, the divergence in drop-size distributions for emulsified and neat fuels occurs in the range of drop temperatures from roughly 512 K to 520 K, similar to the range of 503 K to 520 K reported above for the divergence with varying air temperature. Both changes in air temperature and air pressure lead to a divergence in drop-size distributions for emulsified and neat hexadecane at drop temperatures of approximately 515 K. This is a reasonable drop temperature to expect microexplosions in a practical system compared with the upper limit of 539 K in a pure system.

In addition to the comparative results for emulsions versus neat fuels, the drop-size data for the neat fuels alone provide some interesting and unique data with which to compare predictions from computer models for spray evaporation at elevated temperatures and pressures. Such comparisons are presented in a later section.

Data for both jet-A and hexadecane indicate that emulsified and neat fuels initially atomize to approximately the same drop sizes for a given condition, and evaporate in such a way so as to maintain similar drop sizes at lower air temperatures and pressures. As air temperatures and pressures increase, the drop sizes diverge and the emulsified drops are consistently smaller downstream of the nozzle. For hexadecane, this divergence occurs at a predicted drop temperature on the order of 515 K. Although these results are consistent with what would be expected if microexplosions occurred for the emulsified fuels, it is again possible that the higher specific heat and heat of vaporization of water could delay the evaporation process for emulsions and produce similar results.

3.2 Two-Phase Probe Measurements

Although microexplosions of emulsified drops may produce similar drop-size results to those caused by reduced evaporation rates of the small drops due to the heat-sink effect of water, these two phenomena have opposite effects on the spray evaporation rates. The heat-sink effect would reduce evaporation rates while

microexplosions would enhance the evaporation due to the smaller drop-sizes produced. Therefore a measurement of the comparative evaporation rates of the emulsified and neat fuels would determine the relative importances of the microexplosions versus the heat sink effect.

Such measurements of the fuel vapor concentration across the spray were performed using the two-phase probe described earlier. Measurements were performed at two distances from the nozzle, 19 mm and 57 mm, at temperatures from atmospheric to 650 K, and at a constant pressure of 448 kPa (4.42 atm). Profiles for emulsified and neat hexadecane fuel vapor concentration (hydrocarbon concentration only) at 57 mm from the nozzle are shown in Figure 37 for 509 K and Figure 38 for 646 K. Similar profiles were recorded at other temperatures at 57 mm, and at 19 mm from the nozzle. Equal volume flowrates were used for the emulsified and neat fuels, so that the hydrocarbon concentration for complete evaporation of the emulsified fuel would be only about 80 percent of that for the neat fuel.

The profiles for 57 mm such as those shown in Figures 37 and 38, as well as the profiles at 19 mm, were integrated across the whole spray, accounting for the area weighting factors and correcting the emulsified fuels for the 20 percent hydrocarbon displacement by water, to get a single integrated value for each fuel at a given condition. These integrated hydrocarbon concentrations are plotted as a function of air temperature in Figure 39 for the 19 mm location and Figure 40 for the 57 mm location. (Actually, the effective sampling location for the probe is somewhat upstream of the physical location of the probe tip due to the acceleration of the flow into the probe, but no estimate is included to account for this.)

As shown in Figures 39 and 40, very little, if any, fuel vapor could be measured at 306 K, in agreement with the low vapor pressure of hexadecane at this temperature. However, this is very significant in that it indicates that the aerodynamic separation of drops from the vapor sample works very effectively, even in these finely atomized sprays. The probe itself is heated, so if drops were present in the vapor sample, they would be vaporized and the measured values would be greater. This room temperature (approximately) measurement also indicates that the heated probe is not affecting the sample by vaporizing the spray either before or after entering the probe and prior to the "vapor only" separation point 25 mm downstream of the probe tip. The data in

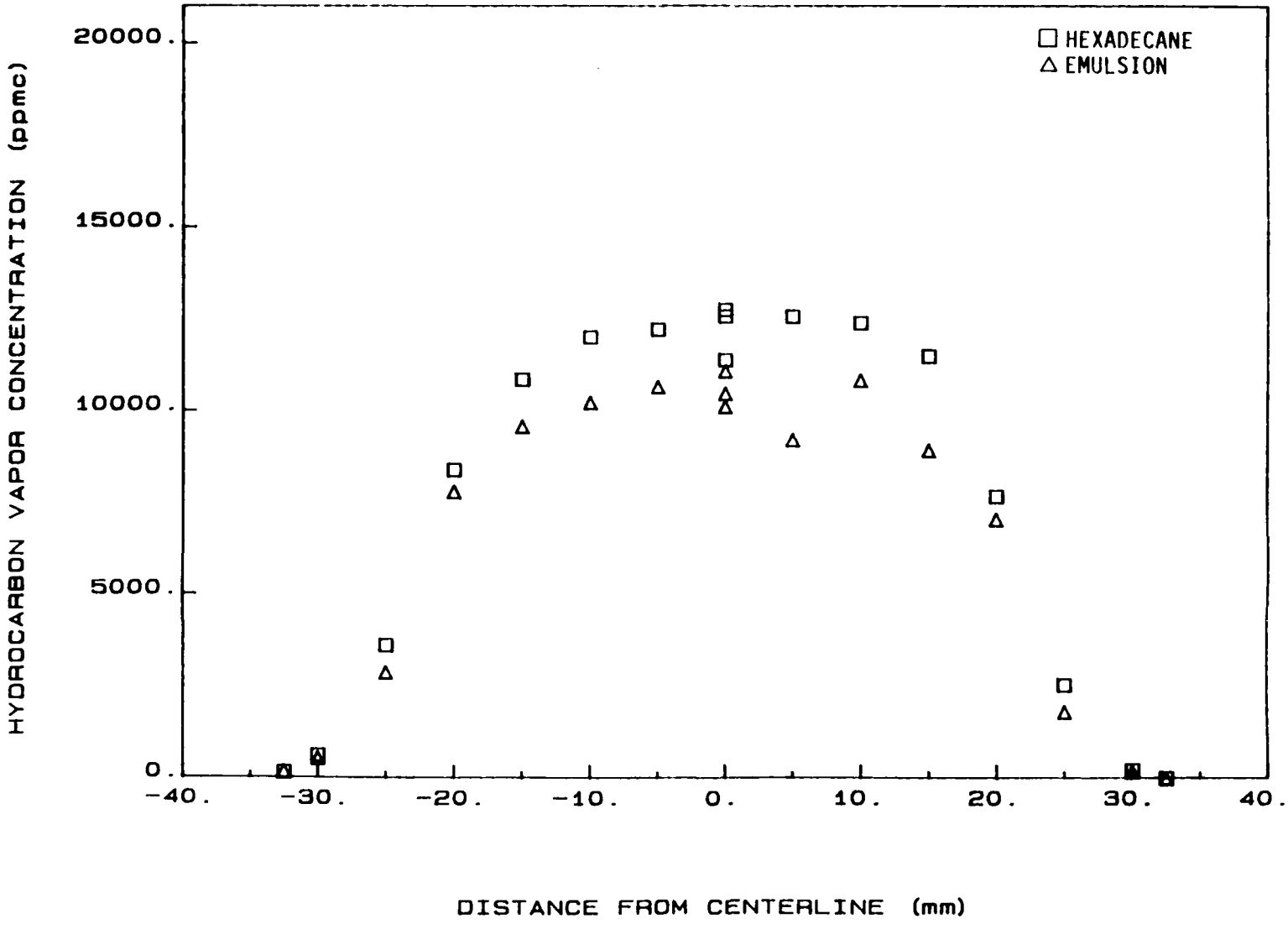

FIGURE 37. HYDROCARBON VAPOR CONCENTRATION AT 57 mm
509 K, 4.42 atm

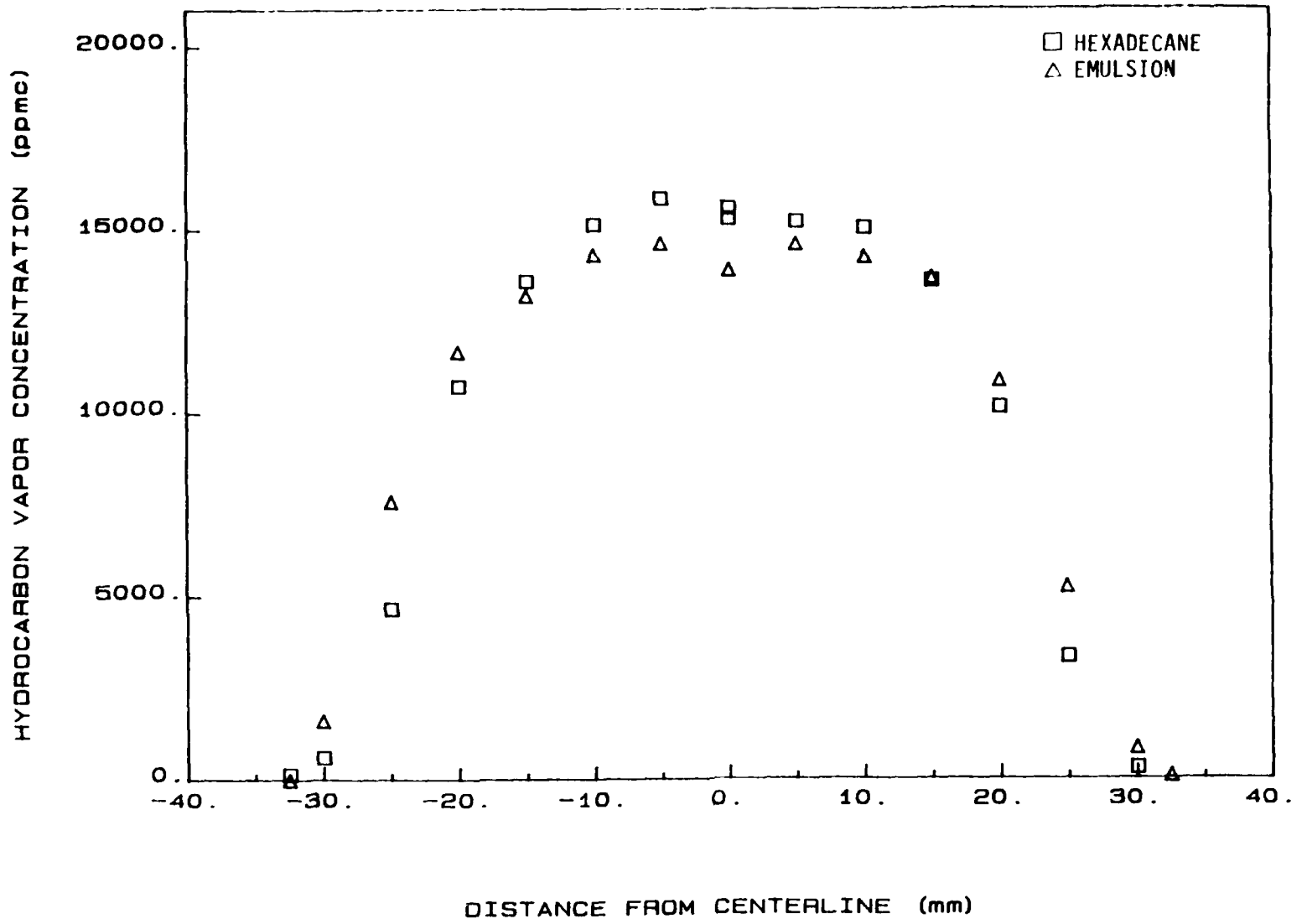

FIGURE 38. HYDROCARBON VAPOR CONCENTRATION AT 57 mm
646 K, 4.42 atm

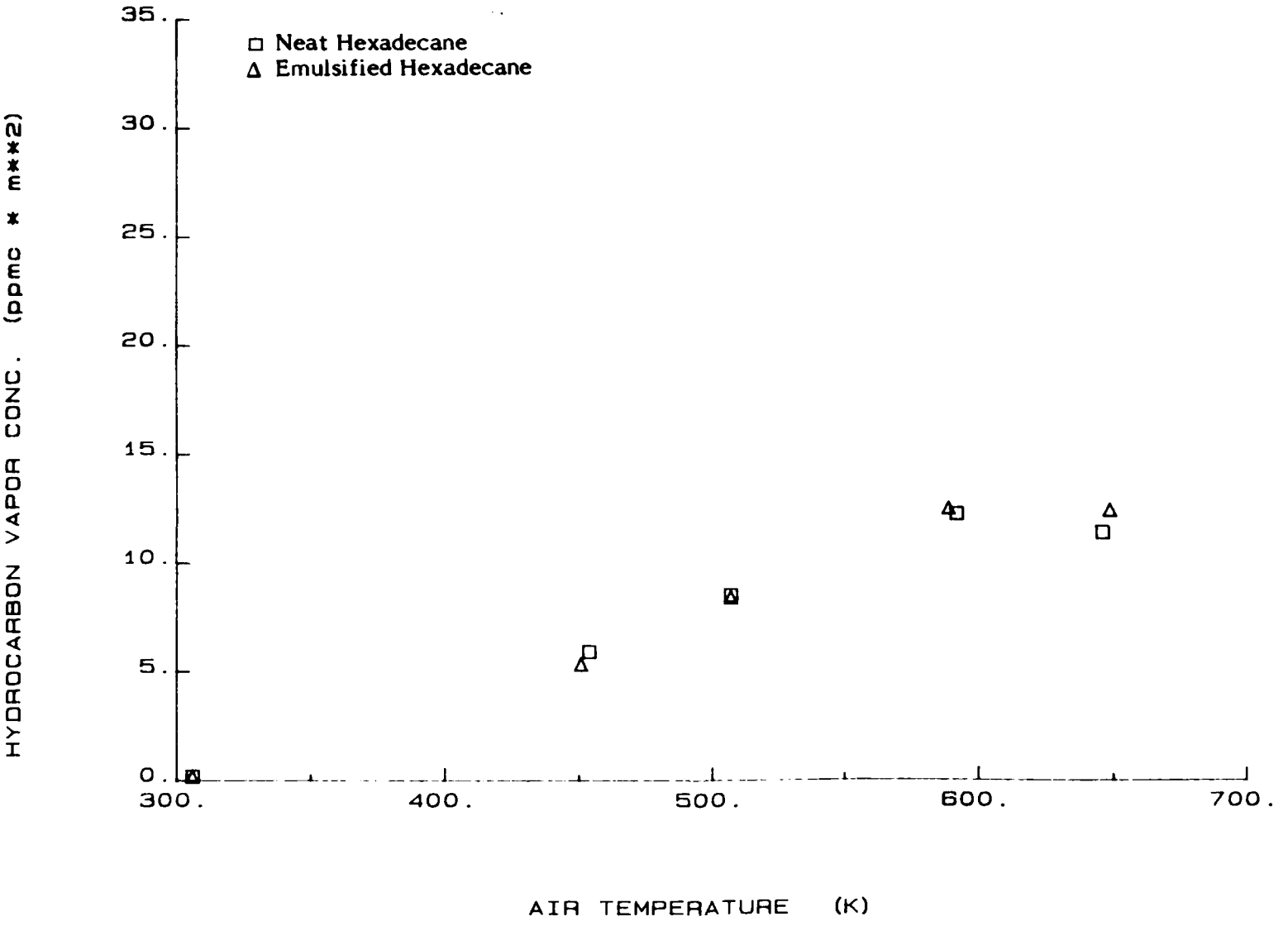

FIGURE 39. COMPARISON OF HYDROCARBON VAPOR CONCENTRATION FOR EMULSIFIED AND NEAT HEXADECANE AT 19 mm

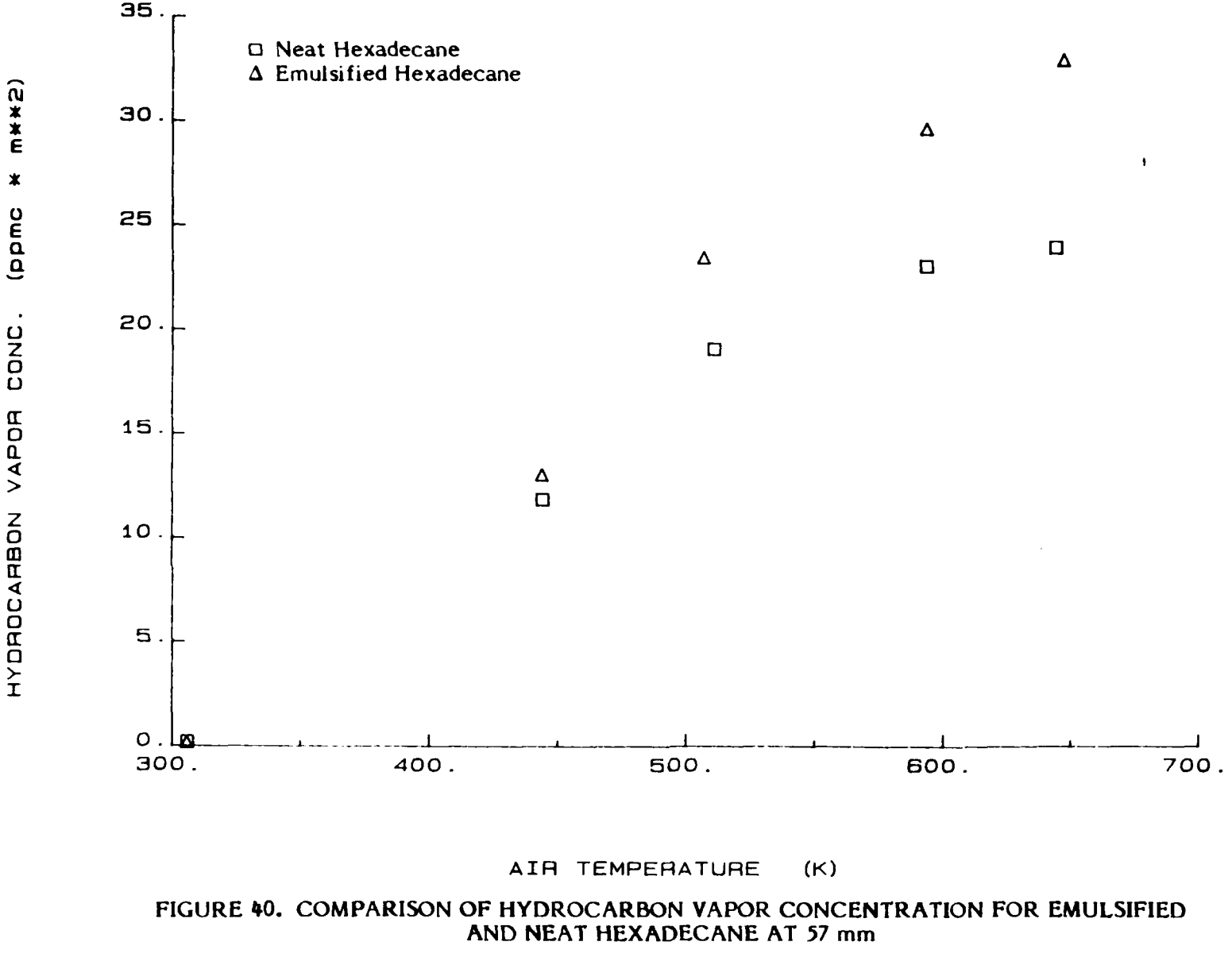

FIGURE 40. COMPARISON OF HYDROCARBON VAPOR CONCENTRATION FOR EMULSIFIED AND NEAT HEXADECANE AT 57 mm

Figure 39 indicate that at 19 mm, the vaporization of the neat and emulsified fuels is similar within the precision of the measurement. At 57 mm, the emulsified fuel is vaporizing faster at elevated temperatures. This observation lends strong support to the idea that sufficient microexplosions are occurring to enhance the vaporization rate beyond any reduction caused by the heat-sink effect of the water.

3.3 Comparison of Computer Predictions and Measured Spray Parameters

The data for the evaporation of neat hexadecane at elevated temperatures and pressures provides not only a reference for the emulsified fuel data, but also a set of data for comparison with predictions from the computer model. Diagnostics have been described which provided a measure of both drop-size distributions as a function of distance from the nozzle and hydrocarbon vapor concentration. The computer model described earlier in this report was used to predict these values in a form comparable with the experimental results. Results for predicted versus measured changes in drop-size distribution are presented first, followed by comparisons for the fuel vapor concentration.

The computer model does not predict initial drop-size distribution upon atomization, but requires this as an input. The experimental values measured at 16.4 mm were used as a calibration point and different parameters for the Rosin-Rammler size-distributions at the nozzle exit were used until a reasonable match was obtained at 16.4 mm. The computer model and experimental values were not matched closer to the nozzle because of the sampling bias effects of the laser beam discussed previously. That is, too close to the nozzle, the large drops on the outer periphery cause a significant increase in the measured SMD, an effect not included in the computer model. Thus, the comparison between predicted and measured size distributions should be made for the trends of SMD and N as a function of distance from the nozzle and air temperature.

Predictions from the computer model are compared with experimental results for a series of tests at 448 kPa (4.42 atm), and a temperature of 450 K in Figure 41, 509 K in Figure 42, 547 K in Figure 43, 593 K in Figure 44, and 646 K in Figure 45. The lines in each figure are the model predictions and the symbols are the experimental values. In each figure, the upper line and data are for the Rosin-

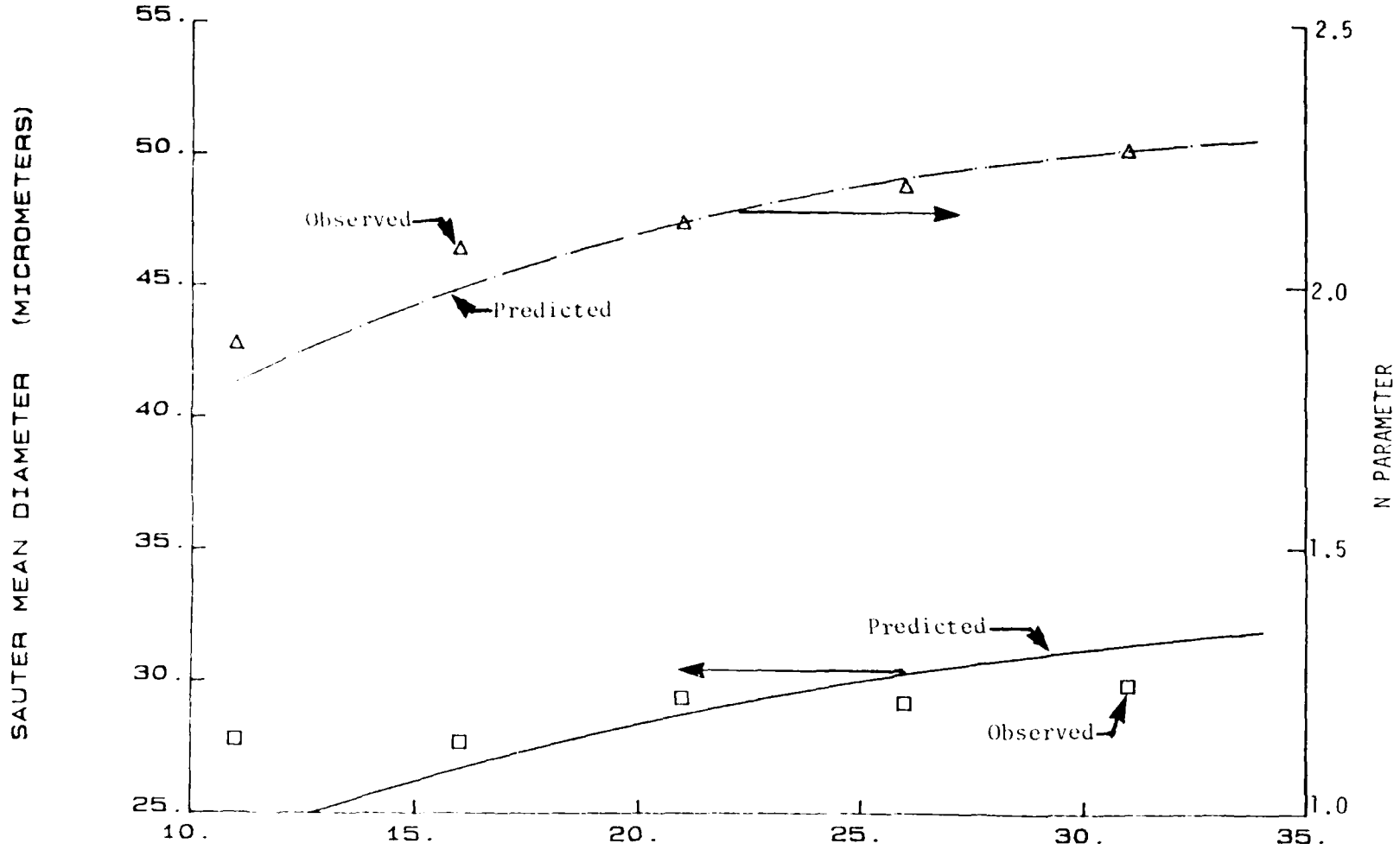

FIGURE 41. COMPARISON OF PREDICTED AND OBSERVED SMD AND N PARAMETER, 450 K, 448 kPa

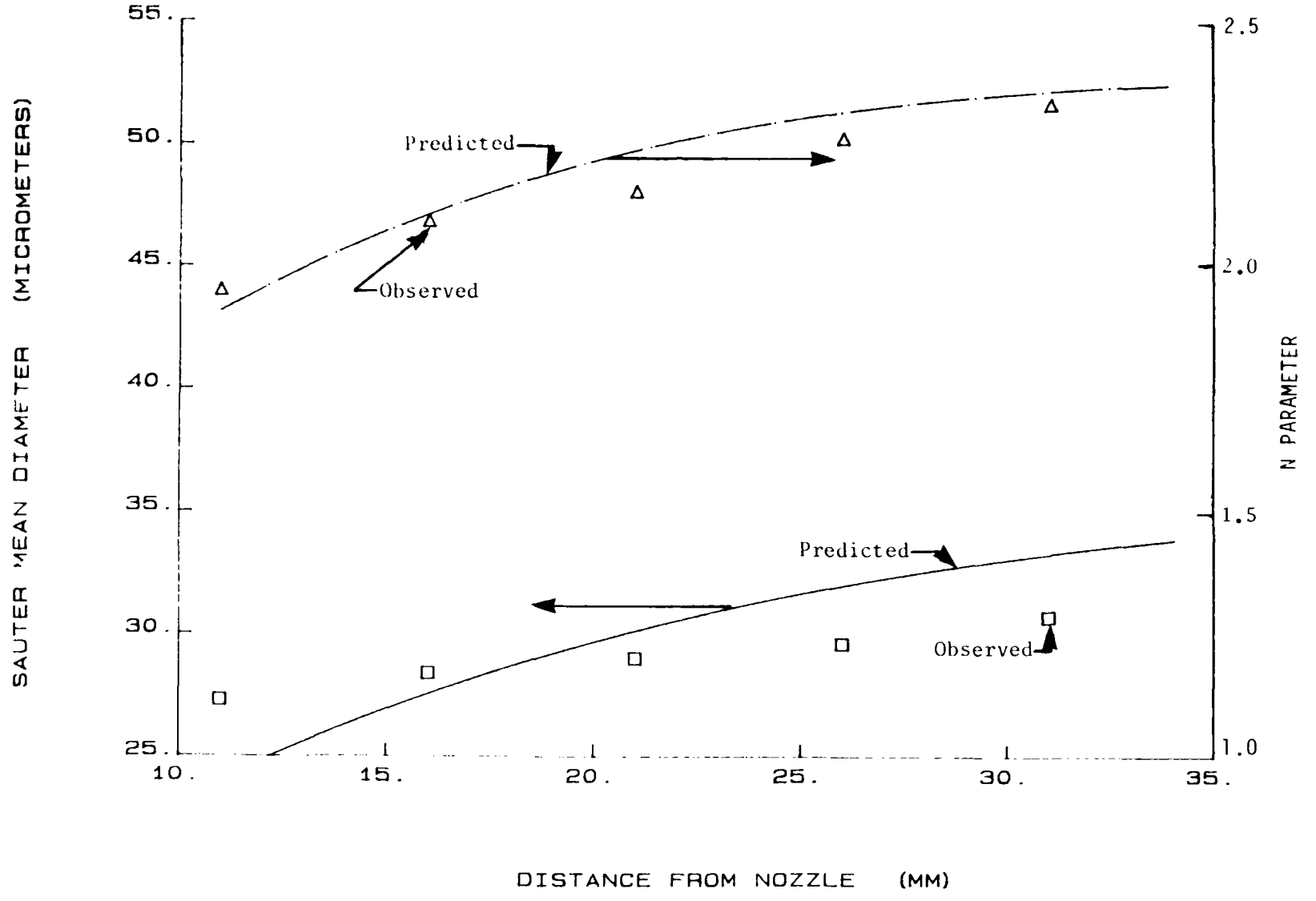

FIGURE 42. COMPARISON OF PREDICTED AND OBSERVED SMD AND N PARAMETER, 509 K, 448 kPa

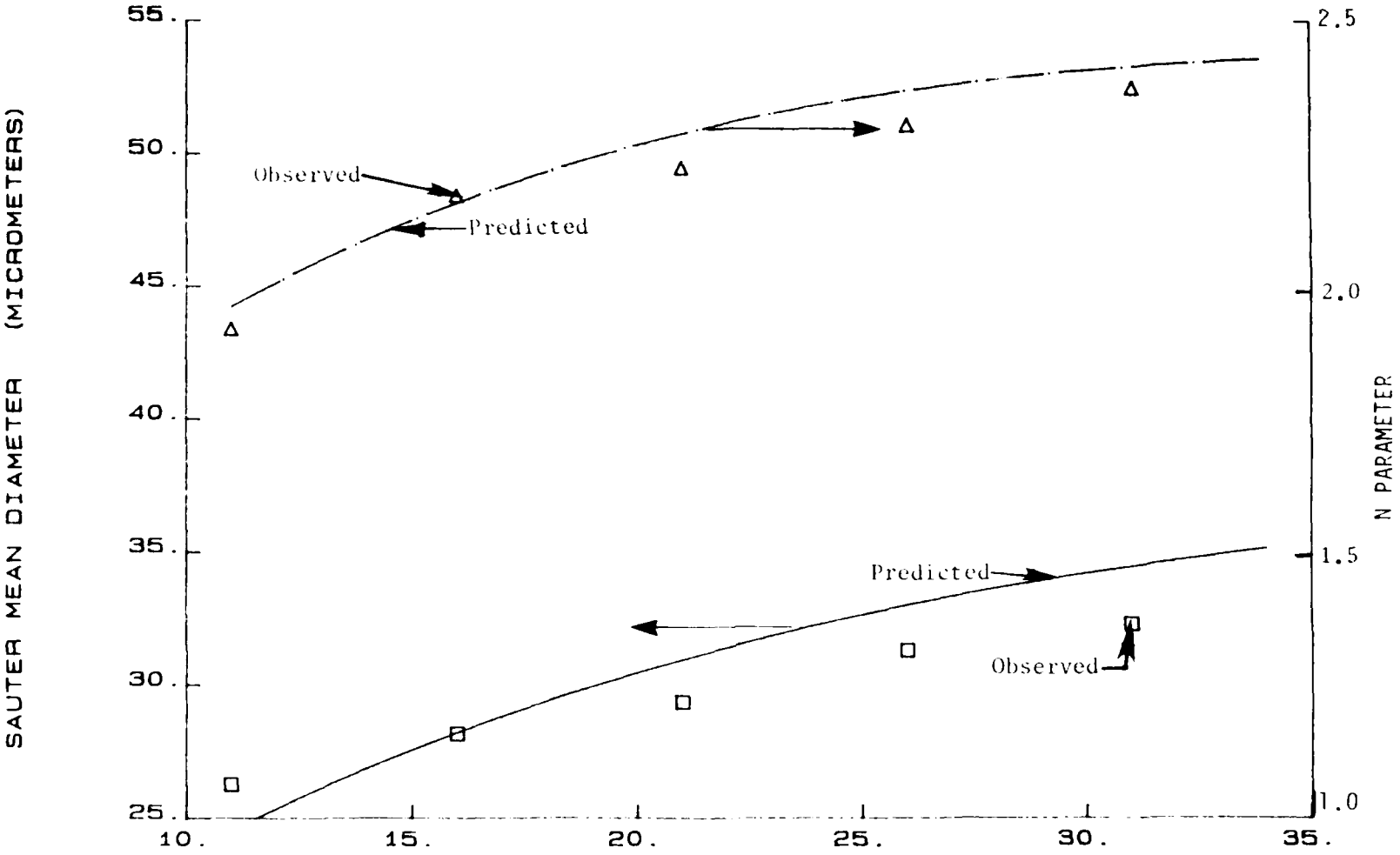

FIGURE 43. COMPARISON OF PREDICTED AND OBSERVED SMD AND N PARAMETER, 547 K, 448 kPa

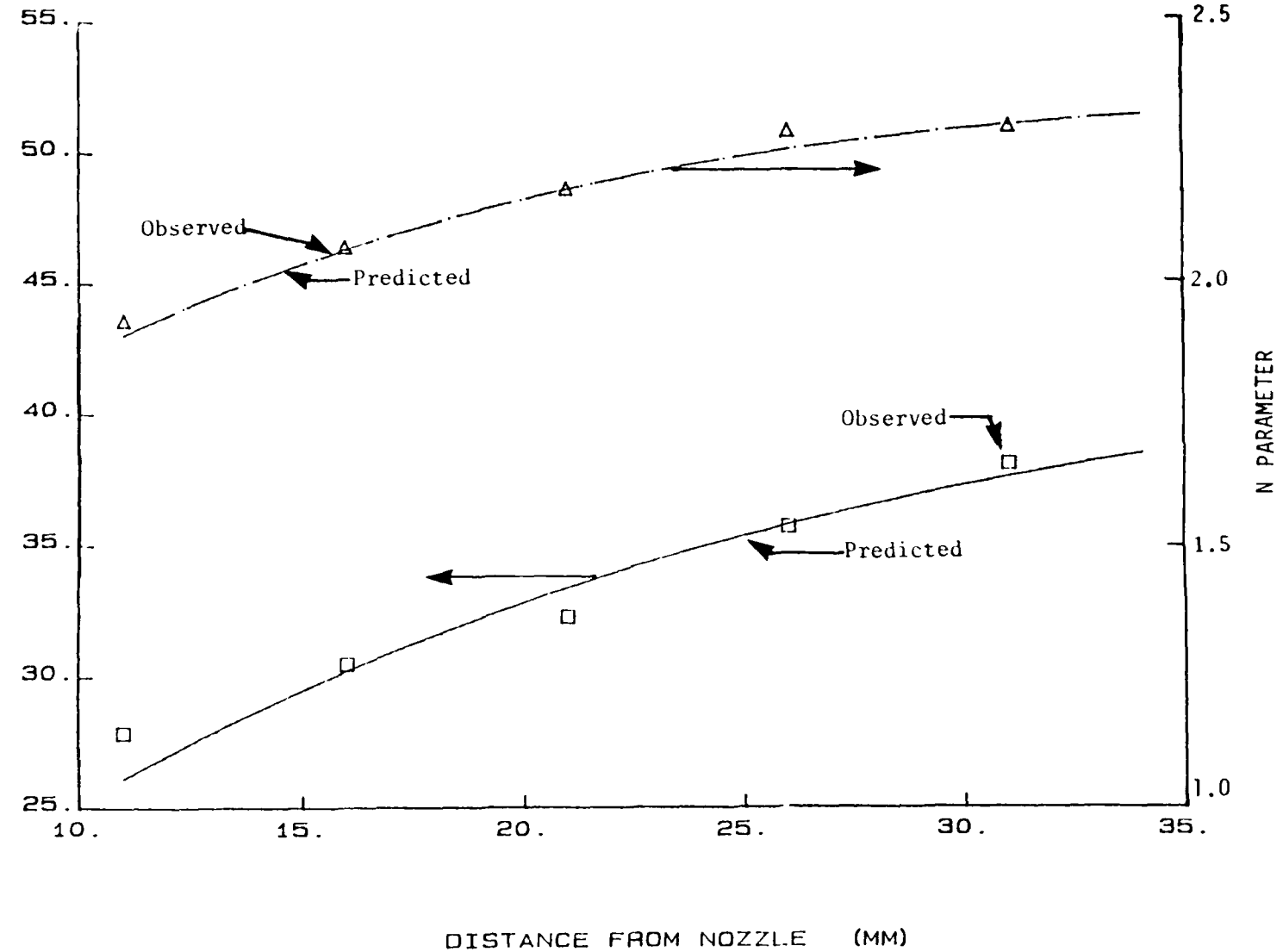

FIGURE 44. COMPARISON OF PREDICTED AND OBSERVED SMD AND N PARAMETER, 593 K, 448 kPa

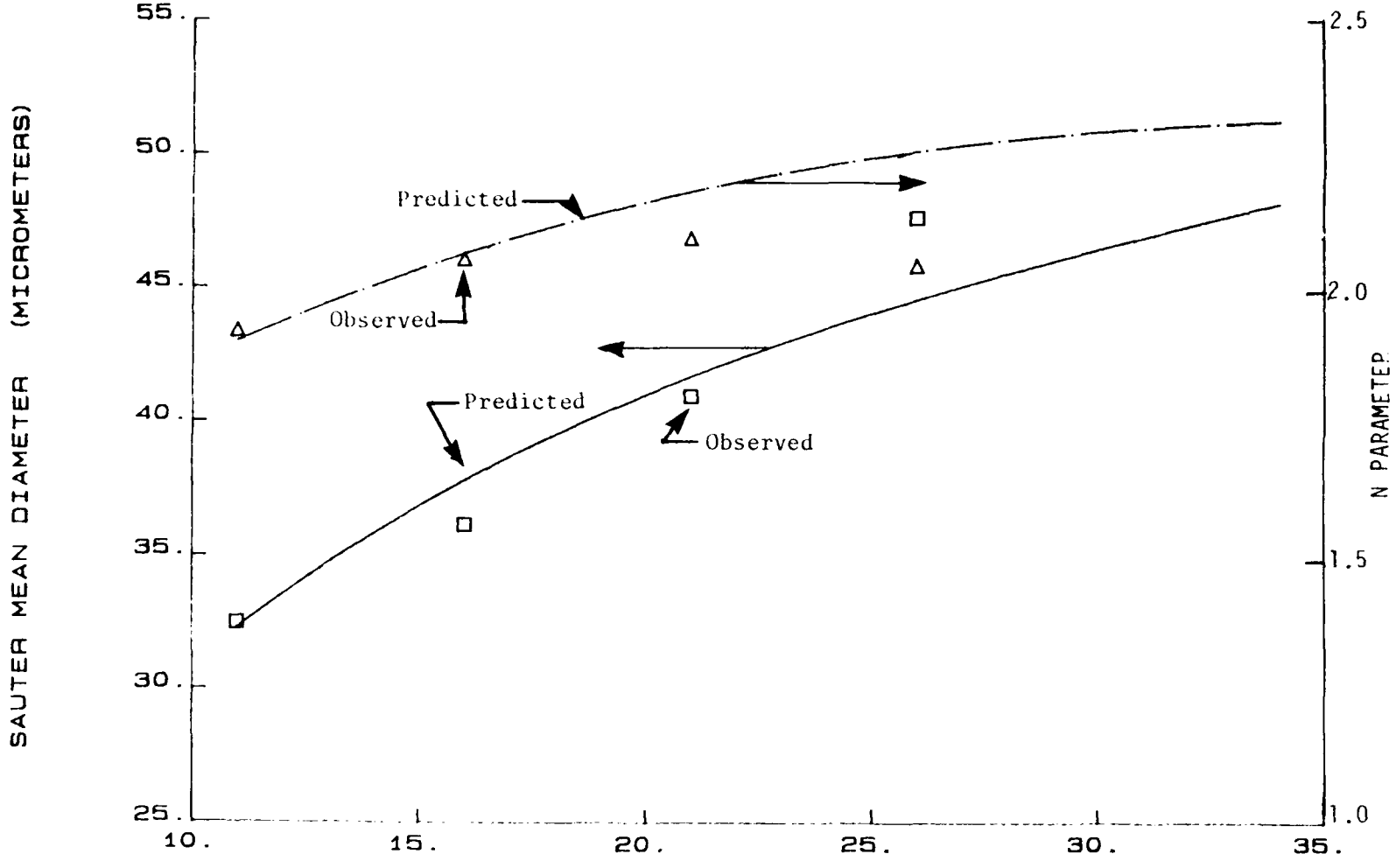

FIGURE 45. COMPARISON OF PREDICTED AND OBSERVED SMD AND N PARAMETER, 646 K, 448 kPa

Rammler N parameter, and for each case, the predicted and measured trends a fairly well, with both indicating a narrower distribution (larger N) going downst from the nozzle, corresponding to the evaporation and removal from the distrib of the smaller drops. Figure 45 for 646 K does show a discrepancy between pred and measured N values, but the measured value is somewhat in error due to l steering problems. At the highest temperatures, the correction technique for e due to steering of the laser beam by thermal gradients cannot completely correc light-scattering signal, with the results that a systematic error is introduced ca the measured N to be smaller than its true value and the SMD to be larger tha true value. This limits the application of this instrument at some point downstrea the nozzle.

The predicted and measured SMD's are shown in the lower parts of Figures 4 Notice that both the lines for the computer model predictions and the syn representing the measured values increase more rapidly going downstream at higher temperatures. These trends seem to be predicted fairly accurately, with a some exception in Figure 45. The errors in SMD's due to beam steering are usually severe than the errors in N's. The predicted and measured SMD's also diverge clo the nozzle due to the sampling effects discussed earlier, which also cause some o differences between the predicted and measured values at the lower temperature particular, the measured values being higher than predicted close to the nozzle lower downstream.

The computer model was also used to predict the fuel vapor concentration i spray cone, and these values were used for comparison with the two-phase p measurements for the hexadecane spray. The comparison at 19 mm downstream o nozzle is shown in Figure 46, and at 57 mm downstream in Figure 47. The comp model assumes a uniform concentration in the radial direction to the edge of the s cone as shown in Figure 5. It is encouraging that the values are of similar magnitu but there are some considerable differences that are due to both simpli assumptions in the model and questions about the two-phase probe. These re could be improved by a measurement of the liquid-phase fuel concentration along the vapor phase. Such a measurement is possible with the two-phase probe, and w allow the fraction of fuel which is vaporized to be calculated more accurately measurement of the liquid fuel concentration as a function of radial displace

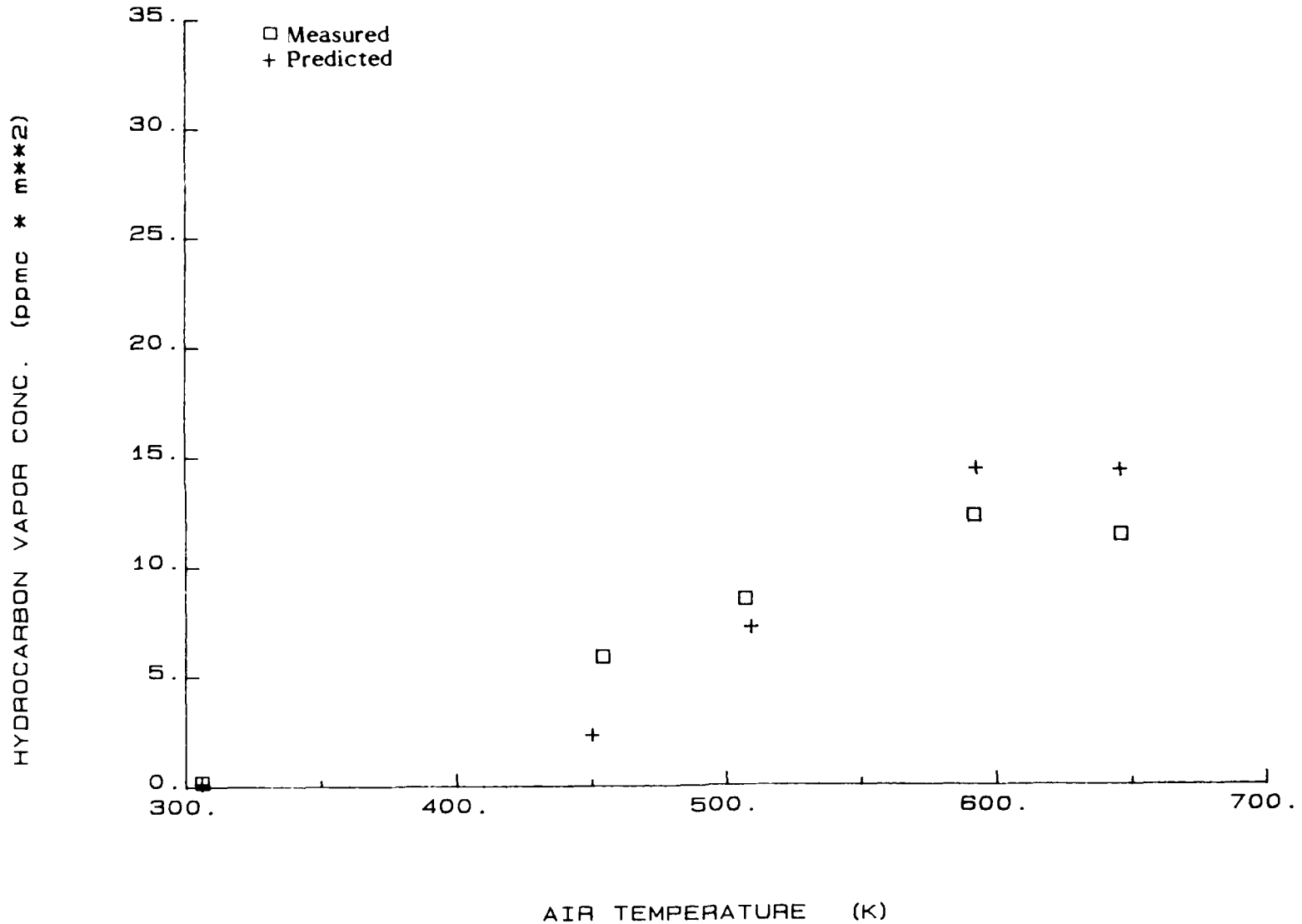

FIGURE 46. COMPARISON OF PREDICTED AND MEASURED HYDROCARBON VAPOR CONCENTRATION AT 19 mm

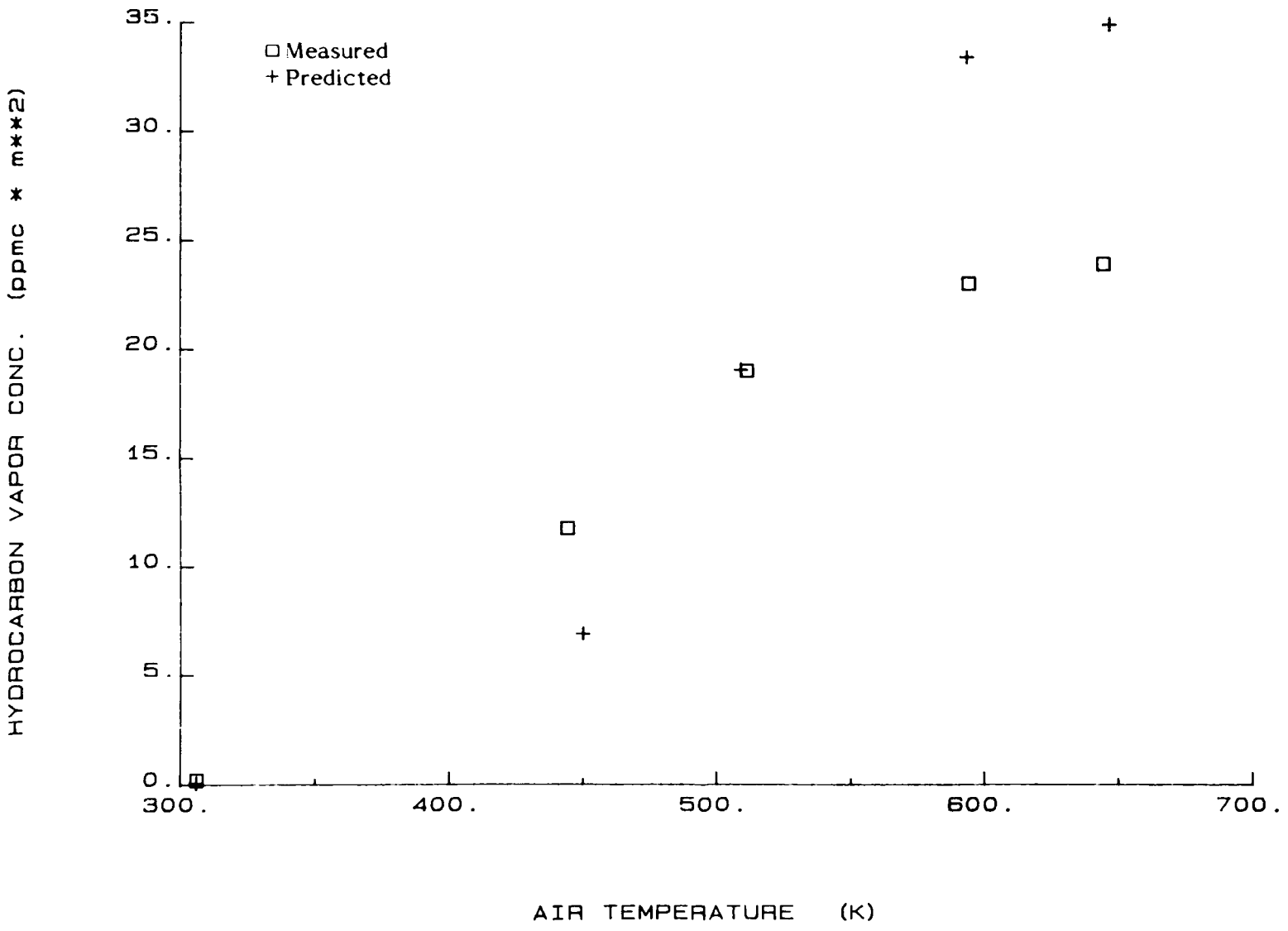

FIGURE 47. COMPARISON OF PREDICTED AND MEASURED HYDROCARBON VAPOR CONCENTRATION AT 57 mm

from the nozzle axis would also allow a check of the trajectory portion of the computer model.

The detailed comparison presented here between predicted and measured drop-size distributions and fuel-vapor concentrations for fuel sprays into elevated temperature and pressure air shows the promising capabilities of these diagnostic techniques for model verification. Verification data for fuel spray models is severely lacking, and these diagnostics demonstrate an approach to model verification.

3.4 Drop-Size Measurements in Burning Sprays

The measurements and modeling discussed earlier have been used for non-burning sprays injected into uniform temperature air flowing coaxially with the fuel spray. It was also of interest to attempt drop-size measurements in a burning spray. Because of the sharp temperature gradients and unsteadiness of the combustion process, the results would be difficult to interpret, but it could be a useful experimental diagnostic instrument. Two types of problems are present when making drop-size measurements in burning sprays. First, the flame produces high levels of visible and near-infrared radiation coinciding with the response range of the detectors in the sizing instrument, and orders of magnitude higher in intensity than the desired scattered radiation from the HeNe laser. Secondly, the strong gradients in temperature and air/fuel vapor concentration result in beam steering problems even worse than those in the non-burning evaporating sprays. Just as for sprays evaporating in elevated-temperature air, the beam steering results in extraneous amounts of light being recorded on the inner detector rings, resulting in significant errors in the computed drop-size distribution.

Drop-size measurements were attempted with JP5 in emulsified (20-percent water) and neat form in two different types of flames. First the disc-in-duct combustor described earlier was used. Then the flame was stabilized downstream of the nozzle using two rectangular flame holders, placed near the top and bottom of the spray, 42 mm downstream of the nozzle and separated by 25 mm.

For both flame configurations, the phase-sensitive detection, optical filtering, and restriction of the field-of-view of the detector described in the EXPERIMENTAL

APPARATUS section were effective in preventing interference from the flame radiation in the scattered-light measurement. However, the extreme thermal gradients in the flame regions prevented reasonable data from being obtained due to excessive beam-steering problems. For the case where the flame was stabilized downstream of the spray nozzle, drop-size data were obtained from the nozzle up to the beginning of the visible flame. For these fairly fine and dilute sprays, the evaporation at the flame front is so rapid and the temperature gradients so steep that no meaningful data were obtained within the burning portion of the spray. When the flame was stabilized downstream of the nozzle, the measured SMD was fairly constant to within about 4 mm of the visible flame, and then increased from there to the edge of the flame front where data could no longer be acquired.

It appears that drop-size measurements in burning sprays are not possible with the diffraction-based instruments unless other approaches are used to alleviate the beam steering problems. In addition, the vaporization is so rapid that very good spatial resolution would also be required for the conditions of this experiment. Techniques to overcome the other problem of interference of flame radiation have been developed and described here.

IV. SUMMARY AND DISCUSSION

Significant progress has been made during this program in three general areas. First, diagnostics have been developed for measuring spray characteristics, including drop-size distributions and vaporized fuel concentrations, in elevated-temperature and pressure-evaporating sprays. Second, these diagnostics have been used to determine the relative atomization and evaporation characteristics of fuels emulsified with water and their neat counterparts in polydisperse high-velocity fuel sprays. The purpose of these comparative measurements has been to determine if microexplosions can occur in emulsified fuels with sufficient frequency and intensity to enhance the overall evaporation rate when compared with neat fuels. Third, these experimental measurements, when combined with predicted results from a spray trajectory and evaporation computer model, have led to a better understanding of fuel spray evaporation.

The data presented here for emulsified and neat hexadecane indicate a divergence in drop size distributions at a predicted drop temperature of about 515 K. The predicted spontaneous nucleation temperature of water in hexadecane is about 539 K. However, the presence of particles, bubbles, or dissolved gases would lower the actual nucleation temperature below the predicted value. The emulsions used in these tests were ultrasonicated to keep them uniformly mixed before entering the test section, and bubbles may have been created within the water or at the water/surfactant/fuel interface. Thus, the observed divergence in the drop-size distributions of neat and emulsified fuels occurs at a predicted drop temperature reasonably close to the expected nucleation temperature of water.

The trends for drop-size distributions observed for emulsified and neat jet-A were qualitatively similar to those seen for the hexadecane blends. Because of the multicomponent nature of jet-A, drop temperatures are more difficult to estimate and no attempt was made to calculate those temperatures here.

The measurements with the two-phase probe allow a distinction between drop-size differences caused by the heat-sink effect of water (due to its large sensible and latent heat of vaporization) and microexplosions. The heat-sink effect will reduce the evaporation rate of emulsions relative to the neat fuel, while the microexplosions

should increase it. Vapor-phase measurements show that the emulsified and neat fuels initially evaporate at about the same rate, but further from the nozzle and at higher temperatures and pressures the emulsified fuel evaporates about 40 percent faster. Microexplosions are the probable explanation for these experimental results. Thus, even in a turbulent high-pressure air stream where internal drop mixing is enhanced, microexplosions can occur, creating smaller droplets to enhance the overall evaporation rate; the effect is apparently sufficient to overcome the reduction in evaporation rate due to the high heat capacity of water. The effect of air pressure on microexplosions was discussed earlier, but it should also be mentioned that while increasing pressure enhances the probability of microexplosions, the intensity of the disruption is expected to be reduced.[23]

This research does not resolve the question about why emulsification of fuels with water reduces soot formation, but it does verify that microexplosions cannot be excluded as an explanation even in turbulent air streams.

Aside from the questions about emulsified fuels, the diagnostics and model discussed here have application to spray evaporation problems in general. Faeth's[11] review article on spray models indicates that there is a scarcity of experimental confirmation of evaporation codes. In order to verify spray models, several diagnostic devices are required, and two have been described here.

Measurements with the drop-sizing instrument have shown that nozzle calibrations obtained at atmospheric conditions cannot be assumed to be an accurate estimate of nozzle performance in a combustor. The drop-sizing instrument as modified for this work can be used to obtain initial spray sizes of many types of sprays at elevated temperatures and pressures. However, laser beam steering caused by temperature and concentration gradients limits its application at some point downstream of the nozzle. For the experiments described here, data could be obtained only for the first 20 percent or so of the evaporation process.

Two-phase or phase-discriminating probes offer the capability of determining fuel vaporization rates within a drop-laden fuel spray. The aerodynamics separation appears to work well even for the fine sprays (SMD $\cong$30 micrometers) used in this work, as indicated by the room temperature tests with hexadecane. The probe did

seem to exhibit some hysterisis with changes in air temperatures that is not yet understood. It would be desirable to test and confirm the operation of a two-phase probe using an independent technique such as a non-intrusive optical absorption method.

V. CONCLUSIONS

Drop-size distributions and fuel vapor concentrations have been determined at a variety of elevated temperatures and pressures within sprays of jet-A and hexadecane and their emulsions with 20 percent water. These results indicate that microexplosions occur in the emulsified fuel at some conditions in spite of the high drop-to-air Reynolds numbers and the air turbulence which serve to enhance internal drop circulation and reduce the probability of microexplosions.

Modifications have been developed and described which, for the first time, allow the Malvern laser-diffraction drop-sizing instrument to be used in high-temperature rapidly-evaporating sprays. Modifications are also described for this instrument to overcome problems associated with high background light levels such as flame radiation. However, in the case of flames, the beam-steering problems become very severe. A calibration procedure for the Malvern has been developed and published which results in agreement with calibration verification reticles to within the accuracy of the reticles. This procedure, described in Reference 3 of Appendix B, should alleviate the differences between instruments which have been so troublesome in the past.

Results have also been reported for a two-phase probe. This appears to be a powerful diagnostic instrument for spray model verification, but more work needs to be done to resolve questions concerning its operation.

The computer model for spray trajectory and evaporation described here predicts many of the trends observed experimentally for both the drop-size data and fuel vapor concentration data.

The air pressure and temperature have a considerable effect upon initial atomization of the spray, with increasing air density improving atomization. This has important consequences when using drop-size calibrations obtained at atmospheric conditions to predict performance of gas-turbine combustors at elevated pressure, or at the low air densities typical of altitude-relight conditions.

VI. RECOMMENDATIONS

The results from this program suggest several other interesting areas for applications of techniques developed here.

1. The diagnostics which were developed in this program to study secondary atomization in emulsified fuel could be used to examine secondary atomization in azide/fuel mixtures, or other blends designed for enhanced atomization.

2. The comparisons of predictions from the spray model with measured quantities show some interesting capabilities for the model. The computer model should be expanded to include more of the sampling effects and the spray/air momentum exchange, and a more thorough comparison made with existing experimental data as well as newly acquired data.

3. The two-phase probe tests were limited in scope, but indicated a powerful technique for spray model verification. This technique should be expanded to include liquid-fuel analysis. Also, the results should be determined independently by an optical absorption technique to develop more confidence in the probe.

4. It is shown in this report that increasing air density improves atomization. The effect of density and temperature need to be documented more generally for subatmospheric and elevated pressures. This has important implications for modeling gas-turbine combustion and altitude-relight problems.

5. Dense fuel sprays cause errors for the drop-sizing instrument due to multiple-scattering of photons off more than one drop. This effect has been examined experimentally and some empirical correction factors developed, but a theoretical study is desirable to develop a more general correction scheme.

VII. ACKNOWLEDGEMENTS

This work has resulted from contributions of a number of people, whose efforts we wish to acknowledge. The Office of Naval Research, with technical monitoring by M.K. Ellingsworth, provided funds for this program under Contract No. N0014-80-K-0460. Mr. R.C. Haufler performed much of the experimental work. Much of the computer model was based on work done by Professors J.S. Chin and A.H. Lefebvre at Purdue. Assistance in the computer programming was provided by Mr. T.J. Callahan. Dr. B. Weiner of Malvern provided ideas in the use of the drop sizing instrument. Dr. D.W. Naegeli at this laboratory and Drs. J.J. Sangiovanni, A. Vranos, and J. McVey of UTRC provided helpful ideas and Ms. S.J. Douvry and Mr. J.W. Pryor helped in manuscript preparation. The experimental work was performed at the U.S. Army Fuels and Lubricants Research Laboratory, operated for the U.S. Army Belvoir R&D Center.

VIII. REFERENCES

1. Moses, C.A., Presented at the Western States Section of the Combustion Institute, University of California, La Jolla, California, (1976).

2. Klarman, A.F., Rollo, A.J., and Scott, H.C., Naval Air Propulsion Center, Trenton, New Jersey, Report No. NAPC-PE-7, (1978).

3. Spadaccini, L.J., and Pelmas, R., Paper presented at the American Chemical Society Meeting, San Francisco, (1976).

4. Kinney, R., and Lombard, P., Second Symposium on Water-in-Fuel Emulsions in Combustion, The U.S. Coast Guard Report CG-D-50-79, p. 84, (1979).

5. Callahan, T.J., Ryan, T.W., III, O'Neal, G.B., and Waytulonis, R.W., SAE Paper No. 830553, (1983).

6. Gollahalli, S.R., Nasrullah, M.K., and Brashi, J.H., Combust. Flame, 55, 93, (1984).

7. Rao, V.K., and Bardon, M.F., Combust. Flame, 55, 73, (1984).

8. Law, C.K., Lee, C.H., and Srinivasan, N., Combust. Flame, 37, 125, (1980).

9. Gollahalli, S.R., Combust. Sci. Tech., 19, 245, (1979).

10. Lasheras, J.C., Kennedy, I.M., and Dryer, F.L., WSS 80-11, presented at the Western States Section of the Combustion Institute, 1980 Spring Meeting, Irvine, California, (1980).

11. Faeth, G.M., Prog. Energy Combust. Sci., 9, 1, (1983).

12. Dodge, L.G. and Cerwin, S.A., to appear in Liquid Particle Size Measurement Techniques, edited by J.M. Tishkoff, (1984).

13. Collins, M.H., Transactions of SAE, Paper No. 690515, (1969).

14. McVey, J.B., Kennedy, J.B. and Owen, F.K., WSCI 76-28, presented at the 1976 Fall Meeting of the Western States Section, Combustion Institute, La Jolla, California, (1976).

15. Wadleigh, K.R. and Oman, R.A., MIT Gas Turbine Laboratory Report on ONR Contract N5 ori-07878, (1956).

16. Chin, J.S. and Lefebvre, A.H., AIAA-83-0068, (1983).

17. Spalding, D.B., Fourth Symposium (International) on Combustion, Williams and Wilkins Co., p. 847, (1953).

18. Frossling, N., "On the Evaporation of Falling Droplets", Gerlands Beitrage zur Geophysik, 52, 170, (1938).

19. Allen, T., Particle Size Measurements, Third Edition, Chapman and Hall (1981) p. 139, 140.

20. Mugele, R.A., and Evans, H.D., "Droplet-Size Distribution in Sprays," Ind. Eng. Chem., 43, 1317 (1951).

21. Dodge, L.G. and Moses, C.A., Interim Rpt. No. SwRI 6287/2, Contract No. N00014-80-K-0460, (1982).

22. Avedisian, C.T., ASME 81-WA/HT-43, (1981).

23. Avedisian, C.T., Trans. ASME, J. Heat Transfer, 104, 750, (1982).

24. Law, C.K., Combust. Sci. Tech., 17, 29 (1977).

APPENDIX A

FUEL SPRAY COMPUTER MODEL - MATHEMATICS

For purposes of discussion, the model is divided into three parts called (1) Thermodynamics, (2) Aerodynamics, and (3) Drop-Size Distribution. Each section is discussed in order. An overall flow chart is shown in Figure A-1.

Thermodynamics

This part of the model computes the heat-up of the drop, the final steady-state temperature, and the fuel and air properties necessary for those calculations. This part of the model is identical to that described by Chin and Lefebvre (Ref. A1 and A2) except that some of the fuel property data were taken from the American Petroleum Institute Data Book (Ref. A3). The results from this model are very similar to those presented by Chin and Lefebvre when the model is used for quiescent fuel sprays. The integration of this part of the model with the other sections to be described allows the examination of sprays in situations where both spray and air are moving with a nonzero relative velocity. The mathematics are outlined below, but a more detailed derivation is given by Chin and Lefebvre (Ref. A1 and A2) which in turn is based on the theories described by Spalding (Ref. A4).

The steady-state temperature is determined as follows. The mass transfer rate, $\dot{m}$, from a drop is given by,

$$\dot{m}_F = 2\pi D \, (k_g/c_{p,g}) \quad \ln \, (1+B) \tag{A1}$$

where D is the diameter, k_g is the thermal conductivity of the gas, $c_{p,g}$ is the specific heat at constant pressure, and B is either B_M, the mass diffusion transfer number if mass diffusion is controlling, or B_T, the

AD-A141 958 MECHANISMS OF SMOKE REDUCTION IN THE HIGH-PRESSURE COMBUSTION OF EMULSIFI..(U) SOUTHWEST RESEARCH INST SAN ANTONIO TX L G DODE ET AL. MAY 84 SWRI-6287/3 2/2

UNCLASSIFIED N00014-80-K-0460 F/G 21/2 NL

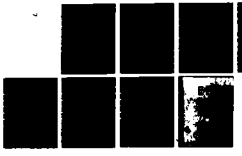

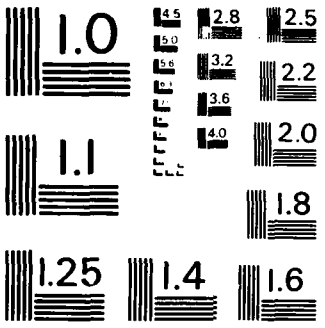

FIGURE A-1 FLOW CHART OF SPRAY MODEL

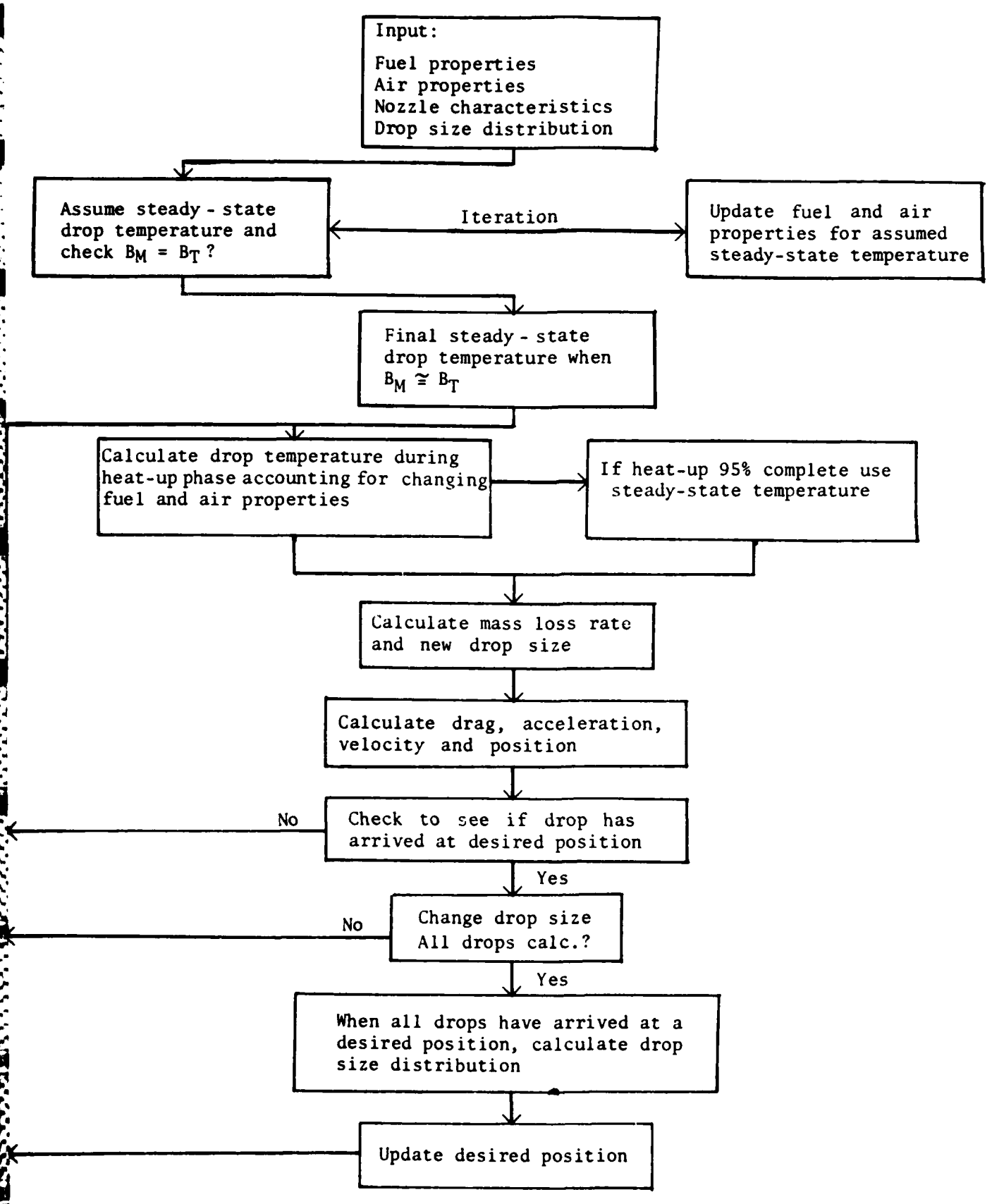

thermal diffusion transfer number if heat transfer is controlling and the Lewis number is assumed to be unity. B_M is defined as

$$B_M = (Y_{F,s} - Y_{F,\infty}) / (1 - Y_{F,s}) \quad (A2)$$

where $Y_{F,s}$ and $Y_{F,}$ are the fuel mass fractions at the drop surface and in the ambient air, respectively, and $Y_{F,s}$ is

$$Y_{F,s} = P_{F,s} M_F / (P_{F,s} M_F + (P - P_{F,s}) M_A) \quad (A3)$$

where $P_{F,s}$ is the fuel vapor pressure at the drop surface, P is the ambient pressure, and M_F and M_A are the molecular weights of fuel and air, respectively. The vapor pressure was calculated using the method recommended by the American Petroleum Institute Data Book (Ref. A3) called Procedure 5A1.10, "Vapor Pressures of Pure Hydrocarbons."

The thermal diffusion transfer number B_T for an evaporating drop is

$$B_T = c_{p,g} (T_\infty - T_S) / L \quad (A4)$$

where T_∞ and T_s are the ambient air temperature and drop surface temperature and L is the latent heat of fuel vaporization corrected from the normal boiling point to the actual surface temperature.

The accuracy of Equation (A1) is very dependent on the choice of values for k_g and c_{p_g}. As recommended by Chin and Lefebvre (Ref. A1) a reference temperature was chosen as the drop surface temperature plus 1/3 of the difference between ambient air and surface temperatures. Similarly a reference value of the fuel vapor mass fraction was taken as the value just outside the surface plus 1/3 of the difference between the value at infinity and just outside the surface. Using these reference conditions denoted by "r" the specific heat of the gas is given by,

$$c_{p,g} = Y_{A,r} \, (c_{p,A} \text{ at } T_r) + Y_{F,r} \, (c_{p,V} \text{ at } T_r) \tag{A5}$$

and the thermal conductivity by,

$$k_g = Y_{A,r} \, (k_A \text{ at } T_r) + Y_{F,r} \, (k_V \text{ at } T_r) \tag{A6}$$

At steady-state conditions, $B_M = B_T$ or from Equations (A2) and (A4)

$$\frac{Y_{F,s} - Y_{F,\infty}}{1 - Y_{F,s}} = \frac{c_{p,g} \, (T_\infty - T_{s,st})}{L} \tag{A7}$$

where $T_{s,st}$ is the desired surface temperature under steady-state conditions. Assuming that the fuel vapor concentration in the ambient air is zero ($Y_{F,\infty} = 0$) and substituting for $Y_{F,s}$ from Equation (A3) then (A7) becomes

$$\frac{P}{P_{F,s}} - \frac{M_F}{M_A} \frac{L}{c_{p,g} \, (T_\infty - T_{s,st})} - 1 = 0 \tag{A8}$$

In solving Equation (A8) to determine the steady-state surface temperature $T_{s,st}$, some of the variables can be specified, P, M_F, M_A, and T_∞ but the remaining three variables are functions of temperature, with L being related to the heat of vaporization at the normal boiling point $L_{T,bn}$ by,

$$L = L_{T,bn} \left[(T_{cr} - T_s) \, / \, (T_{cr} - T_{bn}) \right]^{0.38} \tag{A9}$$

where T_{cr} is the critical temperature and T_{bn} is the normal boiling point of the fuel. In order to solve (A8) it is necessary to first assume a value for $T_{s,st}$. That temperature is used to calculate a reference temperature T_r which in turn is used to calculate those quantities specified in Equations (A5) and (A6) used to calculate $c_{p,g}$ and k_g, and to calculate L as specified in (A9). If the assumed value of $T_{s,st}$ is too low, the left side of Equation (A8) will be positive. An iterative procedure must be used to continue specifying $T_{s,st}$ until Equation (A8) is satisfied within the desired accuracy. That procedure results in a

determination of the steady state surface temperature $T_{s,st}$ and the transfer number $B=B_M=B_T$. The steady state quiescent evaporation constant $\lambda_{q,st}$ can then be determined from,

$$\lambda_{q,st} = 8\ k_g\ \ln\ (1+B)\ /\ \rho_F\ c_{p,g} \qquad \text{(A10)}$$

where ρ_F is the fuel density. Frossling (Ref. A5) has shown that convective effects can be accounted for in the case where heat transfer rates are controlling by,

$$\lambda_{c,st} = \lambda_{q,st}\ (1 + 0.276\ Re_D^{0.5}\ Pr_g^{0.33}) \qquad \text{(A11)}$$

where $\lambda_{c,st}$ is the steady-state evaporation constant corrected for convective effects, Pr_g is the Prandtl number for the gas, and Re_D is the Reynolds number using the relative velocity between the drop and the gas. This velocity should include a fluctuating component in the case of turbulent flow. Turbulence intensities were not measured in these experiments, but a value of 20 percent of the axial velocity was used as an estimate. The effective velocity used to calculate Re_D for the evaporation calculation was taken as the sum of the fluctuating component (20 percent of the air velocity) plus the difference between the drop and air velocities. These computations specify the steady-state properties of the drop.

The evaporation which occurs during the drop heat-up period is significant in many practical situations, with the drop being completely evaporated before reaching steady-state conditions is some instances. Chin and Lefebvre (Ref. A2) have predicted that high air pressures and convective effects, which are often absent in laboratory experiments, both tend to increase the relative importance of the heat-up period relative to the steady-state phase of drop evaporation. Because the experiments conducted in this study were of real sprays at high pressures and relative velocities, it was necessary to model the heat-up period in detail.

Chin and Lefebvre (Ref. A2) have shown that the rate of change of drop surface temperature is given by,

$$dT_S / dt = (\dot{m}_F L / c_{p,F} m) ((B_T / B_M) - 1) \quad (A12)$$

where $\dot{m}_F$ is specified by Equation (A1) with $B=B_M$ during the heat-up period, and $\dot{m}$ is the drop mass,

$$m = (\pi/6) \rho_F D^3 \quad (A13)$$

The change of drop size with time is given by (Ref. A2),

$$dD / dt = -4 k_g \ln (1+B_M) / \rho_F c_{p,g} D \quad (A14)$$

The drop temperature asymptotically approaches the steady-state temperature, and it was assumed that when the temperature had risen to 95 percent of the difference between the initial fuel temperature and the steady-state temperature, that the heat-up calculations could be terminated and steady-state properties used.

Aerodynamics

The approach used was a much more simplified version of the one developed at the University of Sheffield and described in several papers, e.g., Boyson and Swithenbank (Ref. A6). A cylindrical coordinate system was used where x is the axial distance, y the radial distance, and z the angular position, with corresponding velocities in the axial (u), radial (v), and tangential (w) directions. For this work, the tangential velocities were assumed zero.

The equations of motion of a particle (drop) neglecting all forces except drag, are,

$$\dot{u}_p = -F (u_p - u_\infty) \quad (A15)$$

$$\dot{v}_p = \frac{w_p^2}{y_p} - F\,(v_p - v_\infty) \qquad \text{(A16)}$$

$$\dot{w}_p = \frac{v_p\, w_p}{y_p} - F\,(w_p - w_\infty) \qquad \text{(A17)}$$

where the "p" subscripts refer to the particle and the "∞" subscript refers to the free stream, and F is given by,

$$F = (18\,\mu g / \rho_p\, D_p^2)\,(C_D\, Re / 24) \qquad \text{(A18)}$$

where μ_g is the gas viscosity, ρ_p is the particle density, D_p is the particle diameter, C_D is the drag coefficient, and Re is the Reynolds number defined as,

$$Re = \frac{D_p\, \rho_g}{\mu_g} \left| \vec{u}_p - \vec{u}_\infty \right| \qquad \text{(A19)}$$

The drag coefficient, C_D, is given by (Ref. A7),

$$C_D = 27\, Re^{-0.84} \qquad 0 \quad Re - 80 \qquad \text{(A20)}$$

$$C_D = 0.271\, Re^{0.217} \qquad 80 < Re \leq 10^4 \qquad \text{(A21)}$$

$$C_D = 2 \qquad 10^4 > Re \qquad \text{(A22)}$$

The equations of motion (A15 to A17) are solved numerically using a step size of 1 to 10 μs, and the equations of trajectory are solved in a similar manner,

$$\dot{x}_p = u_p \tag{A23}$$

$$\dot{y}_p = v_p \tag{A24}$$

$$\dot{z}_p = \frac{w_p}{y_p} \tag{A25}$$

These equations describe the trajectory of a particle in a gas stream. For each iteration in the trajectory calculation, the drop size and temperature are updated using the procedure described in the Thermodynamics section.

At the end of each iteration through the trajectory calculations, the current calculated axial position of the particle is checked against a target value. When the particle reaches that target value for axial position, the position, transit time, size, temperature, and other parameters for that drop are frozen and the calculations are repeated for the next larger drop size. After all drops reach a targeted axial position, corresponding to a measurement location, the drop size distribution is calculated, important data are printed out, the target position is moved downstream, and the calculations are repeated.

Drop Size Distribution

The computer model makes all calculations on individual drops of certain sizes, but the instrumentation used to measure the spray works best in characterizing the drop sizes by two parameters which specify a size and width of the distribution. Three distributions may be selected: normal, log-normal, and Rosin-Rammler. The Rosin-Rammler distribution has provided the best fit of the sprays studied and has been used throughout this program. In order to compare the predictions from the computer model with the experimental results, it is necessary to convert the computer predicted drop sizes at a given location into an equivalent set of two parameters specifying the Rosin-Rammler distribution.

If R represents the fraction of the liquid being sprayed contained in drops larger than diameter D, then for the Rosin-Rammler distribution (Ref. A8),

$$R = \exp\left(-(D / \bar{x})^N\right) \qquad \text{(A26)}$$

where $\bar{x}$ represents a size, and N specifies the width of the distribution. It is convenient to specify a spray by a single parameter representing an "average" drop size. However, a straight numerical average is heavily weighted towards the smallest drops which are extremely plentiful but which contain a very small fraction of the total volume of the liquid. For combustion processes, the surface-to-volume ratio is important to evaporation, so an average drop size may be chosen which has a surface-to-volume ratio representative of the actual spray, and such an average is called the surface-volume mean diameter or Sauter mean diameter (SMD). The SMD is related to the Rosin-Rammler parameters by (Ref. A8),

$$SMD = \bar{x} / \Gamma(1-1/N) \qquad N>1 \qquad \text{(A27)}$$

Specifying $\bar{x}$ and N allows the calculation of the SMD, or specifying SMD and N determines $\bar{x}$.

An initial set of drop sizes distributed approximately exponentially in size (i.e., evenly spaced when plotted as ln D) and covering the range of about 6μm to 560μm (corresponding to the response range of the drop sizing instrument) with 16 to 21 different sizes is used in the model. Assuming size classes bounded by these drops as end points, the initial fraction of liquid contained in drops larger than a certain size class is given by Equation (A26).

$$R_i = \exp\left(-(D_{o,i} / \bar{x})^N\right) \qquad 1 \le i \le n \qquad \text{(A28)}$$

$$R_o \equiv 1$$

$$R_{n+1} \equiv 0$$

where "n" is the number of drops, D_o is the initial drop diameter, and the initial fraction of liquid in each size class is,

$$F_{o,i} = R_i - R_{i+1} \qquad o \leq i \leq n \tag{A29}$$

$$F_{o,-1} \equiv 0$$

After evaporation begins, the small drops begin evaporating quickly while the large ones evaporate slowly, changing the fraction of liquid in the different size classes unevenly. Denoting the smallest nonevaporated drop size by "k", the fraction of liquid remaining in any size class is,

$$F_i = \frac{F_{o,i} \left\{ (D_i / D_{o,i})^3 / u_{p,i} + (D_{i+1} / D_{o,i+1})^3 / u_{p,i+1} \right\} /2}{\sum_{j=k}^{n} F_{o,j} \left\{ (D_j / D_{o,j})^3 / u_{p,i} + (D_{j+1} / D_{o,j+1})^3 / u_{p,j+1} \right\} /2} \tag{A30}$$

$$k \leq i \leq n$$
$$(o \leq k \leq n)$$

where

$$D_0 \equiv D_1$$

$$u_{p,0} \equiv u_{p,1}$$

$$D_{n+1} \equiv D_n$$

$$u_{p,n+1} \equiv u_{p,n}$$

and $u_{p,i}$ is the axial velocity of the ith drop, D_i is the instantaneous drop size, and $D_{o,i}$ is the initial drop size of the ith drop. Each size class is characterized by the drops making up the end points, and the initial fraction of liquid in a size class is modified by the average loss of volume of the end point drops. The velocity term is added to account for the fact that as the drops slow down they increase their relative concentration, and thus their weighting factor, in the sample volume.

The cumulative fraction of liquid in all size classes including and larger than the ith class is,

$$R_i = \sum_{j=i}^{n} F_i \qquad k \leq i \leq n \qquad \text{(A31)}$$

This instantaneous value of R_i is related to the drop sizes and Rosin-Rammler parameters by Equation (A28) with the initial drop size $D_{o,1}$ replaced by the instantaneous value D_i,

$$R_i = \exp\left(-(D_i / \bar{x})^N\right) \qquad k \leq i \leq n \qquad \text{(A32)}$$

Taking the natural logarithm of both sides twice and excluding i=k (R_i=1), Equation (A32) becomes,

$$\ln_e(\ln_e(1 / R_i)) = N \ln_e D_i - N \ln_e \bar{x} \qquad k+1 \leq i \leq n \qquad \text{(A33)}$$

This has the form of the equation of a straight line, y=mx+b, if the following definitions are used,

$$y = \ln_e(\ln_e(1/R))$$

$$m = N$$

$$x = \ln_e D$$

$$b = -N \ln_e \bar{x}$$

Thus, by determining a least squares fit of the straight line through the data $\ln_e(\ln_e(1/R_i))$ versus $\ln_e D_i$, the Rosin-Rammler parameters are given by,

$$N = m \text{ (the slope)} \qquad \text{(A35)}$$

and

$$\bar{x} = \exp\ (-b\ /\ N)$$

A standard routine is used to perform the least squares operation and the Rosin-Rammler parameters and the SMD (from Equation (A27)) are determined at each target value of the axial location corresponding to the position where experimental data are obtained. Although the initial distribution at the nozzle is an ideal Rosin-Rammler distribution, the distribution downstream does not correspond exactly to the Ro· ·Rammler equation due to the different evaporation rates for the diffe nt sized drops, and the degree of fit is determined by the correlat - coefficient of the straight line through the computed data.

APPENDIX A
REFERENCES

A1. Chin, J.S., and Lefebvre, A.H., "Steady State Evaporation Characteristics of Hydrocarbon Fuel Drops," AIAA-82-1176, presented at the AIAA/SAE/ASME 18th Joint Propulsion Conference, June 21-23, 1982.

A2. Chin, J.S., and Lefebvre, A.H., "The Role of the Heat-Up Period in Fuel Drop Evaporation," to be published.

A3. Anon., Technical Data Book - Petroleum Refining, Second Edition, American Petroleum Institute, Division of Refining, Washington, D.C., 1970.

A4. Spalding, D.B., Some Fundamentals of Combustion, Butterworths Scientific Publications, 1955.

A5. Frossling, N., "On the Evaporation of Falling Droplets", Gerlands Beitrage zur Geophysik, Vol. 52, pp. 170-216, 1938.

A6. Boyson, F., and Swithenbank, J., "Spray Evaporation in Recirculating Flow," Seventeenth Symposium (International) on Combustion, The Combustion Institute, 1979, pp. 443-453.

A7. Dickerson, R.A., and Schuman, M.D., "Rate of Aerodynamic Atomization of Droplets," J. Spacecraft and Rockets," January - February 1965, pp. 99-100.

A8. Allen, T., Particle Size Measurement, Third Edition, Chapman and Hall, 1981, pp. 139, 140.

APPENDIX B

LIST OF PUBLICATIONS RESULTING FROM CONTRACT

Five publications and/or presentations have resulted from this contract to date:

1. "Diagnostics for Fuel Sprays as Applied to Emulsified Fuels," by L.G. Dodge and C.A. Moses, accepted for presentation at the Twentieth International Symposium for Combustion, August 1984.

2. "Drop-Size Measurements in Evaporating Sprays of Emulsified and Neat Fuels," by L.G. Dodge and C.A. Moses, presented at the 1983 International Gas Turbine Conference, ASME Paper 83-FT-231.

3. "Calibration of Malvern Particle Sizer," by L.G. Dodge, accepted for publication in Applied Optics, July 1984.

4. "Extending the Applicability of Diffraction-Based Drop-Sizing Instruments," by L.G. Dodge and S.A. Cerwin, presented at the ASTM Symposium on Liquid Particle Size Measurement Techniques, and accepted for publication in Liquid Particle Size Measurement Techniques, edited by J.M. Tishkoff, to appear 1984.

5. "Atomization and Evaporation of Emulsified and Neat Jet Fuel in Real Sprays," by L.G. Dodge and C.A. Moses, presented at the Fall 1982 meeting of the Western States Section of the Combustion Institute.

At least one further paper describing the computer spray model is anticipated.

YEARLY DISTRIBUTION LIST

No. of Copies		No. of Copies	
3	Mr. Keith Ellingsworth Mechanics Division Material Sciences Division Office of Naval Research 800 North Quincy Street Arlington, VA 22217	6	Technical Information Division Naval Research Laboratories 4555 Overlook Ave. S.W. Washington, DC 20375
1	Mr. Dick Strucko Code 2705 David Taylor Naval Ship R&D Center Anapolis, MD 21402	12	Defense Documentation Center Bldg. 5 Cameron Station Alexandriz, VA 22314
1	Professor C.K. Law Dept. of Mechanical Engineering & Astronautical Sciences Northwestern University Evanston, IL 60201	1	Professor F.L. Dryer Mechanical and Aerospace Engineering Dept. Princeton University Princeton, NJ 08544
1	Mr. William Wagner Naval Air Propulsion Center, PE-71 1440 Parkway Avenue Trenton, NJ 08628	1	Professor A.M. Mellor Department of Mechanical Engineering & Mechanics Drexel University Philadelphia, PA 19104
1	Dr. Robert D. Ingebo NASA-Lewis Research Center Propulsion Laboratory 21000 Brookpark Road Cleveland, OH 44135	1	Mr. John Marek NASA-Lewis Research Center Propulsion Laboratory 21000 Brookpark Road Cleveland, OH 44135
1	Mr. Dan A. Grogan 05-R CP6 R.802 Department of the Navy Naval Sea Systems Command Washington, DC 20362	1	Dr. C. Thomas Avedisian Assistant Professor Sibley School of Mechanical & Aerospace Engineering Upson & Grumman Halls Cornell University Ithaca, NY 14853
	LETTER OF TRANSMITTAL ONLY Defense Contract Administration Services Management Area - San Antonio P.O. Box 1040, Main Post Office 615 E. Houston St. San Antonio, TX 78394	1	Dr. Edward J. Mularz Head, NASA Combustion Fundamentals Section Propulsion Laboratory Research & Tech Laboratories U.S. Army Aviation R&D Cmd. NASA-Lewis Research Center 21000 Brookpark Road Cleveland, OH 44135

No. of Copies	
1	Professor Craig T. Bowman Department of Mechanical Engineering Bldg. 520 Stanford University Stanford, CA 94305
1	Dr. John McVey United Technologies Research Center Silver Lane East Hartford, CT 06108
1	Mr. Harold Simmons Parker-Hannifin Corp. Gas Turbine Fuel Systems Div. 17325 Euclid Avenue Cleveland, OH 44143
1	Professor William A. Sirignano G.T. Ladd Professor and Head Mechanical Engineering Department Carnegie-Mellon University Pittsburgh, PA 15213
1	Dr. Julian Tischkoff AFOSR/NA Bolling AB, D.C. 20332
1	Mr. William Clark Code 3246 Naval Weapons Center China Lake, CA 93555
1	Dr. Abdi S. Najad AFWAL/PORT Wright Patterson AFB, OH 45433
1	Professor A.H. Lefebvre School of Mechanical Engineering Purdue University West Lafayette, IN 47907
1	Dr. Donald R. Hardesty Combustion Research Division Sandia National Laboratories Livermore, CA 94550

No. of Copies	
1	Professor E. Dan Hirleman Mechanical Engineering Department Arizona State University Tempe, AZ 85287
1	Professor Norman Chigier Department of Mechanical Engineering Carnegie-Mellon University Schenley Park Pittsburgh, PA 15213
1	Commander U.S. Army Belvoir R&D Center Attn: STRBE-VF, M.E. LePera Ft. Belvoir, VA 22060
1	Professor S.C. Yao Mechanical Engineering Department Carnegie-Mellon University Pittsburgh, PA 15213
1	Mr. George Opdyke, Jr. Manager, Combustor Section Avco Lycoming Division 550 South Main Street Stratford, CT 06497
1	Mr. Robert E. Jones Head, Combustor Research Section NASA-Lewis Research Center 21000 Brookpark Road Cleveland, OH 44135
1	Dr. J. E. Peters Engineering Department University of Illinois Champaign-Urbana, IL
1	Professor G.M. Faeth Department of Mechanical Engineering The Pennsylvania State University University Park, PA 16802

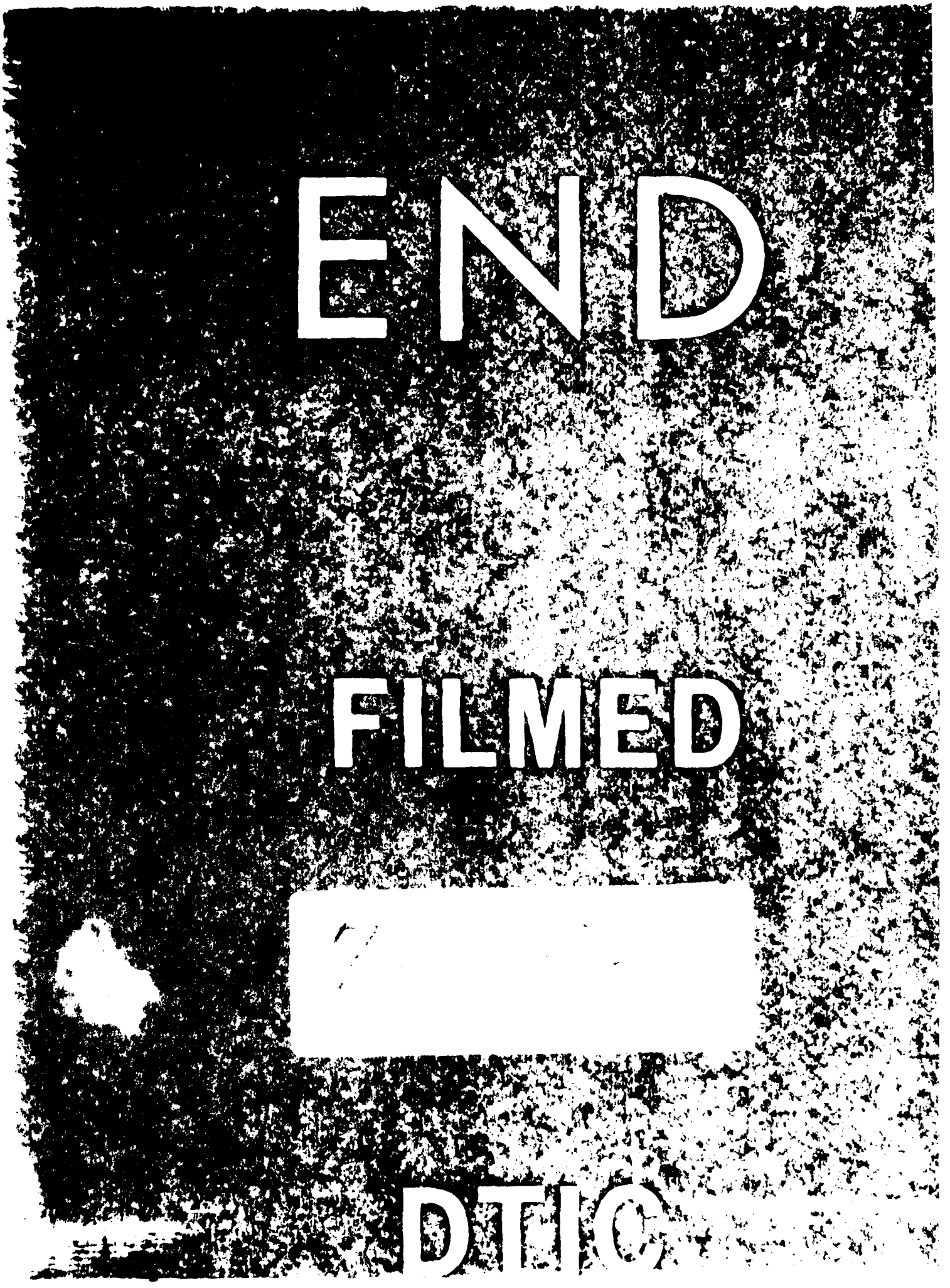
END
FILMED
DTIC